MIXING-CONTROLLED REACTIVE TRANSPORT IN CONNECTED HETEROGENEOUS DOMAINS

A Thesis
Presented to
The Academic Faculty

by

Rulan Gong

In Partial Fulfillment
of the Requirements for the Degree
Doctor of Philosophy in the
School of Civil and Environmental Engineering

Georgia Institute of Technology
December 2013

MIXING-CONTROLLED REACTIVE TRANSPORT IN CONNECTED HETEROGENEOUS DOMAINS

Approved by:

Dr. Jian Luo, Advisor
School of Civil and Environmental Engineering
Georgia Institute of Technology

Dr. Huaming Yao
School of Civil and Environmental Engineering
Georgia Institute of Technology

Dr. Aris Georgakakos
School of Civil and Environmental Engineering
Georgia Institute of Technology

Dr. Guillermo Goldsztein
School of Mathematics
Georgia Institute of Technology

Dr. Philip Roberts
School of Civil and Environmental Engineering
Georgia Institute of Technology

Date Approved: November 12, 2013

ACKNOWLEDGEMENTS

My years pursuing the Ph.D. at Georgia Tech have been, and will always be, one of the most precious and memorable experiences in my life. It is a journey full of joy and happiness, accompanied with frustrations, hardships, encouragement, friendship and love. Now I am finally approaching the end, and I know I am greatly indebted to many people for supporting me and accompanying me along this journey.

First of all, my sincere gratitude goes to my advisor Dr. Jian Luo. His abundant knowledge, scientific intuition and passion for research have set a high standard of an excellent researcher, an outstanding professor, and a professional engineer for me to follow in the years to come. It has always been helpful and challenging to learn from and to work with him. Every meeting and discussion with him made me feel full of hope and energy, and gave me a better prospect of where our research was heading for, especially when I was discouraged and self-doubted by difficulties and obstacles. This dissertation would never have been completed without his patient encouragement and constant guidance. My gratitude to him can never be over expressed for all the kind advice, the brother-like care and the many opportunities that he provided to stimulate my growth during the past six years.

My hearty thanks also go to my committee, Dr. Aris Georgakakos, Dr. Philip Roberts, Dr. Huaming Yao, and Dr. Guillermo Goldsztein, for taking the time to engage with my work. Their encouraging remarks and critical assessment of my thesis, and their insights and inspiring suggestions to my research will be invaluable for my future work.

A special thank is given to Dr. Jinsong Chen at Earth Sciences Division, Lawrence Berkeley National Lab. Dr. Chen offered me a wonderful opportunity of seven-month

internship to work for inverse modeling in Geophysics. His mathematical insights and technical advice were essential to the completion of the research project, which provides a great chance to enrich my research experience in Earth Sciences.

I would also like to thank all my colleagues in Environmental Fluid Mechanics and Water Resources research group and all my friends at Georgia Tech — Chunhui Lu, Yiming Chen, Chia-Jeng Chen, Feng Zhang, Aaron True, Fangzhou Liu, Martin Kistenmacher, Naiyu Wang, David Murphy, Yiwei Cheng, Alex Abdelnour. I am grateful to them for offering me technical knowledge, pleasant and stimulating discussions on sciences as well as on life, and all the help and friendship along the road. It has been enjoyable to discuss research ideas with them, to work with them, to share tough times and happy times with them. And there are so many other people who have helped me from the School of Civil and Environmental Engineering, and from Georgia Tech. My gratefulness cannot be fully expressed on this small page. Although their names are not listed here, I thank them all.

Finally and most importantly, my deepest gratitude and love go to my parents, Xiaohua Gong and Xiuming Zhang, who have cared, loved and believed in me for all these years, to my beloved husband, Shan Huang, who has been a constant source of support and encouragement for me, to my aunt's family here at Atlanta, Xiaohong Gong, Zhesheng Cheng, Dale and Eileen, for their long time accompany and unconditional love and support, and to my loving grandparents, whose uprightness of character, dedication to work and family, and intellectual curiosity have been, and will always be, a continual source of inspiration to me. Without them, my life would never be as pleasant and fulfilling. This dissertation is dedicated to them.

TABLE OF CONTENTS

LIST OF TABLES

LIST OF FIGURES

SUMMARY

Reactive transport models are essential tools for predicting contaminant fate and transport in the subsurface and for designing effective remediation strategies. Sound understanding of subsurface mixing in heterogeneous porous media is the key for the realistic modeling of reactive transport. This dissertation aims to investigate the extent of mixing and improve upscaling effective macroscopic models for mixing-controlled reactive transport in connected heterogeneous formations, which usually exhibit strongly anomalous transport behavior.

In this research, a novel approach is developed for an accurate geostatistical characterization of connected heterogeneous formations transformed from Gaussian random fields. Numerical experiments are conducted in such heterogeneous fields with different connectivity to investigate the performance of macroscopic mean transport models for simulating mixing-controlled reactive transport. Results show that good characterization of anomalous transport of a conservative tracer does not necessarily mean that the models may characterize mixing well and that, consequently, it is questionable that the models capable of characterizing anomalous transport behavior of a conservative tracer are appropriate for simulating mixing-controlled reactive transport. In connected heterogeneous fields with large hydraulic conductivity variances, macroscopic mean models ignoring concentration variations yield good prediction, while in fields with intermediate conductivity variances, the models must consider both the mean concentration and concentration variations, which are very difficult to evaluate both theoretically and experimentally.

An innovative and practical approach is developed by combining mean conservative and reactive breakthrough curves for estimating concentration variations, which

can be subsequently used by variance transport models for prediction. Furthermore, a new macroscopic framework based on the dual-permeability conceptualization is developed for describing both mean and concentration variation for mixing-controlled reactive transport. The developed approach and models are validated by numerical and laboratory visualization experiments. In particular, the new dual-permeability model demonstrates significant improvement for simulating mixing-controlled reactive transport in heterogeneous media with intermediate conductivity variances.

Overall, results, approaches and models from this dissertation advance the understanding of subsurface mixing in anomalous transport and significantly improve the predictive ability for modeling mixing-controlled reactive transport in connected heterogeneous media.

CHAPTER I

INTRODUCTION

1.1 Motivation and Background

Contaminants released from agriculture, industry, urban runoff/storm water, and municipal point sources have the potential to contaminate groundwater and soil. Modeling reactive transport is essential to the design of remediation strategies for contaminated groundwater and soil and to risk assessment. Mixing-controlled reactive transport with reaction rates limited by mixing processes represents a particular challenge in reactive transport modeling, especially in connected heterogeneous media where transport shows anomalous behavior. The present research is motivated by the following observations and challenges:

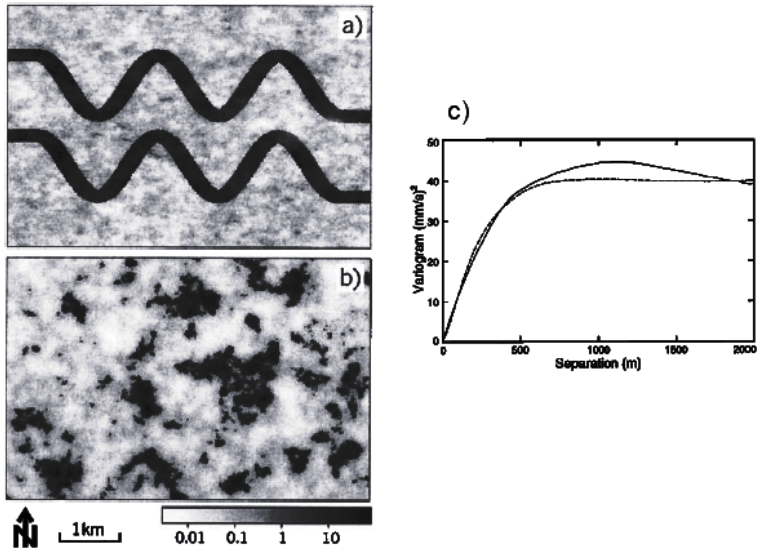

Figure 1.1: Two hypothetical hydraulic conductivity fields constructed by Western et al., [2001], with similar covariance functions but different degrees of connectivity. a) Connected conductivity pattern. b) Random conductivity pattern. c) Omnidirectional variograms for the aquifer conductivity patters in a) and b), respectively

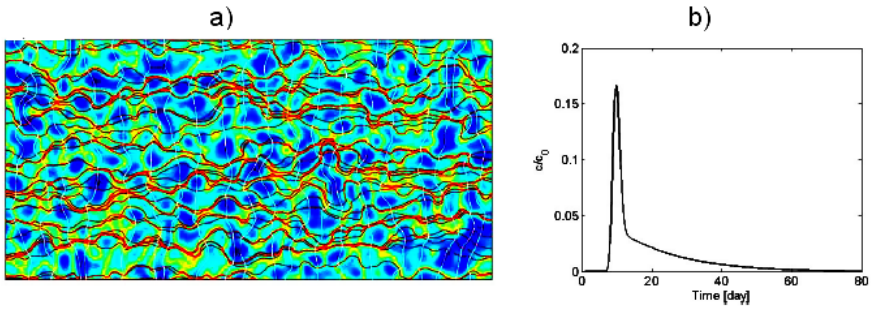

Figure 1.2: Connected heterogeneous medium with small-scale preferential flow paths and outflow breakthrough curves with enhanced tails. a) Connected conductivity field. b) Mean breakthrough curves

1. A major problem for subsurface contaminant transport is the identification of natural heterogeneity of the geologic formation. Conventional geostatistical framework for site characterization considers hydrogeological parameters and geophysical attributes as spatial random functions, and describes the heterogeneity by a distribution of conductivity values, combined with a covariance function (or a variogram function) of separation distance and the associated parameters such as means, variances, and integral lengths. These conventional spatial statistics are simple yet efficient in many applications such as characterization of large data sets, interpolation or extrapolation using kriging or cokriging methods, inverse modeling, Monte Carlo simulations, and stochastic analysis. However, it has been found in a number of field experiments that spatial statistic properties of second order (mean and covariance function) are not sufficient to characterize the matrix heterogeneity. For example, [*Western et al.*, 2001] constructed two hypothetical aquifers with similar covariance functions but have very different conductivity pattern, as shown in Figure 1.1. The connected features such as the thin bands of high-conductivity flow path in Figure 1.1a is of particular interest in practice because connected heterogeneous formations usually exhibit strongly anomalous transport behaviors. As

illustrated in Figure 1.2, the preferential flow in small-scale high-conductivity paths, slow flow in low-permeability zones, and mass exchange between them all contribute to the enhanced tailing for the outflow breakthrough curves. It remains unclear how macroscopic models work for mixing-controlled reactive transport in heterogeneous media with different connected features.

2. Anomalous transport behavior, which is often observed in groundwater transport in heterogeneous formations, refers to non-Gaussian types of behavior of the breakthrough curves that deviate from the classical Gaussian models of macroscopic advection-dispersion equation (ADE), which relies on the assumption that dispersion behaves macroscopically as a Fickian diffusive process. At both laboratory and field scales, various anomalous transport behaviors have been observed in heterogeneous formations, such as irregular, non-Gaussian shape of plume distribution, multimodal concentration breakthrough curve, or anomalously long concentration breakthrough curve tails. Since the macroscopic ADE model (that has a normal bell-shape concentration distribution with a growing width being proportional to square root of time) is unsuccessful for characterizing anomalous transport for a conservative tracer, different nonlocal methods have been developed to describe effective transport of anomalous conservative transport, such as continuous time random walks (CTRW), multirate mass transfer (MRMT), fractional advection-dispersion equations (fADE), and memory functions. Although all these models have been successful in reproducing observed conservative transport, it is unknown whether models representing conservative transport can be extended to reactive transport.

3. The prediction of contaminant fate and transport in the subsurface on the regional scale requires characterization of spatial variability and uncertainty of

hydraulic parameters, as well as reaction kinetics. Because complete characterization is usually unavailable, macroscopic models have been commonly used to describe flow and transport behavior on the large scale in an average sense without the details of pore-scale parameter fields. Major challenges in developing macroscopic transport models include development of good macroscopic frameworks that describe major flow and transport features and derivation of upscaled effective parameters that appropriately characterize hydraulic heterogeneity and reaction kinetics. Conventional techniques for collecting hydrogeologic data rely heavily on flux-averaged breakthrough curves in conservative tracer tests, which measure the average concentration in the outflow. These data are then used to fit physical transport parameters for calibrating macroscopic models. For predicting reactive transport, the common procedure is to couple the macroscopic transport models with chemical reaction kinetics determined in perfectly mixed laboratory experiments. In many cases, such macroscopic transport models can accurately describe the spreading of conservative solute. However, they may cause erroneous predication for mixing-controlled reactive transport because they ignore the micro-scale incomplete mixing, which may play a significant role in predicting mixing-controlled reaction rates.

1.2 Research Objectives

The research in this dissertation is aimed at improving the scientific understanding of subsurface mixing in anomalous transport and the predictive ability for modeling mixing-controlled reactive transport in connected heterogeneous media. To accomplish this objective, the specific research objectives are:

- Investigating geostatistics for characterizing connectivity properties in different heterogeneous fields.

- Improving the understanding of the behavior of mixing-controlled reactive transport in connected heterogeneous media and the performance of classical macroscopic transport models.

- Develop an innovative and practical approach that combines conservative and reactive breakthrough curves to estimate concentration variation.

- Develop a new macroscopic framework for describing both mean and concentration variation for mixing-controlled reactive transport.

The present work is conducted through numerical, analytical, and experimental approaches. Specifically, numerical experiments are conducted to simulate both conservative and reactive transports; analytical derivations are performed on the macroscopic transport framework development; and laboratory visualization experiment conducted by Dr. Harvey's research group at Massachusetts Institute of Technology will be analyzed and used to validate the developed models.

1.3 Outline of the Thesis

This thesis is organized into 7 chapters, including the introduction and the summary given later in the dissertation.

Chapter 2 reviews the mixing mechanisms for subsurface solute transports, and summarizes macroscopic models for anomalous transport in the literature. In addition, the importance of modeling concentration fluctuations is explained in this chapter.

Chapter 3 develops a novel numerical framework for an accurate geostatistical characterization of connected heterogeneous formations transformed from Gaussian random fields. And the two-cluster function of a two-cut indicator field is introduced to quantify connectivity properties that explain different degrees of visual connectivity.

Chapter 4 presents numerical test cases of mixing-controlled reactive transport with a bimolecular precipitation reaction at local equilibrium in heterogeneous domains with different degrees of connectivity, to examine the performance of macroscopic one-dimensional models.

Chapter 5 develops an innovative and practical approach for estimating concentration variation. Numerical experiments, as well as laboratory visualization experiments conducted by Dr. Harvey's group at Massachusetts Institute of Technology are analyzed and used to validate the developed approach.

Chapter 6 presents a new macroscopic modeling framework to upscale mixing-controlled reactive transport in heterogeneous media. The concentration variance behavior is emphasized. Numerical experiments are conducted and experimental data are examined to validate the developed model as well.

Finally, **Chapter 7** summarizes the major research findings and conclusions, and outlines future research needs.

CHAPTER II

LITERATURE REVIEW

This chapter reviews current upscaling models for subsurface reactive transports in heterogeneous fields. The review emphasizes current research focusing on mixing-controlled reactive transports, but general reactive transport models are also summarized to provide additional context. This review is aimed at achieving a general perspective on technical issues associated with spreading and mixing mechanisms for subsurface reactive transport, and with challenges in macroscopic modeling for mean and concentration variance.

2.1 Upscaling of Flow and Transport in Heterogeneous Media

Many processes in hydrology depend on the scale of observation. Typical examples of multiscale processes are turbulence, catchment hydrology, and flow and transport in porous media. With an extremely fine resolution on the conductivity field, numerical simulations of velocity field are capable to accurately capture the effects of spatial variability of the conductivity on the velocity field [*Ababou et al.*, 1988, 1989; *Bellin et al.*, 1992, 1994; *Bellin and Rubin*, 1996; *Dykaar and Kitanidis*, 1992a, b; *Hassan et al.*, 1998a, b; *Salandin and Fiorotto*, 1998;*Rubin*, 2003; *Cirpka*, 2006]. However, large-scale flow simulations can become computationally intensive since huge level of details are included, and the fully resolved heterogeneity will likely not be available at field site. On the other hand, in most cases we are only interested in the large-scale/regional transport properties, instead of the very details of the velocity and concentration distributions. Therefore, the so-called *upscaling* approaches, that describes flow and transport behaviors adequately on the large scale in an average

sense without the loss of important details, are needed.

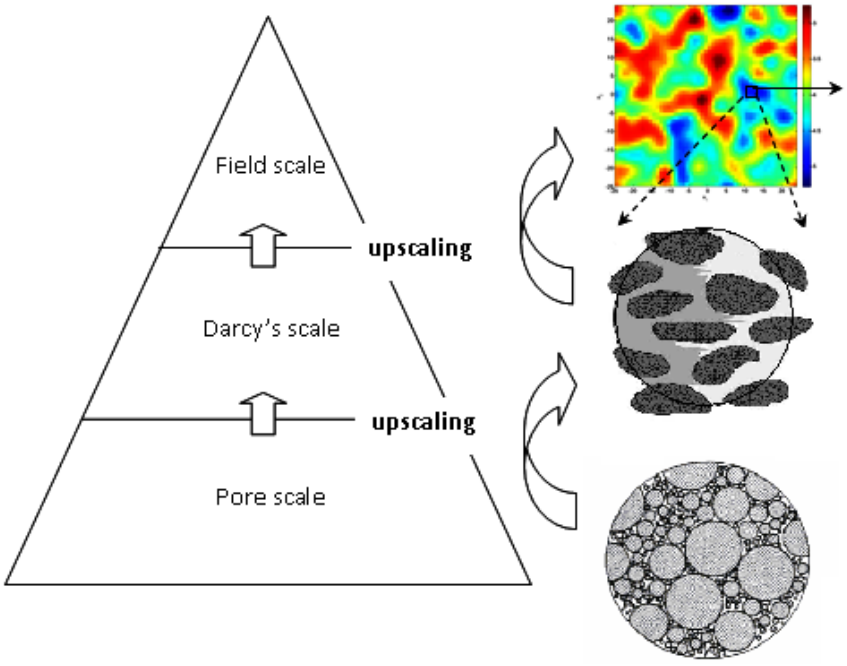

Figure 2.1: A representation of upscaling processes. The Darcy scale figure was given by *Ginn, et al.*, [2002], and the pore scale figure was given by *Bear*, [1972]

There are essentially two upscaling problems when developing an effective transport model for field application: one is from pore-scale to the Darcy's scale, and the other from the Darcy's scale to field scale, as shown in Figure 2.1, although other intermediate scales, such as bench scale, integral scale, pilot scale, may be defined [*Sturman et al.*, 1995]. The Darcy's scale serves as a bridge between the pore scale and the field scale and cannot be ignored because it is practically impossible to solve a field-scale problem directly based on pore-scale models. Even with the advancement of supercomputing techniques, it is impossible to identify the detailed pore-scale structures for a large domain. In addition, we may roughly estimate the spatial and temporal scales of flow and transport behaviors for these two upscaling problems: (1) consider pore size $\sim 1mm$ and molecular diffusion coefficient $\sim 10^{-9}$

m^2/s, then the transverse diffusive timescale is $\sim 10^3 s$ and the corresponding spatial scale is $\sim 1cm$ for an average flow velocity $1m/day$, (2) consider permeability correlation length $\sim 1m$, local-scale transverse dispersivity $\sim 1mm$ and average flow velocity $\sim 1m/day$, then the traverse dispersion timescale is $\sim 10^7 s$ and spatial scale $\sim 10^2 m$. Thus, for field-scale applications, the latter would be more important. This thesis focuses on the scale-up issues of mixing and reaction from the Darcy's scale to the field scale.

A common framework of upscaling is the stochastic one. In the stochastic framework, heterogeneities are modeled as stochastic, time-independent fields with given statistical properties. The characteristic large scale behavior then follows from appropriately defined averages over the ensemble of all possible aquifer realizations[*Dentz, et al.*, 2002]. In many cases, we characterize spatial fields by their statistical moments (the mean value, the variance and the spatial or temporal moments)[*Dagan*,1988]. The ensemble average can be evaluated by either numerical or analytical approaches. The numerical approach, which is also known as *Monte Carlo* simulations, relies on repeated random sampling to compute the results: we generate a large number of realizations, perform the simulation for each realization, and take the average over all of them [*Tompson and Gelhar* 1990; *Bellin et al.* 1992; *Chin and Wang* 1992]. On the other hand, analytical approaches are based on inferring the statistics of a dependent varying quantity (e.g., the mass flux of a solute) from those of the independent (e.g., the velocity field) [*Cirpka*, 2005], and both Lagrangian [*Dagan*, 1989] and Eulerian [*Gelhar*, 1993] frameworks have been well established in hydrogeology. The temporal behaviour of transport coefficients in a medium with spatial fluctuations in the conductivities was investigated by [*Dagan*, 1984, 1988, 1991] using a Lagrangian approach, neglecting the influence of the local dispersion [*Kitanidis*, 1988]. In Eulerian framework, the increase of macroscopic dispersion coefficients due to spatial fluctuations in the hydraulic conductivities for the case of a saturated aquifer has

been investigated by [*Gelhar and Axness*, 1983], which describes the transport processes on asymptotically large scales, while gives little information on the time scales necessary to reach this asymptotic situation. Both approaches described above have been generalized by various authors to include other kinds of heterogeneities [e.g., *Chrysikopoulos et al.*, 1990; *Bellin et al.*, 1993; *Miralles-Wilhelm and Gelhar*, 1996; etc].

The general frameworks described above provide a conceptual platform for upscaling flow and transport in heterogeneous fields. The scaled-up issues of mixing associated with reactive transport will be discussed next.

2.2 The Scale-up Issues of Mixing and Spreading

In heterogeneous porous media, the concepts of mixing and dilution should be distinguished from that of spreading. Spreading, which has been the subject of macrodispersion studies, is a macroscale phenomenon, which describes the spatial extent of the mean concentration field, primarily controlled by aquifer heterogeneities [*Gelhar and Axness*, 1983; *Dagan*, 1984; *Neuman et al.*, 1987; *Kitanidis*, 1994]. Hydraulic heterogeneity of the formation alone leads to a spatially varying specific-discharge field. As a result, a solute cloud introduced into the domain becomes increasingly irregular in shape with a constant concentration. The parts of the plume that are in high-velocity regions over a certain period of time are sheared off from the parts in low-velocity regions. As a consequence, the plume boundary, exhibiting sharp concentration gradients, increases in size. The amount of spreading experienced by a plume undergoing strictly advective transport in a heterogeneous domain depends on the size of the plume [e.g., *Kitanidis*, 1988]. At the limit of point-like injection, no spreading would occur at all, that is, the plume would remain a Dirac pulse [e.g., *Dentz et al.*, 2000]. In such a situation, the exact travel distance passed by the point-like plume would depend on the exact starting location, and the uncertainty of locating the plume

position could be expressed by macrodispersion expressions [e.g., *Fiori and Dagan*, 2000]. In other words, enhanced plume spreading in a heterogeneous porous medium does not necessarily imply it is being significantly diluted because the spreading is mainly caused by spatially varying advection which stretches the plume but does not dilute the solute mass.

Mixing implies that two species occupy the same spatial volume. For one species, mixing is equivalent to dilution, indicating the decay of peak concentrations or more uniformly distributed solute mass as it dissolves into a larger volume. The mechanisms that may create mixing include (1) hydrodynamic dispersive mixing, associated with fluctuations in transport velocity resulting in fingering and steep concentration gradients that are subsequently smoothed through local dispersion and molecular diffusion, (2) kinetic mass transfer, associated with nonequilibrium sorption and stagnant pore structures, (3) chromatographic mixing, caused by different mobility of compounds, and (4) hydrodynamic instabilities, as in variable-density flow when a heavier fluid overlays a lighter fluid. In this work, we are interested in the first two mechanisms because the last two processes are fast and reaction rates may not be limited by mixing.

The problem of incomplete mixing and species segregation may occur in any scale if the complete mixing scale of reaction to occur is inconsistent to the numerical discretization scale of flow and transport. For each upscaling problem in Figure 2.1, there are two scales: the support scale and the target scale. The general upscaling rule defines complete mixing at the support scale, evaluates incomplete mixing at the target scale, and eventually develops effective upscaled models for the target scale. For example, at the pore scale, the Navier-Stokes (NS) -based continuum is assumed complete mixing and molecular diffusion is considered as the primary mixing mechanism, and at the Darcy's scale, the extent of incomplete mixing is evaluated to upscale an effective pore-scale dispersion coefficient [e.g., *Tartakovsky et al.*, 2009].

Similarly, for upscaling an effective reactive transport model at field scale, incomplete mixing is evaluated based on the complete mixing assumption at the Darcy's scale, which may be described by the effective pore-scale dispersion upscaled from the pore scale [*Kapoor et al.*, 1997; *Gramling et al.*, 2002]. Thus, any transport behavior, including the anomalous transport behavior which is the focus of this dissertation, observed at the target scale may be caused by (1) similar behavior at the support scale; (2) the upscaling or averaging process, i.e., the integrated behavior of many support-scale behavior; and (3) both (1) and (2). In this research, we will not start from the pore-scale simulation, but assume complete mixing at small Darcy's scale ($\sim cm$ [*Zheng and Gorelick*, 2003]).

Dilution and mixing in heterogeneous aquifers are current topics of research in subsurface hydrology. A motivation for these studies has been to develop better methods for the evaluation of reactive transport controlled by the rate of mixing of the interacting compounds. A basic requirement for reactions to take place is the mixing of the reacting compounds. As long as the degradation process is not limited by slow reaction kinetics, the rate of mixing of the interacting compounds controls the rate of transformations. The implication of the upscaling approaches suggest that parameters derived by upscaling are not appropriate for the description of processes on the micro-scale. Therefore, it is not appropiate to apply the macrodispersion equation to problems in which micro-scale mixing is the limiting factor, such as mixing-controlled reactive transport discussed in this research, which will be explained next.

2.3 Mixing-Controlled Reactive Transport Models

2.3.1 Macroscopic Reactive Transport Models

Upscaling macroscopic reactive transport models is necessary for predicting contaminant fate and transport in heterogeneous subsurface because detailed characterization of spatial variability and uncertainty of hydraulic parameters is usually unavailable

at field sites. Macroscopic models of mean concentrations, usually calibrated by flux-averaged breakthrough curves of a conservative tracer and coupled with reaction kinetics determined in laboratory experiments, may inaccurately predict breakthrough curves of reactive species for mixing-controlled reactive transport because of the neglect of concentration variations at local scale, which may not be a problem for conservative transport focusing on mean concentrations but may play a significant role in evaluating effective reaction rates for nonlinear reactions limited by solute mixing [e.g., *Molz and Widdowson*, 1988; *MacQuarrie and Sudicky*, 1990; *Kitanidis*, 1994; *Kapoor et al.*, 1997; *Cirpka and Kitanidis*, 2000a; *Raje and Kapoor*, 2000; *Cirpka*, 2002; *Gramling et al.*, 2002; *Dentz and Carrera*, 2007; *Luo et al.*, 2008].

Since reactive transport is very sensitive to the nature of reactions [*Rubin*, 1983, *Willmann, et al.*, 2010], it is important to identify the type of reactions when extending upscaled effective macroscopic transport models to reactive transport. Reactions can be classified as linear or nonlinear, as controlled by kinetics (slow) or equilibrium (fast), as homogeneous (all reactants in the same phase) or heterogeneous, etc [*Willmann, et al.*, 2010]. *Selroos and Cvetkovic*, [1992]; *Bellin et al.*, [1993]; *Roth and Jury*, [1993]; *Rubin et al.*, [1997]; *Haggerty and Gorelick*, [1998]; *Lawrence et al.*, [2002]; *Berkowitz et al.*, [2008] investigated the heterogeneous sorption problems with emphasis on the spatial and/or temporal distribution of concentrations. [*Margolin et al.*, 2003] showed that effective transport in heterogeneous media under linear kinetic reactions occurring homogeneously throughout the domain can be represented by the same nonlocal model as conservative solutes. For equilibrium or nonlinear kinetic reactions, *Rezaei et al.* [2005] and *De Simoni et al.* [2005, 2007] showed that equilibrium reaction rates are controlled by mixing and depend on the species concentrations in a nonlinear way.

A particular challenge lies in predicting mixing-controlled nonlinear reactive transport, i.e., reaction is relatively faster than transport processes so that reaction rates

are limited by solute mixing. Examples of mixing-controlled reactive transport include bioreactive transport in steady state, and equivalent equilibrium reaction [*Cirpka et al.*, 2008], among others. While macroscopic models are fairly well understood and applicable for conservative transport, dilution and reactive mixing are still difficult to predict.

The common procedure for predicting mixing-controlled reactive transport in heterogeneous domains is to determine physical transport parameters by fitting model results to flux-averaged breakthrough curves of a conservative tracer, and to determine the reactive parameters in perfectly mixing laboratory experiments. However, such macroscopic models may inaccurately predict breakthrough curves for mixing-controlled reactive transport. As pointed out by [*Kitanidis*, 1994; *Kapoor et al.*, 1997; and *Ginn et al.*, 1995], among others, macrodispersion parameters describing the increase of the second central spatial moment of a conservative tracer cannot directly be used for the scale-up of reactive transport. Applying spreading-related macrodispersivities to problems of mixing-controlled reactive transports leads to an overestimation of mixing and reaction rates, and thus to erroneous mass balances [*MacQuarrie and Sudicky*, 1990; *Ginn et al.*, 1995; *Miralies-Wilhelm et al.*, 1997].

The key point of poor performance of macroscopic models in such cases is that the mean breakthrough curve alone does not provide information about concentration variations at local scale, which may not be a problem for conservative transport focusing on mean concentrations but may play a significant role in evaluating effective reaction rates for nonlinear reactions limited by solute mixing. Figure 2.2(right panel) shows that even a "perfect" macroscopic model, which may exactly reproduce the flux-averaged breakthrough curve of a conservative tracer (top-right subplot in Figure 2.2), may yield significant errors in predicting concentrations of reactive species (subplots of c_A, $c_B$and c_C in the right panel of Figure 2.2). The inconsistence

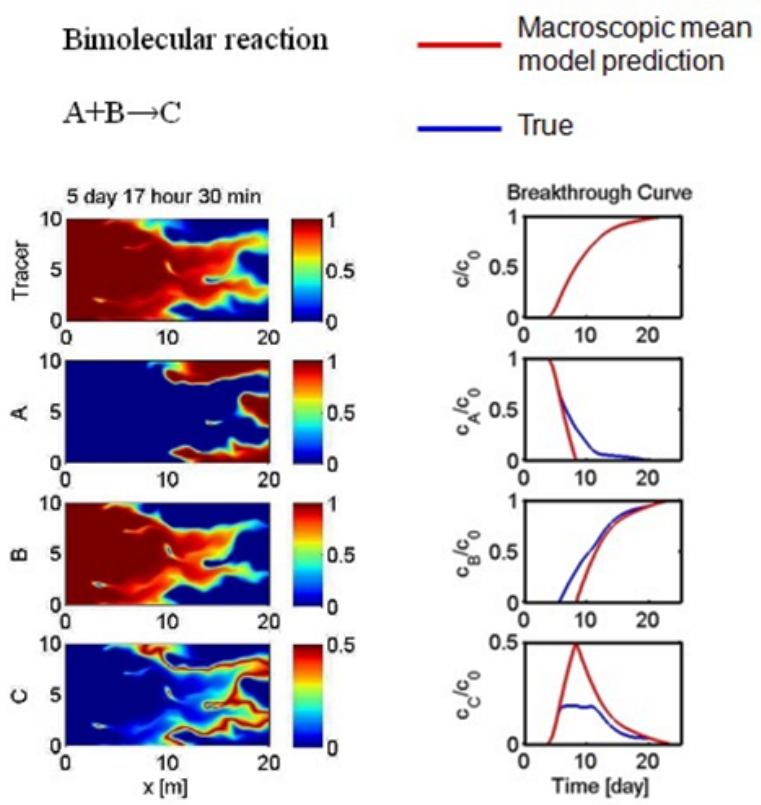

Figure 2.2: Conservative and reactive transports in a heterogeneous medium. Breakthrough curves are measured at the outflow boundary. Reaction is an instantaneous bimolecular reaction. A and B are reactive species, and C is the product

between macroscopic models assuming perfect mixing and the intrinsic solute segregation or incomplete mixing at local scale has become a research focus in stochastic hydrogeology in recent years [*Dentz et al.*, 2010]. Sound understanding of subsurface mixing in heterogeneous porous media is the key for the realistic modeling of reactive transport and is a precondition for assessing natural attenuation processes, designing nuclear waste disposal, and developing effective monitoring network and engineered remediation systems for contaminated sites. Existing methods of modeling the mixing-controlled reactive transport, relying upon the mixing ratio of conservative transport, include stream tube approach [*Cirpka and Kitanidis*, 2000a], framework of analyzing concentration fields[*Fiorotto and Caroni*, 2002, 2003; *Oates*, 2007], and

sampling techniques based on prior information of the breakthrough curve distribution [*Cirpka et al.*, 2008].

2.3.2 Anomalous Transport Behavior

Anomalous transport behavior, primarily characterized by deviations of the average breakthrough curve from Fickian behavior, has been observed in many heterogeneous formations [e.g., *Selroos and Cvetkovic*, 1992; *Hadermann and Heer*, 1996; *Berkowitz and Scher*, 1997, 1998; *Berkowitz et al.*, 2000; *Guswa and Freyberg*, 2000; *Harvey and Gorelick*, 2000; *Haggerty et al.*, 2001; *Zheng and Gorelick*, 2003]. Examples of anomalous transport behaviors include irregular, non-Gaussian shape of plume distribution or enhanced concentration breakthrough curve tails, among others. *Haggerty et al.*, [2000], among others, showed that anomalous transport behavior may provide important information for understanding slow mixing processes because extended tailing behavior usually indicates that some slow processes dominantly control transport at late times. Thus, anomalous transport behavior, particularly enhanced tailing, may serve as an indicator of slow mixing processes occurring in the subsurface and provide valuable information for calibrating appropriate transport models.

To describe anomalous transport behaviors, many sophisticated upscaling macroscopic models have been developed such as fractional macroscopic advective dispersive equation (fADE)[*Benson, et al.*, 2000], continuous-time random walk (CTRW) [*Berkowitz and Scher*, 1998; *Berkowitz et al.*, 2006], nonlocal models with kinetic mass transfer particularly multirate mass transfer(MRMT)[*Haggerty and Gorelick*, 1995; *Silva et al.*, 2009], among others [*Cushman and Ginn*, 2000; *Harvey and Gorelick*, 2000; *Liu et al.*, 2004, 2007; *Barlebo et al.*, 2004; *Zinn et al.*, 2004; *Carrera et al.*, 1998; *Salamon et al.*, 2007]. For conservative tracer transport, all these models are capable of giving fairly good predictions for describing anomalous behaviors, especially enhanced tailing behavior, since mean concentrations are the simulation

target, while reactive transport will still be difficult to predict, since both mean and spatial variability (i.e., concentration variation) should be accounted for describing mixing. *Luo and Cirpka*[2011] showed that only under specific conditions can these improved models be effective, such as in highly-heterogeneous media or nearly homogeneous media with low flux-averaged concentration variances, as reviewed in the next section.

2.3.3 A Recent Observation

A recent work by [*Luo and Cirpka*, 2011] presented numerical test cases of mixing-controlled reactive transport with a bimolecular precipitation reaction at local equilibrium in heterogeneous domains are investigated. The objective was to which extent concentration fluctuations within the solute flux could be neglected in the transfer from breakthrough curves of conservative to reactive compounds. From a strictly theoretical standpoint of view it is clear that neglecting such variations must lead to a mass-balance error, because the transfer from conservative to reactive compound concentrations is nonlinear. However, the studies of [*Edery et al.*, 2009] and [*Willmann et al.*, 2010] indicated good performance, despite the fact that their models could not account for concentration variations in the solute flux.

For the sake of completeness, we briefly describe the hydrogeological settings and the reactive transport in [*Luo and Cirpka*, 2011]: An elliptic inclusion setup was considered for the heterogeneity as shown in Figure 2.3a. An elliptical low-permeability inclusion is embedded in a rectangular two-dimensional homogeneous, isotropic domain. The hydraulic head is fixed at the left and right boundaries, whereas no flow crosses the top and bottom boundaries. The major and minor axes of the ellipse are half of the domain length and width, respectively. Table 2.1 summarizes the hydrogeological parameters used in the numerical case. Solute transport in this domain is essentially controlled by two dimensionless parameters:

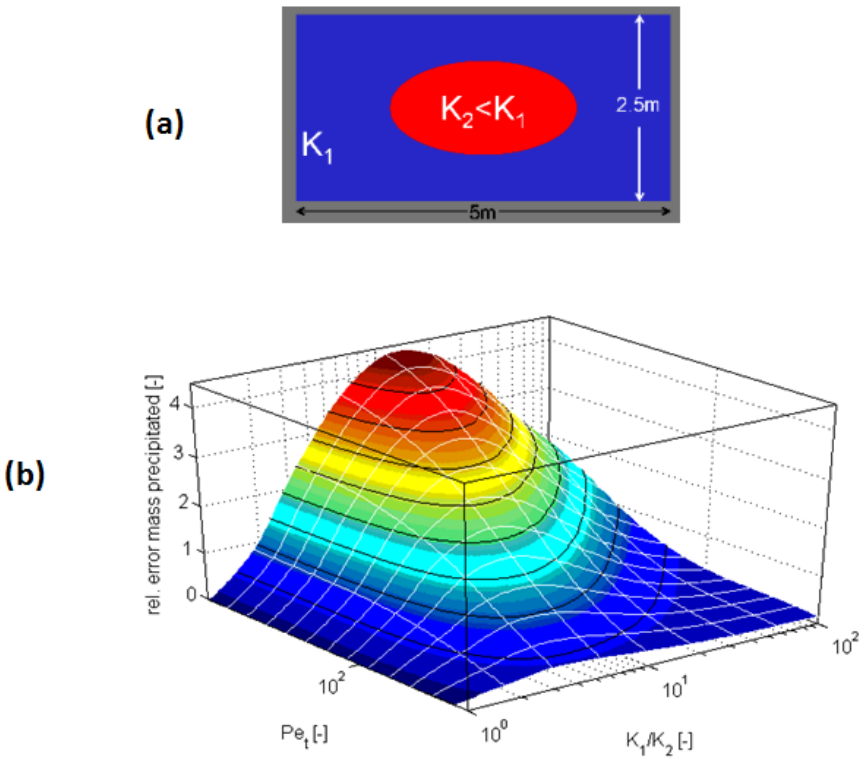

Figure 2.3: Investigation of performance of macroscopic models for predicting mixing-controlled reactive transport in an elliptical, low-permeability inclusion domain. (a) Elliptic Inclusion: The Domain; (b) Relative prediction errors in terms of total product mass

$$K_{rel} = \frac{K_1}{K_2} \tag{2.1}$$

$$Pe = \frac{\overline{v}b^2}{D_t L} \tag{2.2}$$

where K_1 and K_2 are the hydraulic conductivity in the inclusion and matrix, respectively, K_{rel} represents the hydraulic conductivity contrast, $\overline{v}$ is the effective mean velocity within the entire domain, b is the half width of the elliptical inclusion, L is the domain length, D_t is the transverse dispersion coefficient, and Pe is the transverse Péclet number.

Table 2.1: Hydrogeologic parameters for the hydrogeological setup with an elliptical, low-permeability inclusion

Parameter	Symbol	Values
Dimension of domain	$L \times W$	$5m \times 2.5m$
Dimension of elliptical inclusion	$2a \times 2b$	$2.5m \times 1.25m$
Discretization	$\triangle x \times \triangle y$	$0.005m \times 0.005m$
Hydraulic conductivity	K_1	$10^{-3}m/s$
Hydraulic conductivity	K_2	$10^{-5} \sim 10^{-3}m/s$
Mean hydraulic gradient	J	0.01
Effective porosity	θ	0.4
Longitudinal dispersivity	αt	$0.01m$
Transverse dispersion	D_t	$10^{-9} \sim 10^{-6}m^2/s$

And an **instantaneous bimolecular precipitation reaction** was used for numerical modeling and simulations. Assume advective-dispersive transport of compounds A, B and C with concentrations c_A, c_B, and c_C. Aqueous species (solutes) A and B react with each other, forming compound (mineral) C:

$$A + B \rightarrow C \downarrow \tag{2.3}$$

This reaction is assumed to be fast compared to typical transport times, so that it can be treated as in equilibrium. The concentrations of the aqueous species A and B satisfy:

$$c_A \cdot c_B = K_{eq} \tag{2.4}$$

where c_A and c_B are the molar concentrations of the reactive species A and B respectively, and K_{eq} is the chemical equilibrium constant. This reactive transport case can be solved completely relying upon the mixing ratio of conservative transport [*De Simoni et al.*, 2005, 2007]. In the numerical simulations, K_2 and D_t are varied so that K_{rel} ranges across three orders of magnitude ($10^0 \sim 10^2$) and Pe ranges across four orders of magnitude ($10^0 \sim 10^3$). For each combination of K_{rel} and Pe, the steady state flow field and the reactive transport were solved.

The results in [*Luo and Cirpka*, 2011] indicate largest errors in macroscopic one-dimensional models for intermediate conductivity contrasts and high Péclet numbers (Figure 2.3b). With respect to total and peak mass-balance errors, increasing the degree of heterogeneity beyond a critical value led to an improvement of the performance. The comparably good performance in highly heterogeneous cases can be attributed to: (1) small fractions of the water flux passing through low conductivity inclusions so that, while the fronts lag extremely behind in such inclusions, their contribution to the overall breakthrough curve is not that big; and (2) efficient mixing between water fluxes that have experienced low-conductivity zones and those that have not caused by transverse dispersion over short diffusion lengths within preferential flow zones downstream of inclusions. In media with intermediate hydraulic conductivity contrast, such models may still yield significant errors in predicting mixing-controlled reactive transport. The decisive point is that such models conceptualize a single concentration within the solute flux in the mobile domain. Therefore, they cannot account for any effects caused by concentration fluctuations within the flux. For example, the multirate mass transfer model can describe anomalous transport behavior by varying local memory functions for characterizing incomplete mixing in the immobile domains. However, for the flow flux leaving a domain, only the mobile contributions count. Thus, such models with a single flux mobile concentration are strictly impossible to account for variations within the flux, no matter whether reactions are considered in the immobile domains or not.

The importance of modeling concentration variation besides the mean concentration will be further illustrated in the next section.

2.3.4 Modeling Both Mean and Concentration Variation

In practical applications, macroscopic advective-dispersive-reactive models assume that mean concentrations are representative of the actual concentration values and

employ macrodispersion coefficients (large-time limit or scale dependent) for describing solute transport and reaction rates evaluated by mean concentrations and reaction parameters determined in completely-mixed laboratory experiments. For mixing-controlled reactive transport, however, uncertainties of reaction rates caused by concentration variations cannot be neglected. *Kapoor et al.*[1997] indicated that reaction kinetics of a kinetic bimolecular reaction evaluated by average concentrations may over-predict the transformation rate by neglecting the local-scale concentration covariance between reactive species introduced by transport processes. In nearly homogeneous porous media, *Raje and Kapoor* [2000] and *Gramling et al.* [2002] conducted instantaneous, irreversible bimolecular reactive transport experiments and demonstrated that reaction rates were overestimated by the macroscopic model with the transport parameters fitted from conservative tracer tests.

The schematic description of the conventional upscaling macroscopic models is shown in Figure 2.4 , for a conservative transport and a bimolecular reactive transport. The concentration and velocity covariance, $\overline{v_i' c'}$, is described by macrodispersion, while the concentration covariance, $\overline{c_1' c_2'}$, is neglected. Despite the importance in practice, concentration variations are very difficult to evaluate for a specific site. Theoretical approximations based on stochastic hydrogeology theory may not be valid to predict concentration variance at specific locations since they usually yield ensemble behavior only for weakly heterogeneous media. Also, a complete understanding of the geostatistical structure of the hydraulic conductivity field is required, which involves uncertainties in practice. On the other hand, experimental measurements for estimating concentration variance require a number of local-scale samples, which are expensive and challenging to realize even with the advancement of multilevel sampling techniques.

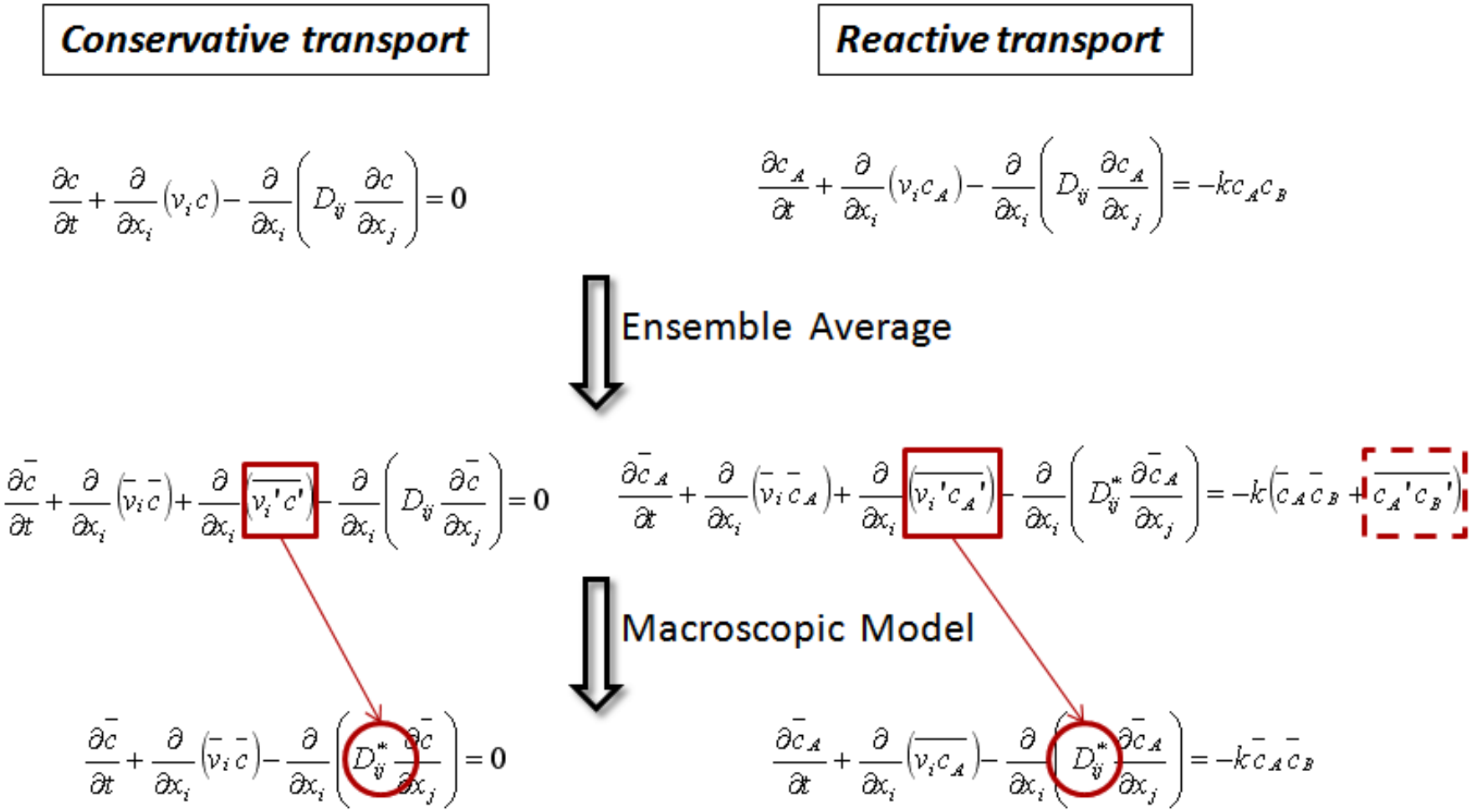

Figure 2.4: Schematic description of upscaling processes of conservative and reactive transports

To account for concentration variance besides mean concentration, two modeling frameworks have been developed. The first approach is to simulate concentration variance in addition to macroscopic mean models [*Kapoor et al.*, 1997]. The mean concentration is described by macroscopic transport models, and the variance is obtained by solving a variance transport equation involving an additional variance destruction coefficient, which is difficult to measure. For reactive transport, the conservative concentration statistics (mean and variance) may be incorporated into the nonlinear reaction kinetics by linearization to evaluate the species covariance matrix, which is subsequently used to correct the reaction rate [*Oates*, 2007]. It has been shown that the probability density function of concentration of a conservative tracer in a randomly heterogeneous medium can be approximated by a beta distribution, which shows bimodal behavior for cases with high coefficient of variation and resembles a Gaussian distribution in low-variance cases [*Fiorotto and Caroni*, 2002, 2003]. Thus, it is also possible to evaluate concentration distributions for reactive species by sampling the beta distribution given the relationship between conservative and reactive components [*Cirpka et al.*, 2008]. Full probability distributions for conservative transport were also recently reported [*Schwede,et al.*, 2008.]. The second modeling framework is based on the effective mixing concept and multiscale measurements. In the analysis of point-like observations of solute breakthrough, longitudinal dispersion does not alter the mean breakthrough time at any location, whereas transverse dispersion balances differences of mean breakthrough time between adjacent streamtubes in heterogeneous formations. Both processes lead to wider local breakthrough curves. Thus, a particular set of point-like measured breakthrough curves within an observation plane may be interpreted as caused by transport with transverse dispersion in a highly variable velocity field or by transport with enhanced longitudinal dispersion rather than transverse exchange, but in a less variable velocity field. This ambiguity

is used in the advective-dispersive streamtube (ADS) approach within an Eulerian-Lagrangian framework [*Cirpka and Kitanidis*, 2000a, b; *Ginn*, 2001; *Ginn et al.*, 2001; *Cirpka*, 2002; *Janssen et al.,* 2006; *Luo and Cirpka*, 2008]. The essence of this approach is to characterize the "right" mixing and "right" advection. The dispersion of the mean concentration breakthrough curve or macrodisperion is the summation of the mean dispersion of local-scale breakthrough curves and the variance of the mean of local breakthrough curves (also referred as the two-particle covariance [*Fiori and Dagan*, 2000; *Pannone and Kitanidis*, 2004]). The "right" mixing is the mean dispersion of local-scale measurements, while the variance of the mean describing the advection variations should not be included for evaluating mixing. The "right" advection is then described by an advective travel-time distribution. Integration of all local concentration breakthrough curves over the entire travel-time distribution yields the mean concentration breakthrough curve at the outflow boundary. *Cirpka* [2002] studied a bimolecular reactive transport case, in which the original reaction terms were maintained, i.e., concentration covariance was not included in the reaction rate, while effective heterogeneity induced mixing was characterized by the effective dispersion tensor [*Dentz et al.*, 2000].

Both numerical and experimental work showed good applicability of these two modeling frameworks [*Cirpka*, 2002; *Janssen et al.*, 2006; *Oates*, 2007; *Cirpka et al.*, 2008]. The essential difference between them is that the first one aims to evaluate effective reaction rates by explicitly accounting for the concentration covariance or the entire distribution, while the latter creates solute segregation by a number of non-interacting streamtubes. The first approach may become complicated for nonlinear, heterogeneous reactions involving many species and different phases because of the challenges in evaluating the covariance matrix [*Miralles-Wilhelm et al.*, 1997]. The latter is more efficient for simulating multi-species reactive transport given the "right" advective travel-time distribution and the effective mixing parameters because within

each streamtube it is a classical one-dimensional transport problem. However, it is only applicable at locations where both point-scale and integral-scale measurements are available, and is difficult to make predictions at locations without multiscale measurements because it is challenging to predict apparent "right" mixing parameters and "right" advective travel-time distributions [*Luo and Cirpka*, 2008].

2.4 Connected Heterogeneous Fields

Connected heterogeneous fields and random heterogeneous fields may share similar geostatistical structures in terms of spatial distributions of hydraulic conductivity [*Zinn and Harvey*, 2003; *Knudby and Carrera*, 2005], but they exhibit different transport behavior, thereby excluding the effectiveness of traditional macrodispersion theory for upscaling effective macroscopic models [*Zinn and Harvey*, 2003; *Fiori et al.*, 2010].

In connected heterogeneous fields, very different flow and transport behaviors can occur even though the conductivity fields have nearly identical lognormal univariate conductivity distributions and nearly identical isotropic spatial covariance functions (Figure 1.1) [*Western et al.*, [2001]; *Zinn and Harvey*, 2003]. Therefore, the traditional macrodispersion theory is no longer effective for upscaling effective macroscopic models. In fact, it has been proven that advection-macrodispersion transport models (a normal bell shape with width growing with the square root of time) fail to characterize anomalous transport behavior, and kinetic mass transfer (particularly multirate mass transfer), non-Fickian or fractional dispersion, continuous time random walk, or more detailed hydraulic conductivity heterogeneities must be incorporated.

There are different patterns for connected heterogeneous fields in the sense that high- or low- conductivity structures are connected (Figure 2.5). In practice, connected fields can be generated through a transformation of the multigaussian field. In this research, we follow the methods by [*Zinn and Harvey*, 2003] , in four steps:

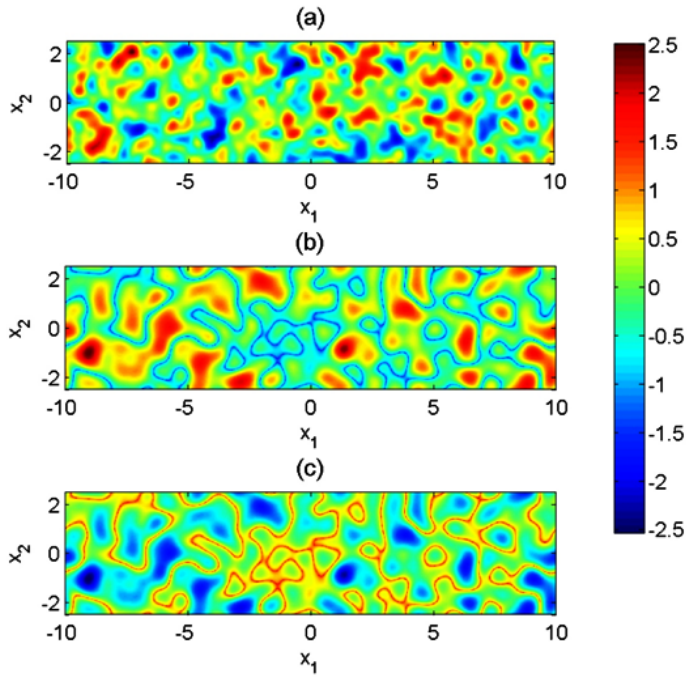

Figure 2.5: Generation of a connected hydraulic conductivity field from a multi-Gaussian field. (a) multi-Gaussian field; (b) low-conductivity structures are connected; c) high-conductivity structures are connected

1. The absolute value of the multigaussian field (zero-mean, unit-variate, Figure 2.5a) is calculated. this transform shifts extreme values to become high values, and values originally close to the mean become low values.

2. The histogram of the values in the field is converted back to a univariate Gaussian distribution by mapping the CDF (cumulative distribution function) value at each point to a standard normal CDF. This transformation can be written explicitly as:

$$Y' = \sqrt{2}\text{erf}^{-1}\left(2\text{erf}\left(\frac{|Y|}{\sqrt{2}}\right) - 1\right) \tag{2.5}$$

where K are the field conductivities, Y' are the transformed values of $\ln(K)$ and Y are the original values. This creates a field in which the extreme low values are connected and the high values form isolated blobs, e.g., the field shown in Figure 2.5b.

3. Increase the block size of the field so that the integral scale matched that of the original multigaussian field.

4. The connected field (Figure 2.5c) is then generated from the low-conductivity connected field by reflecting the values of the low-connected field around the mean, so connected patterns of low conductivity become connected flow paths of high conductivity.

Flow and transport in the connected field has many of the characteristics that are attributed to conductivity fields with layering, bimodal histograms, or large integral scales. However, the connected field is isotropic, univariate lognormal, and has an integral scale much smaller than the domain length. The connected field has behaviors similar to a layered field because the high-conductivity regions form contiguous preferential channels for flow. It also may reproduce some of the behavior of nonstationary fields (i.e., field with integral scales larger than the domain size) because the high-conductivity structures span the entire domain. Finally, the connected field can reproduce anomalous transport behaviors, such as nonequilibrium mass transfer, that are often attributed to fields with bimodal distributions, such as low conductivity blobs embedded in a matrix of uniformly higher conductivity. This is because the connected field also creates regions of low velocity embedded in channels of high velocity, even though the univariate distribution is Gaussian, which is unimodal.

Investigations of mixing-controlled reactive transport in connected heterogeneous domains are proposed in this research, which usually exhibit strongly anomalous transport behavior (Figure 1.2) for a conservative tracer as a result of preferential flow in small-scale high-conductivity paths, slow flow in low-permeability zones, and mass exchange between them.

2.5 Closure

In general, macroscopic models of mean concentrations can provide accurate prediction for mixing-controlled reactive transport only when concentration variations are negligible compared with mean concentrations or for linear reactions. Sophisticated models have been developed to improve the predictive ability of macroscopic mean models for equilibrium and kinetic reactions. However, the underlying implication of perfect mixing for macroscopic models has been a limitation for their applications in mixing-controlled reactive transport, where micro-scale mixing is the limiting factor.

In cases where concentration fluctuations cannot be neglected, both mean and concentration variances should be evaluated in order to transfer information from conservative-tracer data to the transport of reactive compounds when making predictions about reactive transport. In particular, mixing-controlled reactive transport such as equilibrium and nonlinear kinetic reactions are of general interest.

Beside characteristics of flow and solute transport, the natural heterogeneity of the porous media is also an essential factor in the prediction of contaminant fate and transport in subsurface. Connectivity properties are especially important for nonlinear reactive processes, where the flow can develop a channeling behavior. The difficulty lies in evaluating the connectivity, since second order spatial statistical properties are often not sufficient to characterize the field heterogeneity in an appropriate manner. In addition, connected heterogeneous domains usually exhibit strongly anomalous transport behavior, especially enhanced tailing, which may serve as an indicator of mixing processes occurring in the subsurface.

CHAPTER III

GEOSTATISTICAL CHARACTERISTICS OF CONNECTED HETEROGENEOUS FIELDS

Part of the material in this Chapter was recently published by Water Resources Research (Gong, R., Haslauer, C., Chen, Y., Luo, J., 2013, Analytical relationship between Gaussian and transformed-Gaussian spatially distributed fields, Water Resour. Res., 49, 1735-1740, doi: 10.1002/wrcr.20143.)

3.1 Introduction

The spatial dependence structure of naturally occurring parameters, such as hydraulic conductivity (logarithm of hydraulic conductivity values), can be characterized by a multivariate Gaussian distribution with a covariance or variogram function of separation distance. Random fields generated by such statistical approximations based on two-point correlations show a high connectivity of intermediate values [e.g., *Journel and Alabert*, 1990; *Journel and Deutsch*, 1993; *Zinn and Harvey*, 2003]. The spatial structure of hydraulic conductivity influences the velocity field, which in turn influences dependent parameters, such as the spreading behavior of a solute plume. In recent years, a number of studies have demonstrated that flow and transport in heterogeneous fields with preferential flow paths of connected high hydraulic conductivities, referred to connected fields, may exhibit significantly different behavior from that in disconnected heterogeneous fields [e.g., *Fogg*, 1986; *Silliman and Wright*, 1988; *Wen and Gomez-Hernandez*, 1997; *Tidwell and Wilson*, 1999; *Labolle and Fogg*, 2001; *Zinn and Harvey*, 2003; *Zinn et al.*, 2004; *Liu et al.,* 2004, 2007; *Knudby and Carrera*, 2005; *Willmann et al.*, 2008; *Luo and Cirpka*, 2011]. Particularly, connected

high-conductivity paths may lead to early arrival times of contaminant plumes and enhanced tailing behavior due to kinetic mass transfer between fast and slow flow zones. Such anomalous behavior may not be described by classical advection-dispersion models and macrodispersion theory [e.g., *Zinn and Harvey*, 2003; *Liu et al.*, 2004]. The effects of non-Gaussian dependence on macrodispersion based on the Borden data-set have been quantified by *Haslauer et al.* [2012].

Generation of spatial fields that mimic the spatial dependence structure as encountered in nature as closely as possible is important to improve understanding of solute transport in the subsurface. Available approaches for generating connected random fields include the multiple-point geostatistical method with a training image [e.g., *Strebelle*, 2002; *Hu and Chugunova*, 2008], the reorganization method of random fields [*Knudby and Carrera*, 2005], the self-avoiding invasion percolation method [*Stark*, 1991], the sequential indicator simulation method and the simulated annealing method for generating non-Gaussian random fields [see the review by *Gomez-Hernandez and Wen*, 1998], the absolute-value transformation of multivariate Gaussian fields [*Zinn and Harvey*, 2003], and copulas [*Bardossy and Li*, 2008]. Among these approaches, the method proposed by *Zinn and Harvey* [2003] offers a simple approach to generate a spatial dependence structure with different connectivity that is non-Gaussian, but based on a multivariate normal spatial field given two-point spatial correlations. It has been used to investigate flow and transport behavior in heterogeneous fields with a constant spatial covariance or variogram function but with different connectivity [e.g., *Zinn and Harvey*, 2003; *Neuweiler and Cirpka*, 2005; *Knudby and Carrera*, 2005, 2006; *Willmann et al.*, 2008].

The absolute-value transformation defines a new variable by the normal score transform of the absolute value of the original random variable [*Zinn and Harvey*, 2003]:

$$Y'(\mathbf{x}) = -\sqrt{2}\text{erf}^{-1}\left(2\text{erf}\left(\frac{|Y(\mathbf{x})|}{\sqrt{2}}\right) - 1\right) \tag{3.1}$$

where Y is an autocorrelated Gaussian random field with zero mean and variance of unity, $\mathbf{x}$ is the spatial location, and Y' is the transformed random field with connected high conductivities ($-Y'$ is a disconnected field with connected low conductivities). To maintain the zero mean and unitary variance for individual realizations, *Neuweiler and Cirpka* [2005] included a variance term in Eq. (3.1) to correct the variance deviation; and *Knudby and Carrera* [2005] introduced one more step of normal score transform to assure a standard Gaussian distribution of the underlying random field. Linear transformation of Y' can then be applied to generate random fields with non-zero mean and non-unitary variance. Connectivity of the transformed field may be characterized by the number of connected clusters and the two-point cluster function [*Neuweiler and Cirpka*, 2005; *Renard and Allard*, 2011]. Spatial statistical properties of absolute-value transformed variables are different from the original multivariate Gaussian variables. The transformed variable, by construction, is univariate normally distributed with zero mean and unitary variance, which is necessary but not sufficient for the transformed random field to be multivariate normal. The spatial structure of the underlying multivariate Gaussian field is different from the spatial structure of the transformed field, such as the shorter correlation length of the transformed field than that of the underlying Gaussian field. An example of transformed Gaussian field has been shown in Figure 2.5. Y can also be an autocorrelated exponential random field, and Figure 3.1 gives an example of transformed exponential field.

The issue remaining unclear about such transformation is how exactly the spatial correlation changes for the transformed field compared to the underlying Gaussian random field. *Zinn and Harvey* [2003] presented theoretical calculation for the correlation length of the absolute value of the original random field and found a scaling

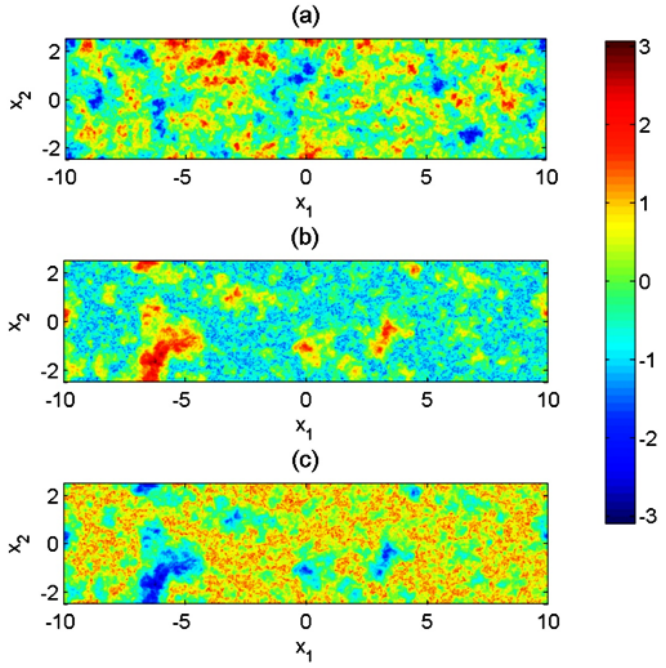

Figure 3.1: Generation of a connected hydraulic conductivity field from an exponential field. (a) exponential field; (b) low-conductivity structures are connected; (c) high-conductivity structures are connected

factor of 1.86 for the isotropic Gaussian covariance function. However, this calculation was valid for $|Y(\mathbf{x})|$, not for the final generated field, $Y'(\mathbf{x})$. *Neuweiler and Cirpka* [2005] found a scaling factor of 1.6 based on Monte Carlo simulations of 10,000 two-dimensional realizations. The common procedure is to first generate two or three-dimensional Gaussian random fields, conduct oriented covariance or variogram analysis for each transformed realization, and then analyze the mean covariance or variogram. *Neuweiler and Cirpka* [2005] analyzed the change of correlation lengths based on 10,000 two-dimensional random fields with 256×256 cells for an isotropic Gaussian covariance model, in which one point was fixed at the domain center. Thus, the actual amount of samples for each spatial distance (from the center to neighboring cells) is 40,000. Such a sampling procedure is computationally demanding for a large number of multi-dimensional realizations. This note aims to provide an accurate estimation of the spatial dependence structure of the underlying

Gaussian structure and the transformed structure, as well as a mapping between any two structures. The type of transformation is arbitrary. Such information is critical for generating connected random fields with predefined spatial correlations and for conducting stochastic analysis of flow and transport in connected random fields.

3.2 Method

Our method to obtain an accurate estimation of the spatial correlation of transformed fields consists of two simple steps: (1) determining a unique mapping of the correlation coefficients of the original multi-Gaussian fields to the transformed correlation coefficients; and (2) mapping the correlation to spatial distance. The method is not limited to the absolute-value transformation, but is applicable to any transformation function, $Y'=g(Y)$.

To establish the relationship between the correlations of transformed random variables and underlying Gaussian random variables, it is sufficient to focus on the joint distribution of two random variables instead of working on multi-dimensional random fields. The standard joint-Gaussian distribution with zero mean and variance of unity for two random variables is described by:

$$f_{Y_1,Y_2}=\frac{1}{2\pi\sqrt{1-\rho^2}}e^{-\frac{1}{2(1-\rho^2)}\left(Y_1^2+Y_2^2-2\rho Y_1 Y_2\right)} \tag{3.2}$$

where ρ is the correlation between Y_1 and Y_2. The correlation of transformed variables, Y_1' and Y_2', can be evaluated by either working on the correlation definition or sampling the joint distribution. For a specified correlation, joint samples of Y_1 and Y_2 can be generated based on the well-known method of Cholesky decomposition. By transforming Y_1 and Y_2 to Y_1' and Y_2', we can then evaluate the new correlation. Discretizing ρ from -1 to 1 and repeating the sampling for each ρ, one can obtain the correlation of transformed variables, ρ', as a function of the original correlation, ρ.

Figure 3.2 shows ρ' as a function of ρ for the absolute-value transform described

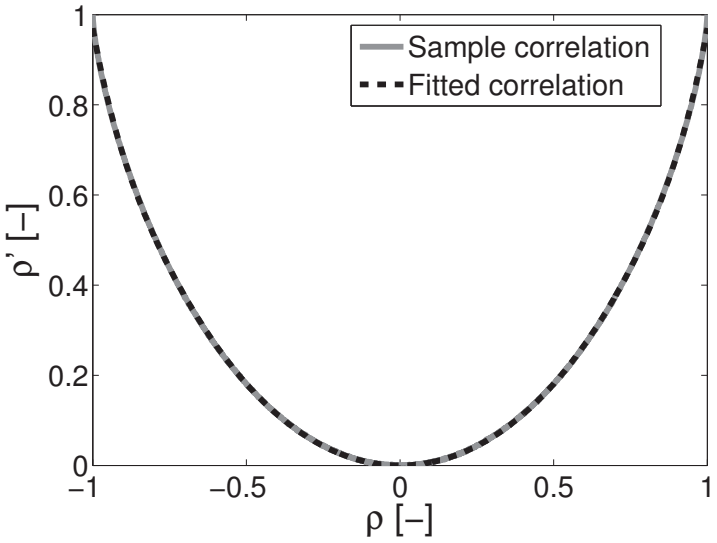

Figure 3.2: Relation between the correlations of an underlying standard normal bivariate distribution, ρ, and its absolute value transformed field, ρ'

by Eq. (3.1). For uncorrelated random variables, the transformed variables remain uncorrelated; and for linearly correlated variables, the transformed variables are positively linearly correlated. A polynomial function with only even contributions can be used to fit ρ':

$$\rho'(\rho) = 0.6559\rho^{10} - 0.8430\rho^8 + 0.3538\rho^6 + 0.1215\rho^4 + 0.6821\rho^2 \tag{3.3}$$

which yields zero for originally uncorrelated variables, and 0.97 for originally linearly correlated variables. The number of terms in the polynomial can be varied to decrease or increase fitting quality.

In geostatistics, various geostatistical parameterizations are available for describing the two-point correlation as a function of spatial distance. If the transformation, such as the absolute-value transformation, does not change the spatial distance between two points, the new correlation of transformed variables, ρ', is constant for a given ρ regardless of the type of geostatistical parameterization. Thus, one can evaluate the spatial correlation of transformed random fields simply by mapping the correlations to corresponding spatial distances using Figure 3.2 or substituting it into Eq. (3.3). For example, for a random field with an isotropic Gaussian covariance function, the correlation of the transformed field can be approximated by:

$$\rho'(h) = 0.6559\rho_G^{10} - 0.8430\rho_G^8 + 0.3538\rho_G^6 + 0.1215\rho_G^4 + 0.6821\rho_G^2 \tag{3.4}$$

where

$$\rho_G(h) = \exp\left(-\frac{h^2}{l^2}\right) \tag{3.5}$$

and l is the correlation length.

Figure 3.3 illustrates the simple mapping procedure: calculating the correlation for a specified distance (Figure 3.3a) and then determining the new correlation for the

transformed field according to the identified relationship in Figure 3.2 (Figure 3.3b). Figure 3.2 provides an accurate estimation of the transformed correlation because of the fine discretization, and Eq. (3.3) provides an easy and fast way to approximate the correlation.

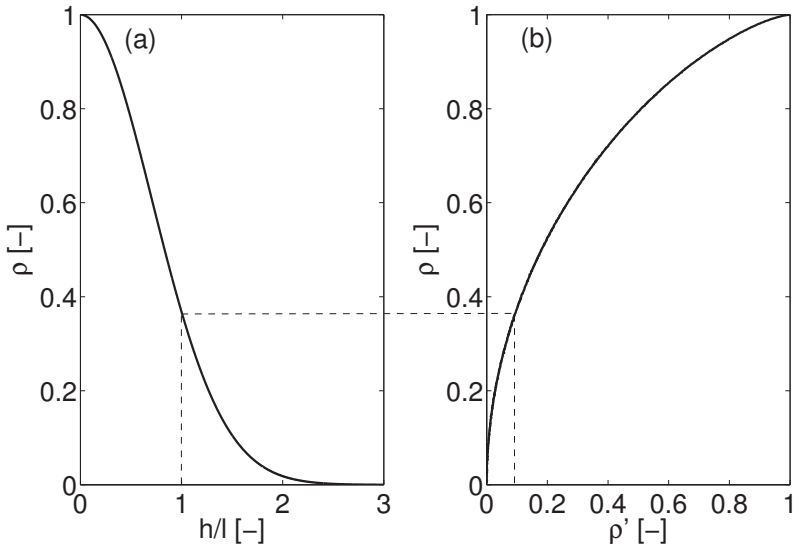

Figure 3.3: Quantile-quantile transformation to evaluate the correlation of the transformed field based on the spatial structure of the underlying field. (a) the original covariance model as a function of distance; and (b) mapping according to the correlation relationship

Figure 3.4 further illustrates the mapping between two different spatial correlation functions, ρ_1 and ρ_2. For a given correlation, $\rho_1 = \rho_2$, Figure 3.4a and 3.4b show the different spatial distance for the two spatial correlation functions. From Figure 3.4a to 3.4c, ρ_1' for the transformed field is obtained at the spatial distance determined in Figure 3.4a. Combining $\rho_2' = \rho_1'$ and the spatial distance determined in Figure 3.4b yields the correlation ρ_2' (Figure 3.4d) as a function of the spatial distance.

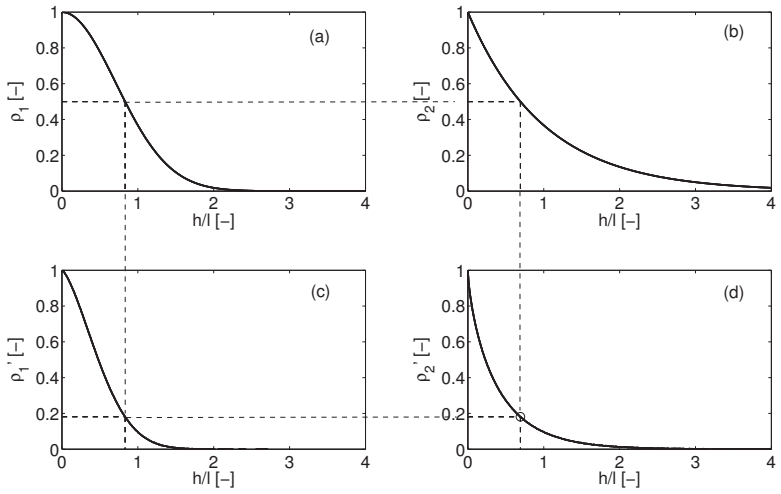

Figure 3.4: Mapping between two geostatistical correlation models. (a) the original correlation for model 1; (b) the original correlation for model 2; (c) the transformed correlation for model 1; (d) the transformed correlation for model 2

3.3 Results and Discussion

3.3.1 Distribution of Transformed Data

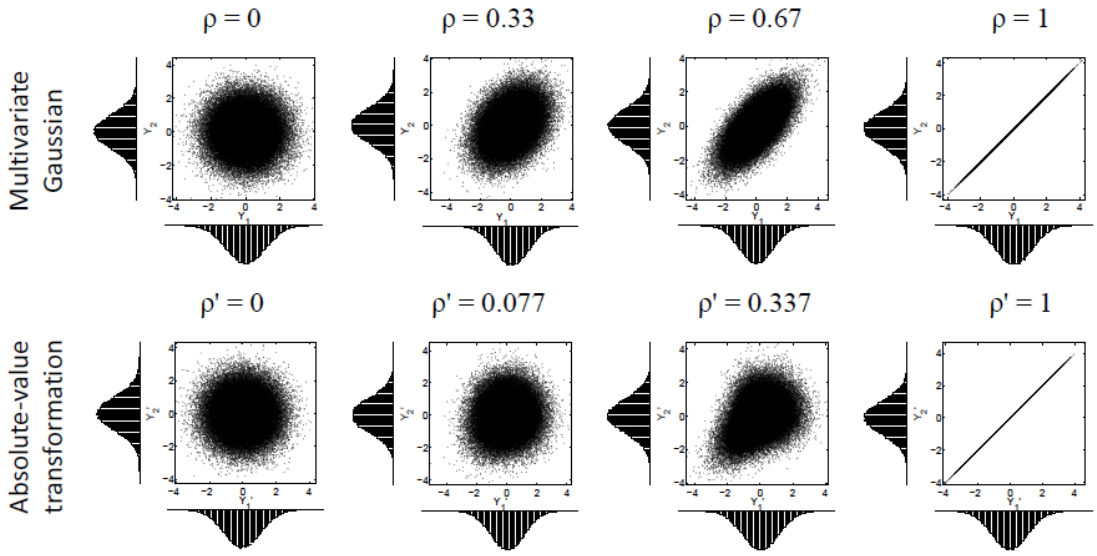

Figure 3.5: Scattered sampling points and marginal histograms before and after the absolute-value transformation

Figure 3.5 shows scattered sampling points and marginal histograms for absolute-value transformation of joint-Gaussian distributions with different correlations. For the absolute-value transformation, only if $\rho = 0$ or $\rho = \pm 1$ the transformed distribution is joint-Gaussian due to the normal score transform. In geostatistics, the first condition represents the case when the two points are far enough separated such that they are essentially uncorrelated and independent, and the second condition represents essentially a single point. For any two different points with short separation distances compared to the correlation length, the transformed data are not multivariate Gaussian, although both marginal distributions are Gaussian.

3.3.2 Correlation Changes for Specific Covariance Models

Figure 3.6 shows the isotropic correlation functions of transformed fields by the absolute-value transformation for Gaussian and exponential covariance models. Any

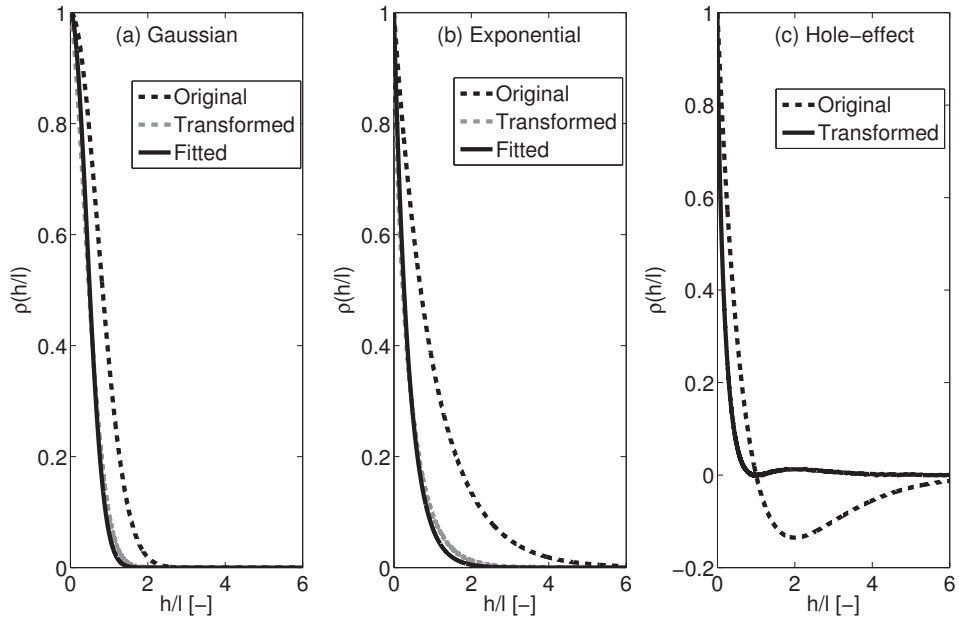

Figure 3.6: Correlations of the underlying and transformed fields for different covariance models. Transformed correlations are fitted by the same type of covariance functions for the Gaussian and exponential models

other commonly used covariance models such as the spherical or matern models can be evaluated. Eq. (3.3) shows that the common covariance model types, such as Gaussian and exponential models, may be changed by the transformation. If the same types of covariance models are used to fit the transformed correlations [*Zinn and Harvey*, 2003; *Neuweiler and Cirpka*, 2005], the original correlation lengths are 1.67 and 2.64 times of the transformed one for the Gaussian and exponential model, respectively. This result implies that one needs to scale up the cell size by 1.67 and 2.64 for connected fields with Gaussian and exponential models in order to maintain the same correlation lengths or to generate Gaussian random fields with larger

correlation lengths for transformation. For example, to generate a connected field with a correlation length of 3 cells for the Gaussian model, one needs to generate a multivariate Gaussian field with a correlation length of 5 cells.

3.3.3 Effect of Anisotropy and Orientation

The mapping method using Figure 3.2 and Eq. (3.3) can be applied to evaluate multi-dimensional anisotropic covariance models. Because the transformation only changes the correlation values and does not change the spatial separation distance, the anisotropic ratio and orientation remain constant. That is, the change ratios of correlation lengths at different directions between underlying and transformed anisotropic fields are identical to the change ratio for isotropic fields, indicating that it is sufficient to investigate the correlation change in one dimension. Thus, to generate anisotropic connected fields, one only needs to apply the absolute-value transform to an isotropic Gaussian field and simply scale the cell size according to the anisotropic ratio.

3.3.4 Inverse Mapping

Scaling the cell sizes of transformed fields according to the correlation length change ratio, as discussed in section 3.2, was used to generate connected fields with similar correlation functions as the underlying Gaussian fields [*Zinn and Harvey*, 2003; *Neuweiler and Cirpka*, 2005]. This method is based on the assumption that the covariance model type is not changed by the transformation, which is not accurate as indicated by Eq. (3.3). In our approach, the inverse mapping of Figures 3.3 and 3.4 or Eq. (3.3) can yield an accurate estimation of the correlation function required for the underlying Gaussian field. Thus, to generate a connected field with a given correlation function, one may first determine the required correlation function, generate the underlying Gaussian field accordingly, and then apply the absolute-value transformation.

3.3.5 Hole-effect Correlation

Non-monotonic correlations are known as the hole-effect structures, often used to represent a dependence form of pseudo-periodicity [*Journel and Huijbregts*, 1978]. Figure 3.2 shows that the negative correlation becomes positive after the absolute-value transformation. Thus, the anti-correlation in a random field with hole-effect correlations cannot be maintained by the absolute-value transformation. In addition, the non-monotonic behavior of hole-effect correlations will be maintained because of the symmetric, monotonic relationship about zero correlation between the original and transformed correlations. Figure 3.6c shows a hole-effect correlation and its transformed correlation. It clearly shows that the transformed correlation structure cannot be described by the original model.

3.3.6 Conclusion

This note investigates the effects of a transformation on the spatial dependence structure of spatially distributed random fields. An efficient method is developed to fast and accurately evaluate the transformed correlation. Results indicate that (1) a transformation of spatially distributed fields usually changes the spatial dependence structure; and (2) the relationship between the dependence structures of the underlying and the transformed field can be expressed analytically, and it is sufficient to do this in one dimension.

We use the developed approach to investigate the change of correlations of connected random fields generated by the absolute-value transformation. Results show (1) the correlation lengths of the underlying Gaussian fields are 1.67 and 2.64 times of those of transformed non-Gaussian fields for Gaussian and exponential covariance models, respectively; (2) the anisotropic ratio does not change; and (3) the anti-correlation in hole-effect correlations cannot be maintained. In addition, the inverse mapping can yield the accurate estimation of the correlation function required for the

underlying Gaussian field, which can be used to generate the connected field with a given correlation function.

3.4 Quantitative Charaterization of Connectivity Patterns

3.4.1 Charateristics of Connected Fields

Heterogeneity of geologic media is an intrinsic feature of natural hydrologic systems, and its effect on subsurface flow and transport often have a substantial influence on the behavior of the system. The characteristics of the spatial structures have been studied since decades [e.g., *Dagan*, 1986; *Gelhar*, 1986; *Neuman*, 1997]. Mostly, we are interested in the flow and transport behaviors on large scales, and the exact distribution and detailed variability of the spatial patterns are unknown. Thus geostatistical techniques (i.e. one- and two-point statistics) and upscaled models are often used. However, a number of studies in various areas of hydrogeology have been demonstrated that traditional geostatistics are not sufficient for capturing and generating appropriate heterogeneity of the underlying field [*Western, et al*, 1998, 2001; *Wen and Gomez-Hernamdez*, 1998], including hydrogeologically important examples such as soil moisture, surface rainfall-runoff [*Western et al*, 1998], and hydraulic conductivity in aquifer formations[*Western et al*, 2001]. These and other studies [e.g., *Fogg*, 1986; *Silliman and Wright*, 1988; *Wen and Gomez-Hernandez*, 1997; *Tidwell and Wilson*, 1999; *LaBolle and Fogg*, 2001; *Zinn and Harvey*, 2003; *Zinn et al.*, 2004; *Liu et al.*, 2004, 2007; *Knudby and Carrera*, 2005; *Willmann et al.*, 2008; *Luo and Cirpka*, 2011] have demonstrated that flow and transport in heterogeneous fields with connected features (i.e., thin connected bands with high- or low- conductivity paths) are hydrologically important, and require special attention. Intuitively, high-conductivity flow paths form preferential flow paths (channeling) which can lead to early breakthrough of contaminants and significant reduction of arrival times; while

low-conductivity flow paths form flow barriers that can result in excessive tailing behavior. The important feature of these connected paths is the degree to which they are interconnected, instead of their sizes or directions.

Quantification of connectivity properties in hydrogeology usually utilizes indicator functions. [*Journel and Alabert*, 1990; *Anderson*, 1997] suggested that indicator geostatistics is an appropriated tool for characterizing connectivity, while *Western et al.* [1998] showed a counter-example in soil moisture patterns. *Western et al.* [2001] inherits the measurements in percolation theory, and introduces two-pint cluster functions and two-cut indicators[e.g., *Torquato et al.*, 1988; *Western et al*, 1998, 2001; *Neuweiler and Cirpka*, 2005]. *Western et al.* [2001] has applied these concepts on soil moisture patterns and hydraulic conductivity in aquifer formations; while *Neuweiler and Cripka* [2005] applied these concepts to investigate the influence of connectivity on the effective relative permeability curves in unsaturated soils. Additionally, *Knudby and Carerra* [2006] defines flow connectivity indicators and transport connectivity indicators, and concludes that the degree of connectivity is process-dependent.

3.4.2 Two-cut Indicator Function

Here we use the two-point cluster function of a two-cut indicator field as a way of quantifying connectivity properties [*Torquato et al.*, 1988; *Western et al.*, 2001; *Neuweiler and Cirpka*, 2005].

Indicator values vary between 0 and 1. The **two-cut indicator field** $I(\mathbf{x})$ is defined by an upper and a lower threshold value, taking value $I(\mathbf{x}) = 1$ if the original value $Y(\mathbf{x})$ at location $\mathbf{x}$ is between the two thresholds, and taking value $I(\mathbf{x}) = 0$ otherwise. The threshold values are flexible and chose by the users, and we consider threshold values for log-intrinsic permeability field since we want to analyze the connected permeability zones.

For clusters of regions with $I(\mathbf{x}) = 1$, we give each cluster an index, and denote

the indexed field as $Cl(\mathbf{x})$. Figure 3.7 gives a simple example of a 10×10 field.

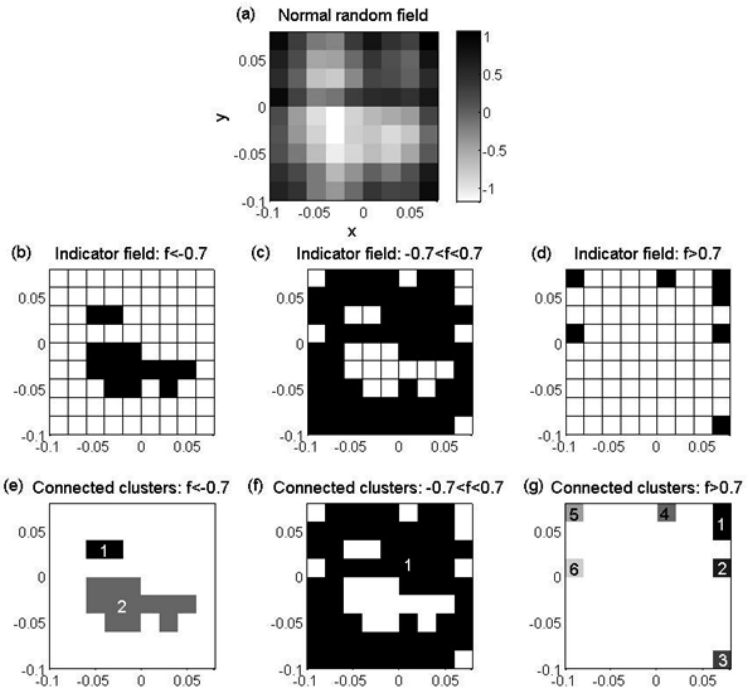

Figure 3.7: 2-cut indicator functions for a simplified 10 by 10 field, with zero mean and variance 1

Then we can define the **two-point cluster function** $C(h)$ as the probability that two points $\mathbf{x}$ and $\mathbf{x\prime}$ with distance $h = |\mathbf{x} - \mathbf{x}'|$ belong to the same cluster [*Torquato et al*, 1988; *Western et al*, 2001; *Neuweiler and Cirpka*, 2005]:

$$C(h) = \frac{\langle I(\mathbf{x}) P(\mathbf{x}, \mathbf{x}') \rangle_{|\mathbf{x}-\mathbf{x}'|=h}}{\langle I(\mathbf{x}) \rangle} \tag{3.6}$$

where

$$P(\mathbf{x}, \mathbf{x}') = \begin{cases} 1 & \text{if } Cl(\mathbf{x}) = Cl(\mathbf{x}') \\ 0 & \text{otherwise} \end{cases} \tag{3.7}$$

In order to perform the averaging process denoted by the angular brackets, we will need to calculate over an ensemble of N fields. For the simplified situation when there

is only one cluster, the two-point cluster function will be identical to the correlation function of the indicator field $I(\mathbf{x})$.

3.4.2.1 Quantification of Connectivity

We are now ready to quantify and compare connectivities for the set of three different fields in Section 3.1, namely, the Gaussian (or exponential) random field, the high-conductivity connected field, and the low-conductivity connected field, having identical correlation functions.

A 2-dimensional random field with 256×256 cells is created by an isotropic Gaussian (or exponential) covariance model, with one point was fixed at the domain center, having mean $\langle Y(x) \rangle = 0$, variance $\sigma^2_{Y(x)} = 1$, and correlation length of 5 cells. The upper threshold value is chosen to be 0.7, and the lower threshold value is -0.7. And we calculate the two-point cluster function (Eq. 3.6) based on 10,000 random fields generated by the same procedure as described in Section 3.1.

Figure 3.8 is an example of random heterogeneous fields with Gaussian covariance model, as well as their two-cluster functions, respectively. The first row indicates normal random field, while the second and the third rows indicate high-value connected field and low-value connected field, respectively. And the 2nd, 3rd, and 4th columns denote connected clusters for $f < -0.7$, $-0.7 < f < 0.7$, $f > 0.7$, respectively. Different fields have different types of connected clusters: the high-value connected field has connected clusters corresponding to the high values ($f > 0.7$); the low-value connected field has connected clusters corresponding to the low values ($f < -0.7$); and the normal random field does not have significant connected phenomenons except for intermediate values ($-0.7 < f < 0.7$), which is consistent with our definition and understanding of the Gaussian field: centered at the mean and scattered at extreme values, and with the understanding that intermediate values tend to be well connected in MultiGaussian-fields [*Knudby and Carrera*, 2006]. The right column of Figure 3.8

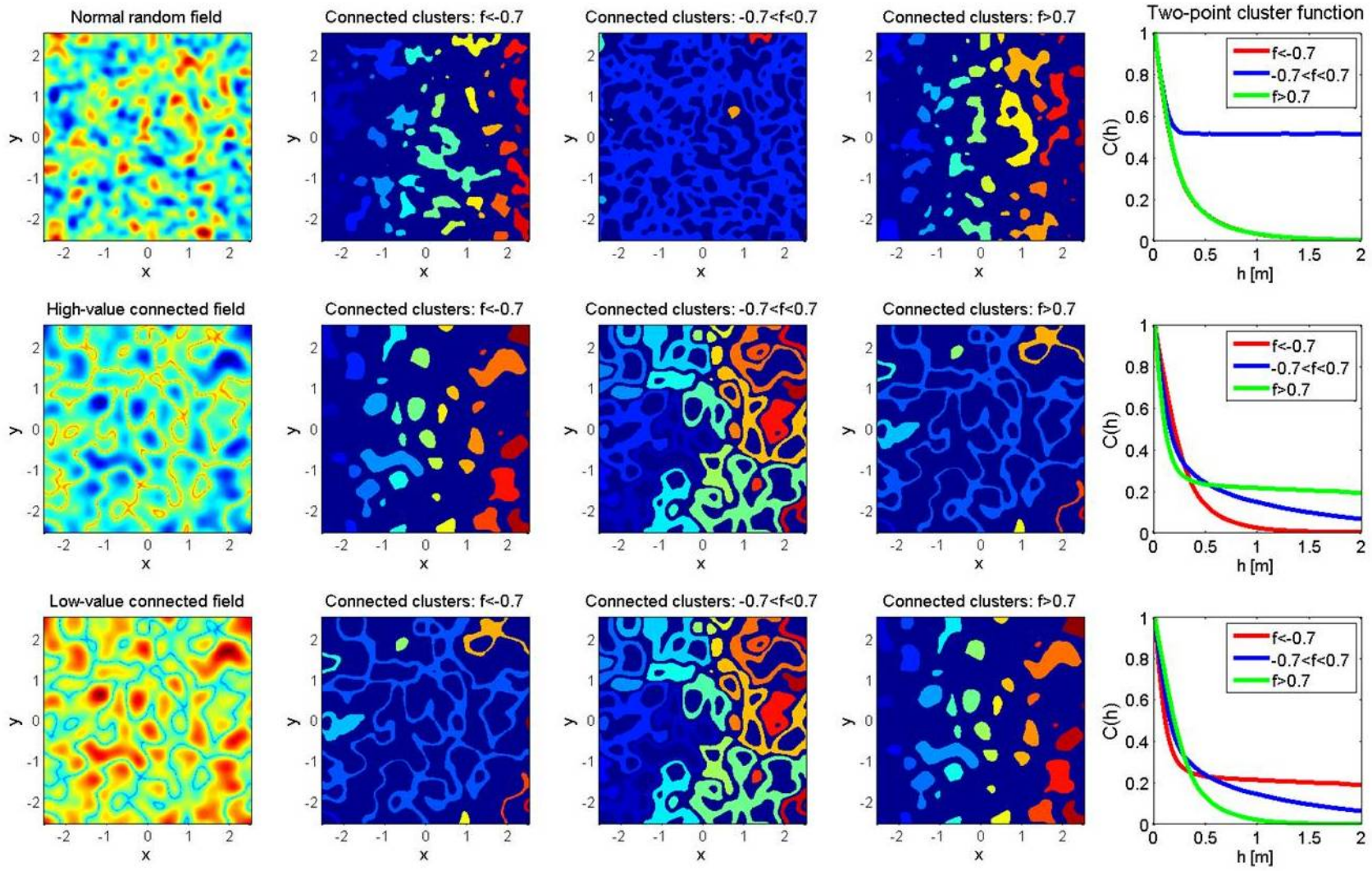

Figure 3.8: Two-point cluster functions for random Gaussian field, high-conductivity connected field, and low-conductivity connected field, respectively

demonstrates the two-point cluster function for each field: the red line indicates low permeability, the blue line indicates intermediate permeability, and the green line indicates high permeability. As for the standard gaussian field (1st row), the red line and the green line are overlapped, suggesting that connectivities on extreme values are symmetric, and both tend to zero as distance between two points increases, meaning that two points with extreme (low or high) conductivity values are not likely to be connected. For intermediate values (the blue line), however, $C(h)$ tends to be stabilized at 0.5 when the distance is large enough ($h \gtrsim 0.2$), meaning that most points of the intermediate values are connected, no matter how far apart they are. As for the high-conductivity connected fields (2nd row), the high-permeability zones are best connected, followed by intermediate zones and low permeability zones; while the low-conductivity connected fields (3rd row) have the opposite order: low permeability zones are better connected than intermediate zones, and the high permeability zones are least connected. By definition, all these observations are consistent with the cluster functions in 2nd, 3rd, and 4th columns.

Figure 3.9 gives another example of random heterogeneous fields with exponential covariance model. As we noticed, exponential covariance models are not as smooth as Gaussian covariance models, which also affects their connectivity. Considering the demonstration of cluster functions (2nd, 3rd, and 4th columns), there are no significantly well connected zones as those in Figure 3.8. In addition, zones with intermediate values are always best connected, among the set of three fields. And, contrary to what happens in fields with Gaussian covariance model, in fields exponential model, high-permeability zones are less connected in high-conductivity connected fields (2nd row), and low-permeability zones are less connected in low-conductivity connected fields (3rd row). This might imply that absolute-value transformation is not suitable for exponential fields: "high-conductivity connected" fields are not truly connected in the high-value zones, and the "low-conductivity connected" fields are

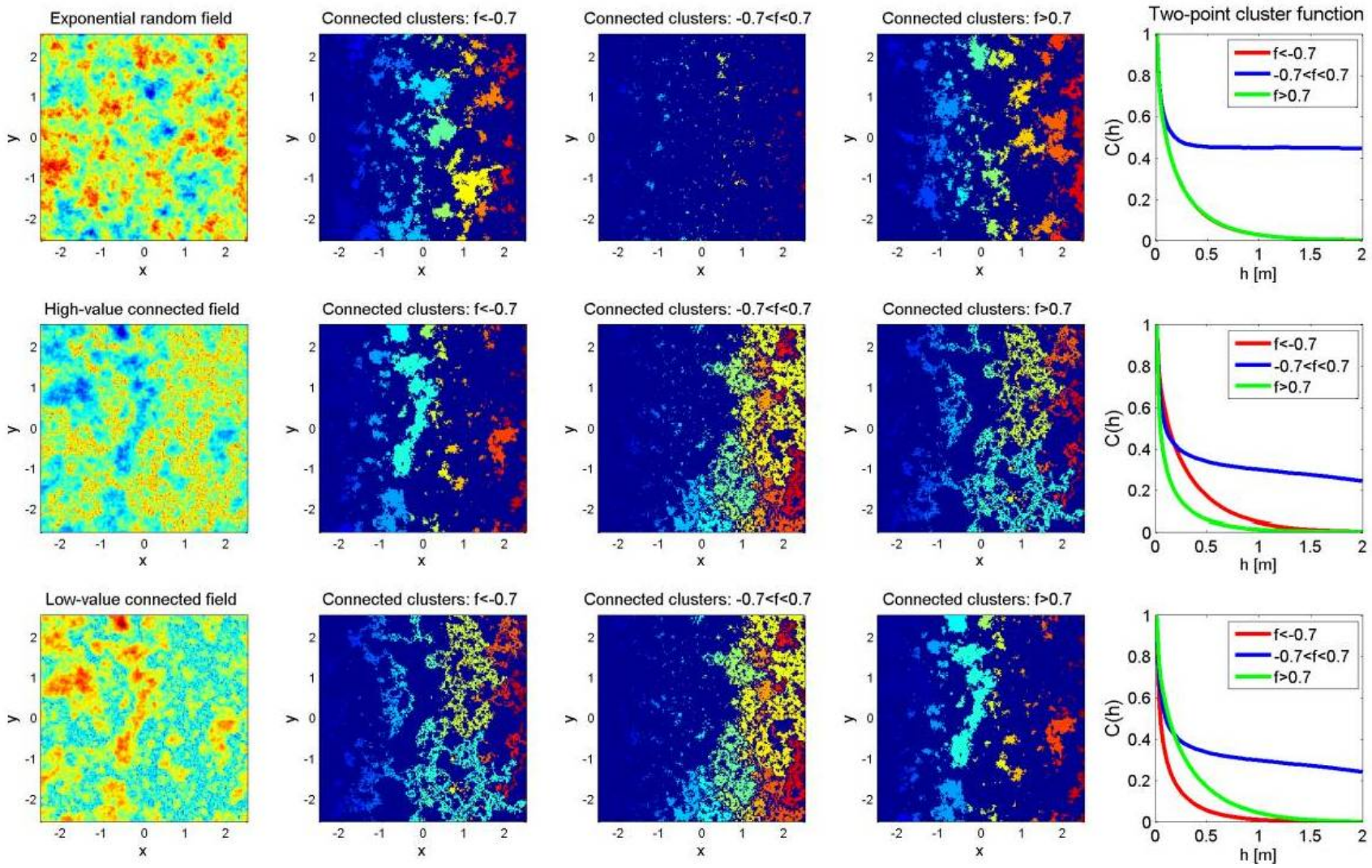

Figure 3.9: Two-point cluster functions for random Exponential field, high-conductivity connected field, and low-conductivity connected field, respectively

not truly connected in the low-value zones. Furthermore, by comparing Figure 3.8 and Figure 3.9, we conclude that fields with Gaussian covariance model have better connectivity than those with exponential covariance model.

3.5 Closure

This chapter has reviewed methods to generate connected fields, especially the efficient absolute value transformation method. Then the change of correlation length of connected random fields generated by the absolute-value transformation has been investigated. We carry out Monte-Carlo simulation and the results indicate that (1) the absolute-value transformation has slight effect on changing the types of covariance models; (2) the correlation length of the original field is 1.67 or 2.64 times of that of the connected field for Gaussian or exponential covariance models; (3) anisotropy is not changed by the absolute-value transformation. This chapter has also summarized connectivity measures in the literature, and discussed two-point cluster function in details. We conclude that two-point cluster functions can identify different degrees of connectivity for connected fields with Gaussian covariance model, but not as reliable when used for connected fields with exponential covariance model, which may be due to the fact that exponential covariance models are continuous but not smooth.

Now that we have studied the characteristics of connected fields, in the following chapters, we will focus on the flow and transport behaviors, especially the macroscopic reactive transport models, and the estimation of concentration variations.

CHAPTER IV

PERFORMANCE OF MACROSCOPIC MODELS IN CONNECTED HETEROGENEOUS MEDIA

4.1 Introduction

The current research is motivated by a previous work by [*Luo and Cirpka*, 2011], in which numerical cases of mixing-controlled reactive transport with a bimolecular precipitation reaction at local equilibrium in structured and normally heterogeneous domains are investigated. They showed that, in cases with intermediate hydraulic conductivity contrast, making macroscopic models fit flux-averaged concentration breakthrough curves better may not improve the prediction of mixing-controlled reactive transport, and it becomes necessary to quantify and account for the variability of conservative concentrations in the flux in order to formulate an appropriate macroscopic transport model that predicts mixing-controlled reactive transport. The objective here was to examine the performance of macroscopic models in predicting mixing-controlled reactive transport in connected heterogeneous media. In other words, we investigated to which extent concentration fluctuations within the solute flux could be neglected in the transfer from breakthrough curves of conservative to reactive compounds.

In connected heterogeneous fields, very different flow and transport behavior can occur even though the conductivity fields have nearly identical lognormal univariate conductivity distributions and nearly identical isotropic spatial covariance functions [*Western et al.*, 2001; *Zinn and Harvey*, 2003]. Therefore, the traditional macrodispersion theory is no longer effective for upscaling effective macroscopic models. In

fact, it has been proven that advection-macrodispersion transport models (a normal bell shape with width growing with the square root of time) fail to characterize anomalous transport behavior, and kinetic mass transfer (particularly multirate mass transfer), non-Fickian or fractional dispersion, continuous time random walk, or more detailed hydraulic conductivity heterogeneities must be incorporated. However, most of such sophisticated macroscopic models consider the mean concentration distribution and ignore the subscale incomplete mixing. From a strictly theoretical standpoint of view, it is clear that neglecting such variations must lead to a mass-balance error, since the transfer from conservative to reactive compound concentrations is usually nonlinear. However, the studies of [*Edery et al.*, 2009] and [*Willmann et al.*, 2010] indicated good performance, despite the fact that their models could not account for concentration variations in the solute flux. The present research aims to improving the understanding of how macroscopic models perform in connected heterogeneous media so that we know when improving macroscopic models is effective and when we need to seek other modeling frameworks.

4.2 Methods

4.2.1 Mixing-Controlled Reactive Transport

We study the same reactive transport as the one conducted by [*Luo and Cirpka*, 2011]. An instantaneous bimolecular precipitation reaction was used for numerical modeling and simulations. Assume advective-dispersive transport of compounds A, B and C with concentrations c_A, c_B, and c_C. Aqueous species (solutes) A and B react with each other, forming compound (mineral) C:

$$A + B \rightarrow C \downarrow \tag{4.1}$$

For simplicity, we assume all stoichiometric coefficients to be one. This reaction is assumed to be fast compared to transport processes, so that it can be treated as in

equilibrium. The concentrations of the aqueous species A and B satisfy:

$$c_A \cdot c_B = K_{eq} \tag{4.2}$$

where c_A and c_B are the molar concentrations of the reactive species A and B respectively, and K_{eq} is the chemical equilibrium constant. The transport equations for the reactive species A, B, and C are given by:

$$\frac{\partial c_A}{\partial t} + \nabla \cdot (\mathbf{v} c_A - \mathbf{D} \nabla c_A) = -r \tag{4.3}$$

$$\frac{\partial c_B}{\partial t} + \nabla \cdot (\mathbf{v} c_B - \mathbf{D} \nabla c_B) = -r \tag{4.4}$$

$$\frac{\partial c_C}{\partial t} + \nabla \cdot (\mathbf{v} c_C - \mathbf{D} \nabla c_C) = r \tag{4.5}$$

where t is the time, $\mathbf{v}$ is the seepage velocity, defined as the specific discharge over porosity, $\mathbf{v} = \mathbf{q}/\theta$, $\mathbf{D}$ is the local dispersion tensor, and r is the reaction rate (precipitation of C, if r positive). A and B have the same reaction rate due to the stoichiometry balance of the bimolecular reaction. For simplicity, we assume local chemical equilibrium is satisfied everywhere at all times. This reactive transport case can be solved completely relying upon the mixing ratio of conservative transport [*De Simoni et al.*, 2005, 2007].

4.2.2 Mixing-Ratio Approach

For the sake of completeness, the mixing-ratio methodology developed by *De Simoni et al.*, [2005] is briefly summarized in the following[*Luo and Cirpka*, 2011]. Define the conservative component:

$$u = c_A - c_B \tag{4.6}$$

which satisfies a conservative transport equation

$$\frac{\partial u}{\partial t} = -\mathbf{v} \cdot \nabla \mathbf{u} + \nabla \cdot (\mathbf{D} \nabla \mathbf{u}) \tag{4.7}$$

Solving equations 4.2 and 4.6 yields the reactive species concentrations:

$$c_A = \frac{u}{2} + \sqrt{\frac{u^2}{4} + K_{eq}} \tag{4.8}$$

$$c_B = -\frac{u}{2} + \sqrt{\frac{u^2}{4} + K_{eq}} \tag{4.9}$$

Thus, $c_A$and c_B can be solely evaluated on the basis of the conservative component, i.e., $c_{A,B}(\mathbf{x}, t) = c_{A,B}[u(\mathbf{x}, t)]$ for given chemical equilibrium constants. On other words, we can directly obtain reactive species concentrations based on conservative breakthrough curves and there is no need to fit a mechanistic model for predicting reactive transport. Thus, the mixing-ratio approach can also be considered as a "perfect" macroscopic modeling approach.

4.2.3 Random Gaussian Heterogeneous Fields

The geological settings follow those in [*Luo and Cirpka*, 2011], containing a two-dimensional, rectangle site of $20m \times 10m$. The mean flow is in direction x, and the variance of log hydraulic conductivity, $\sigma^2_{\ln K}$, is varied from mildly heterogeneous field $\sigma^2_{\ln K} = 0.2$ to relatively strongly heterogeneous field $\sigma^2_{\ln K} = 6$. Table 4.1 lists all hydrological parameters:

The log conductivity fields are generated by the spectral method of *Dykaar and Kitanidis* [1992] on a rectangular 1000×500 cell grid. The steady state flow field is solved for a mean hydraulic gradient of 0.01 in direction x. A streamline-oriented grid for transport with grid resolution identical to that of the rectangular grid is generated using the streamline method of *Cirpka et al.* [1999a, 1999b]. The flowrate in each stream tube is identical. The numerical schemes for solving the transport problem follows [*Cirpka et al.*, 1999a].

Table 4.1: Hydrogeologic parameters for random Gaussian heterogeneous fields

Parameter	Symbol	Values
Dimension of domain	$L \times W$	$10m \times 5m$
Discretization	$\triangle x \times \triangle y$	$0.01m \times 0.01m$
Mean hydraulic conductivity	$\langle K_G \rangle$	$1 \times 10^{-4} m/s$
Variance of hydraulic conductivity	$\sigma^2_{\ln K}$	$0.2, 0.5, 1, 2, 3, 4, 5, 6$
Correlation length	$I_x \times I_y$	$0.2m \times 0.2m$
Mean hydraulic gradient	J	0.01
Effective porosity	θ	0.3
Longitudinal dispersivity	α_L	$0.01m$
Transverse dispersivity	α_T	$0.001m$
Molecular diffusion	D_m	$10^{-9} m^2/s$

Generation of connected random fields used the absolute-value transformation of multivariate Gaussian fields [*Zinn and Harvey*, 2003], which offers a simple approach to generate a spatial dependence structure with different connectivity that is non-Gaussian, but based on a multivariate normal spatial field given two-point spatial correlations. The absolute-value transformation defines a new variable by the normal score transform of the absolute value of the original random variable [*Zinn and Harvey*, 2003]:

$$Y'(\mathbf{x}) = -\sqrt{2}\mathrm{erf}^{-1}\left(2\mathrm{erf}\left(\frac{|Y(\mathbf{x})|}{\sqrt{2}}\right) - 1\right) \tag{4.10}$$

where $Y = \ln K$ is an autocorrelated Gaussian random field with zero mean and variance of unity, $\mathbf{x}$ is the spatial location, and Y' is the transformed random field with connected high conductivities ($-Y'$ is a disconnected field with connected low conductivities).

Figure 2.5 shows some generated realizations of normally, high-conductivity connected and low-conductivity connected fields. All hydrological parameters are identical to those in table 4.1. The connected fields are generated using the method developed in Chapter 3 so that all realizations have the same spatial correlation.

4.3 Results and Discussion

4.3.1 Conservative transport

We are interested in the reactive transport after a long travel distance, i.e., the plume has been sufficiently developed, because it is more common in reality. In our numerical cases, the domain length is 50 times of the correlation length, which is considered as a sufficiently long distance for macrodispersion to describe plume spreading.

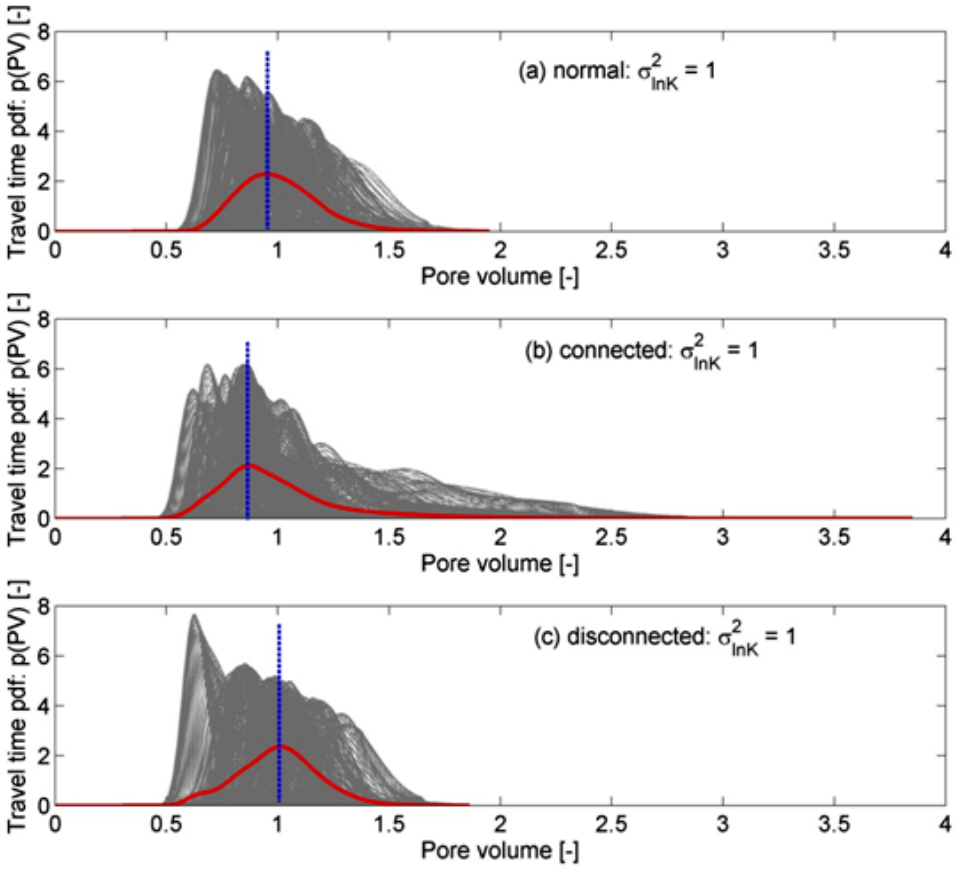

Figure 4.1: Particle travel time density functions at the outflow boundary in one realization with unitary variance of hydraulic conductivity field

Figure 4.1 shows the particle travel time density functions at the outflow boundary in one realization with unitary variance of hydraulic conductivity field. Measurements available in reality are usually the flux-averaged mean of all local-scale values. Figure

4.1 clearly shows that great variations in the local scale or sub-scale are created by hydraulic conductivity heterogeneities. Two major features can be observed from the mean behavior: (1) the mean travel time pdf in the high-conductivity connected field is highly asymmetric with a heavy, long tail, while the mean travel time pdfs in normally and disconnected heterogeneous fields are rather symmetric; and (2) the peak time in the connected field is much earlier than the other two, indicating preferential flow paths in the connected field.

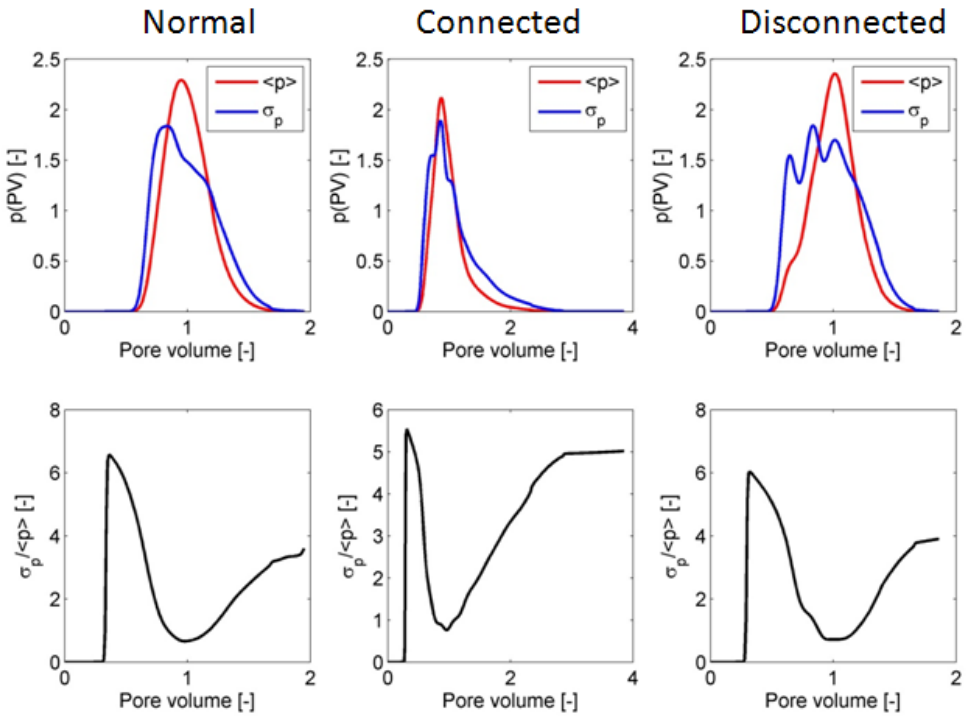

Figure 4.2: Mean travel time pdf, variance and coefficient of variation at the outflow boundary in heterogeneous media with different connectivity and unitary variance of $\ln K$

Figure 4.2 shows the mean, variance and coefficient of variation of the travel time pdf for the specific case. In general, variance follows the similar pattern as the mean, i.e, variance vanishes at early and late times and peaks with the mean. However, the coefficient of variation shows almost opposite pattern as the mean and variance. At early and late times, variances are small but non-negligible compared with the

mean, implying that ignoring such variations may still create relative large errors in predicting reactive transport.

4.3.2 Reactive transport

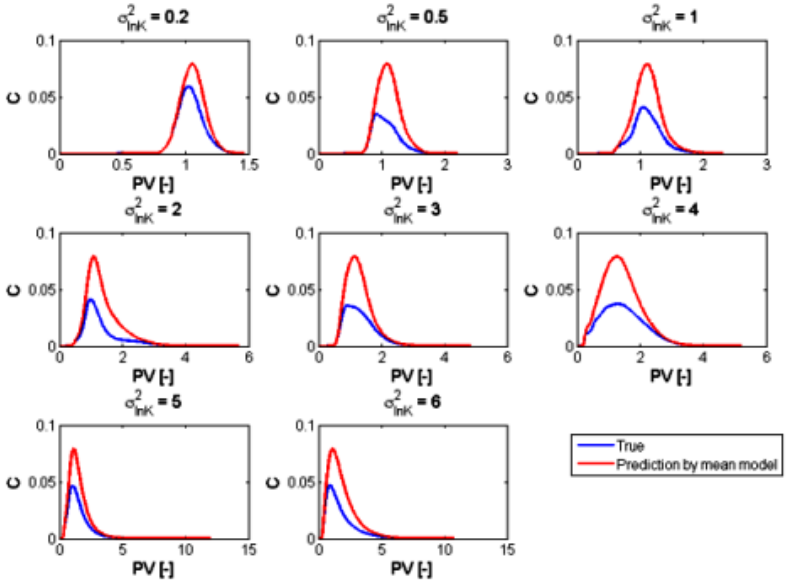

Figure 4.3: Numerical results and prediction by a "perfect" macroscopic model for the flux-averaged concentration difference of compound A between the conservative and reactive cases at the outflow boundary, for Gaussian fields with different variance of hydraulic conductivity

Figures 4.3-4.5 show the product species concentration breakthrough curves of macroscopic models for predicting mixing-controlled reactive transport in normally Gaussian, high-conductivity connected, low-conductivity connected heterogeneous fields, respectively. Clearly, all macroscopic models overestimate the reaction rates, yielding higher peak concentrations and more total product mass. However, by comparing the different types of heterogeneous fields with different variances, we can see the macroscopic model performs much better in connected fields and in fields with small or high variances. This finding is consistent to the results identified in structure media in *Luo and Cirpka* [2011].

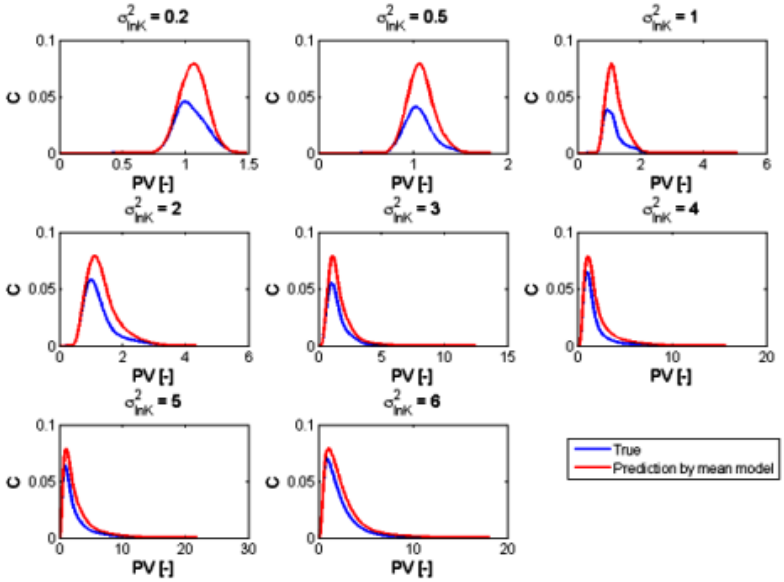

Figure 4.4: Numerical results and prediction by a "perfect" macroscopic model for the flux-averaged concentration difference of compound A between the conservative and reactive cases at the outflow boundary, for connected fields with different variance of hydraulic conductivity

Figure 4.6 shows the results averaged from 20 realizations for each type of heterogeneous fields with different variances. The relative errors for both the total mass and peak concentrations show that (1) the highest error occurs in fields with intermediate variances around 1; the error can be as high as 100%; (2) the macroscopic model performs better in heterogeneous fields with very low (nearly homogeneous) and high variances (highly heterogeneous); (3) at the low variance, the macroscopic model performs best in disconnected fields and worst in connected fields; while at the same high variance, the macroscopic model performs best in connected fields and worst in disconnected fields.

Figure 4.7 shows snapshots of plume development in connected fields with different variances. The plume front is rather uniformly distributed across the domain in the case of a small log-conductivity variance. With increasing variance, the plumes

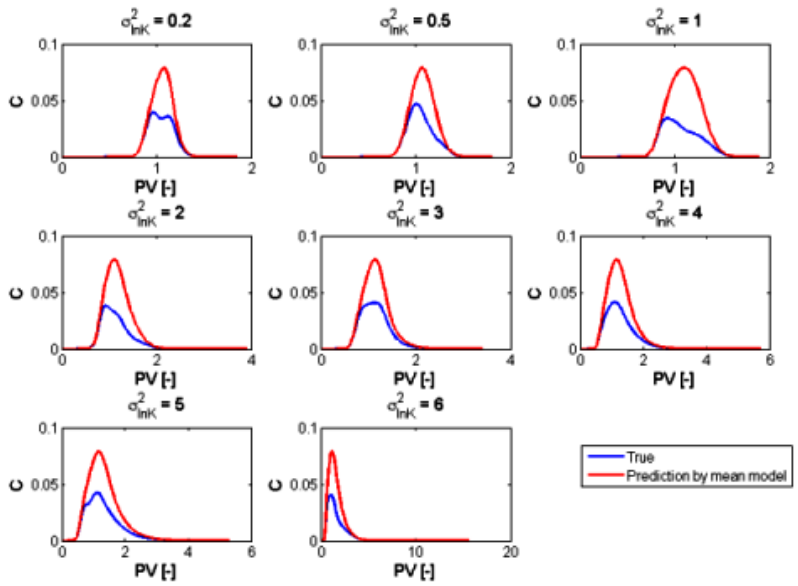

Figure 4.5: Numerical results and prediction by a "perfect" macroscopic model for the flux-averaged concentration difference of compound A between the conservative and reactive cases at the outflow boundary, for disconnected fields with different variance of hydraulic conductivity

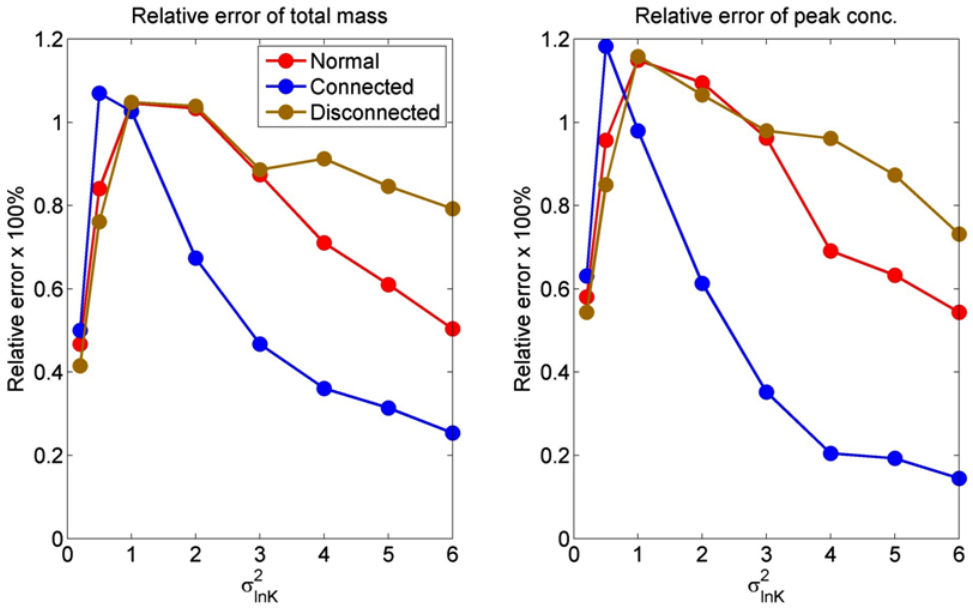

Figure 4.6: Relative errors of total mass and peak concentration predicted by the "perfect" macroscopic transport model in heterogeneous media with different connectivity

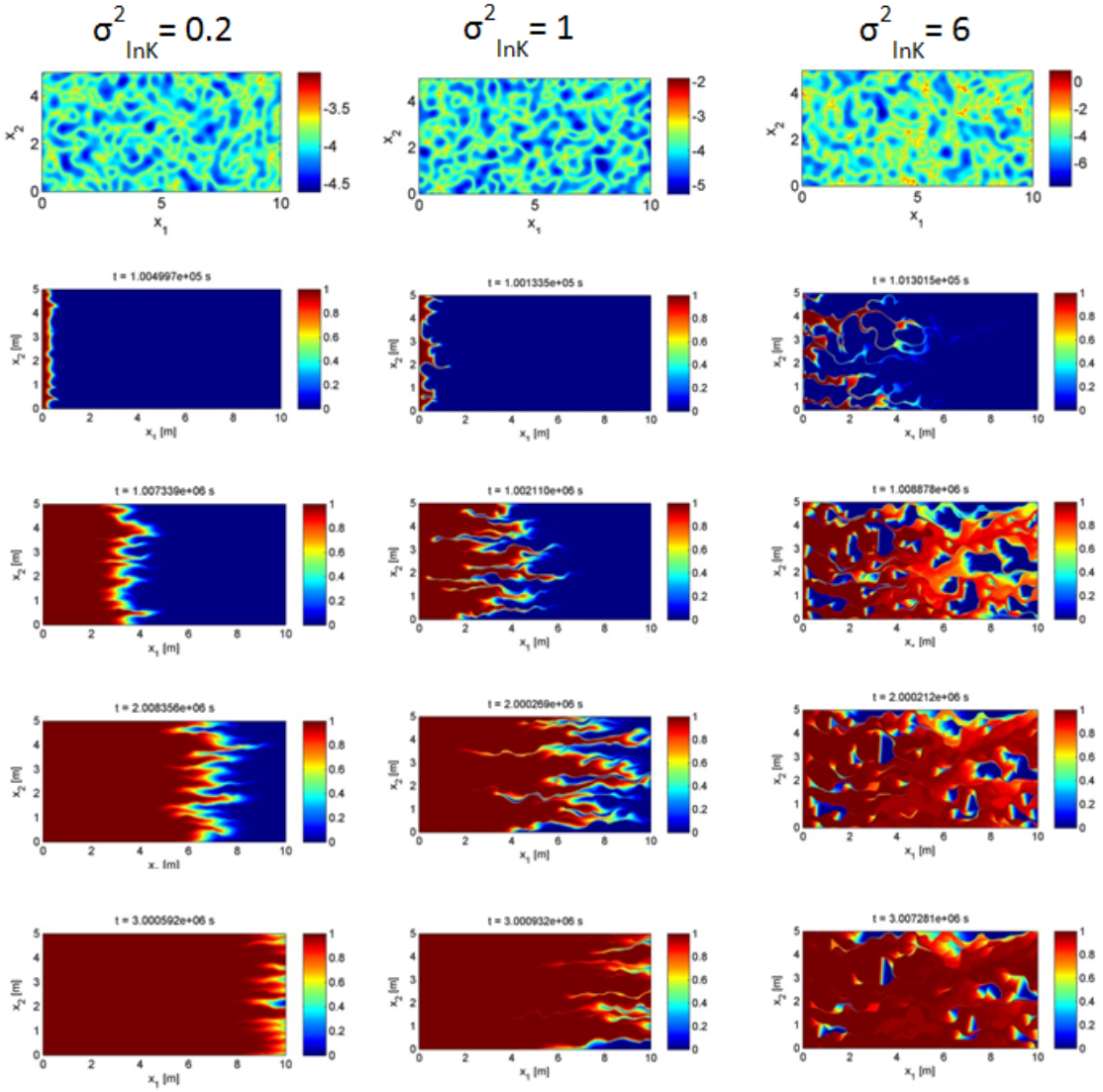

Figure 4.7: Snapshots of plume development in connected heterogeneous media with different connectivity

are stretched, focusing in the zones with large hydraulic conductivities and forming narrow preferential paths. The majority of flow moves along these preferential paths, which accounts for the large proportion in evaluating flux-average breakthrough curves. In the flow focusing areas, shorter transverse distance is required for mixing. Thus, concentration variations in highly heterogeneous fields may become smaller than those in intermediately heterogeneous fields.

4.4 Conclusions

We have presented numerical test cases of mixing controlled reactive transport with a bimolecular precipitation reaction at local equilibrium in different heterogeneous domains. We also investigate random heterogeneous fields with same variance of hydraulic conductivity, but with different connectivity. Specifically, we study Gaussian heterogeneous fields, high-conductivity connected fields, and low-conductivity connected fields. The key objective was to analyze to what extent concentration fluctuations within the solute flux could be neglected in the transfer from breakthrough curves of conservative to reactive compounds. Our results indicate the largest errors in macroscopic one-dimensional models for intermediate conductivity variances. With respect to total mass balance and peak concentration errors, increasing the degree of heterogeneity beyond a critical value led to an improvement of the performance. Our results clearly indicate the need for developing other modeling frameworks to evaluate both mean and concentration variance for simulating mixing-controlled reactive transport in heterogeneous media, particularly in media with intermediate variances of hydraulic conductivity.

CHAPTER V

A STATISTICAL APPROACH TO ESTIMATE CONCENTRATION VARIANCE

Concentration variations are very difficult to evaluate for a specific site both theoretically and experimentally, despite the importance in practice. From a practical view, the information that can be conveniently obtained through tracer tests is integrated breakthrough curves, such as those extracted from a well or through an outflow plane. The objective for this chapter is to develop an innovative approach that relies on the mean or integrated breakthrough curves to estimate concentration variance. The idea is that we will rely upon both conservative and reactive breakthrough curves: conservative breakthrough curves provide the mean behavior while reactive ones are resulted from both mean behavior and the species segregation or incomplete mixing. Thus by combining these two, it is possible to extract the extent of mixing from the reactive breakthrough curves.

5.1 Background

Reactive transport models are essential tools for understanding contaminant plume transport, dilution, and remediation in subsurface media. Spatial variability and uncertainty of hydraulic parameters has been identified as the major challenge in developing appropriate models and upscaling effective transport parameters for predicting the fate and transport of contaminants in natural aquifers. The widely applied macroscopic advection-dispersion equation (ADE) can adequately describe how the mean or spatially averaged concentration of a conservative tracer behaves at the late

time in the absence of detailed information of pore structures and hydraulic conductivities in a mildly random heterogeneous medium. However, such models coupled with chemical reactions have proven unsuccessful for forecasting reactive transport with reaction rates limited by species mixing because macrodispersion implicitly assumes that plume spreading controlled by spatial variations in hydraulic conductivity is equivalent to mixing [*MacQuarrie and Sudicky*, 1990; *Kitanidis*, 1994; *Kapoor et al.*, 1997; *Cirpka and Kitanidis*, 2000; *Raje and Kapoor*, 2000; *Gramling et al.*, 2002; *Dentz and Carrera*, 2007], a prerequisite for multi-species reactions to occur and much more likely to be a limiting factor controlling the overall rate of chemical reactions.

A good macroscopic model should be able to describe both spreading and mixing. In cases when concentration fluctuations cannot be neglected, both mean concentrations and concentration variances should be evaluated for predicting mixing-controlled reactive transport. A specific modeling framework, which accounts for both the mean concentration and its variance, is based on transport equations of the concentration variance in addition to macroscopic mean models [*Kapoor et al.*, 1997]. The variance transport equation involves terms for the generation and destruction of the concentration variance, which are difficult to measure or to predict from statistical metrics of the flow field. From conservative-concentration statistics (mean and variance), attempts have been made to estimate the concentration covariance of reactive species in nonlinear mixing-controlled reactive transport, which is subsequently used to correct reaction rates [*Oates*, 2007]. More elaborate models have targeted the full concentration distribution of conservative species [e.g., *Fiorotto and Caroni*, 2002, 2003], which has been shown to resemble a beta distribution. For specific cases, such as instantaneous bimolecular reactions or biokinetic reactions at steady state, the local statistics of conservative species can be mapped to those of reactive species without relying on linearization [*Cirpka et al.*, 2008, 2011].

In the present research, we are interested in developing an innovative and practical approach for estimating concentration variance. We will assume that only breakthrough curves at the outflow boundary are known, which can be conveniently measured through a tracer test. The conservative breakthrough curve describes the mean concentrations, which are not a function of concentration variations. However, the reactive breakthrough curves are a result of both mean and concentration variations. For example, for a bimolecular reactive transport undergoing advection and dispersion at local scale, we have:

$$\begin{aligned} \text{Conservative} \quad &: \quad \frac{\partial \overline{c}}{\partial t} + \frac{\partial}{\partial x_i}(\overline{v_i c}) + \frac{\partial}{\partial x_i}(\overline{v_i' c'}) - \frac{\partial}{\partial x_i}\left(D_{ij}\frac{\partial \overline{c}}{\partial x_i}\right) = 0 \qquad (5.1) \\ \text{Reactive} \quad &: \quad \frac{\partial \overline{c_1}}{\partial t} + \frac{\partial}{\partial x_i}(\overline{v_i c_1}) + \frac{\partial}{\partial x_i}(\overline{v_i' c_1'}) - \frac{\partial}{\partial x_i}\left(D_{ij}\frac{\partial \overline{c_1}}{\partial x_i}\right) + k\overline{c_1 c_2} = -k\overline{c_1' c_2'} \end{aligned}$$

The left-hand side of the reactive transport equation can be evaluated by the mean and the conservative transport, which yields the macroscopic model prediction without the consideration of concentration variance. The prediction error compared with the true reactive breakthrough curve reflects the effects of concentration variations. We will develop an inverse algorithm with prior information of the distribution shape (such as Beta) and sampling techniques to estimate the concentration variance. More importantly, we will directly use the concentration breakthrough curve instead of a fitted macroscopic model so that the algorithm can be applied to any type of heterogeneous fields. To test the developed method, we will utilize the lab-scale visualization experiments from Dr. C.F. Harvey's research group at MIT (@ *http://web.mit.edu/ harveylab/Reactive_Transport.html*), in which a colorimetric reaction was used to quantify fluid mixing, and the movement of colored dye tracers and colorimetric chemical reactions[*Oates and Harvey*, 2006] were digitally imaged through illuminated chambers [*Zinn* et al., 2004; *Oates*, 2007].

5.2 Method

5.2.1 Estimating Concentration Variance

The beta-distribution function is used to describe the conservative concentration distribution [e.g., *Fiorotto and Caroni*, 2002, 2003]:

$$f\left(c/c_0;\alpha,\beta\right)=\frac{\Gamma\left(\alpha+\beta\right)}{\Gamma\left(\alpha\right)\Gamma\left(\beta\right)}\left(c/c_0\right)^{\alpha-1}\left(1-c/c_0\right)^{\beta-1} \tag{5.2}$$

where the parameters α and β can be evaluated by the concentration mean and variance [*Oates*, 2007]

$$\alpha=\overline{c/c_0}\left(\frac{\overline{c/c_0}\left(1-\overline{c/c_0}\right)}{\sigma^2_{c/c_0}}-1\right) \tag{5.3}$$

$$\beta=\left(1-\overline{c/c_0}\right)\left(\frac{\overline{c/c_0}\left(1-\overline{c/c_0}\right)}{\sigma^2_{c/c_0}}-1\right) \tag{5.4}$$

Given the mean breakthrough curve of conservative tracers alone at the out flow boundary, it is usually impossible to evaluate the species segregation and concentration variance. However, if the mean breakthrough curves of reactive species are known, it is possible to extract the concentration variations from both mean conservative and reactive breakthrough curves. For example, for a bimolecular instantaneous reaction, one can evaluate the concentrations of reactants A and B and the product C by sampling the approximated beta distribution.

The bimolecular instantaneous reaction case can be solved conveniently through a conservative transport problem [e.g., *Cirpka and Valocchi*, 2007]:

$$c_A = \begin{cases} X - (1 - X) & \text{if} \quad X \geq 0.5 \\ 0 & \text{if} \quad X \leq 0.5 \end{cases} \tag{5.5}$$

$$c_B = \begin{cases} 0 & \text{if} \quad X \geq 0.5 \\ (1 - X) - X & \text{if} \quad X \leq 0.5 \end{cases} \tag{5.6}$$

$$c_C = \begin{cases} (1 - X) & \text{if} \quad X \geq 0.5 \\ X & \text{if} \quad X \leq 0.5 \end{cases} \tag{5.7}$$

in which X is the mixing ratio of the solution containing A in the mixture. X is computed by solving the Heaviside problem of conservative transport.

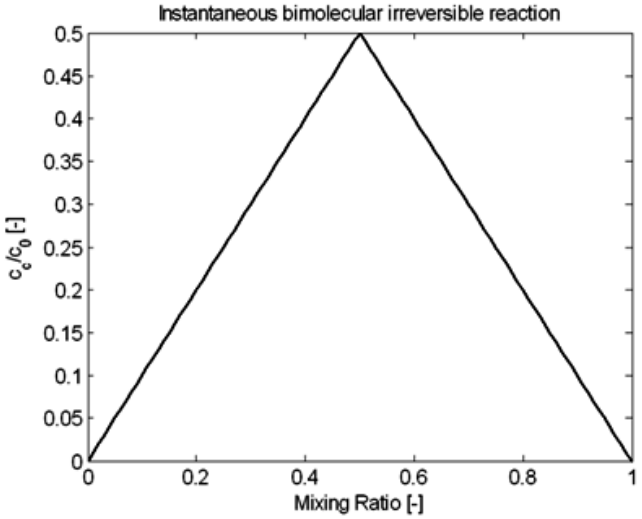

Figure 5.1: Schematic curve that demonstrates the relationship between reactive product concentration and mean concentration for instantaneous bimolecular irreversible reaction

Figure 5.1 is schematic plot that demonstrates the relationship between reactive product concentration and mean concentration for instantaneous bimolecular irreversible reaction. Figure 5.2a shows the 2D contour mesh plot for mean product concentration, and Figure 5.2b shows the contour mesh plot for reactive product concentration variance. We notice that the relation between mixing ratio and coefficient

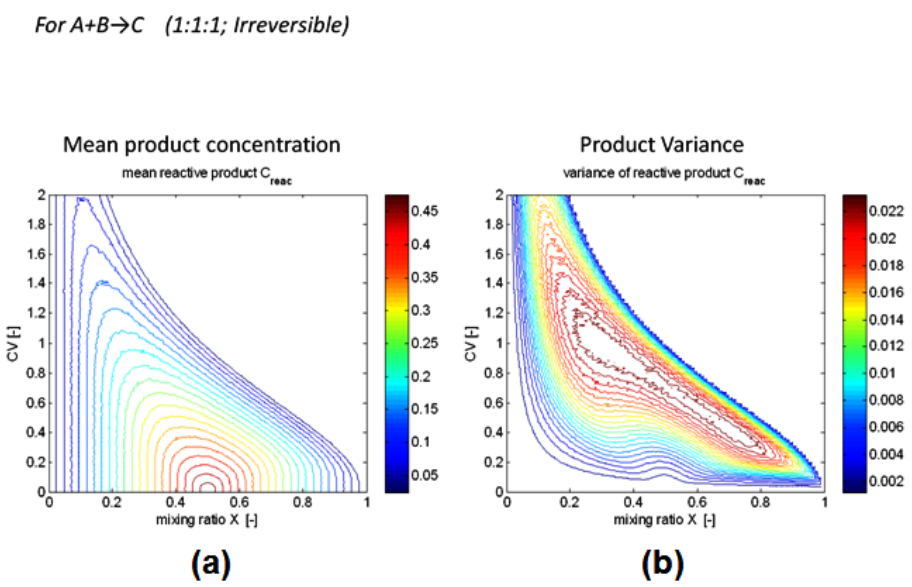

Figure 5.2: 2D mesh plot between mixing ratio, coefficient of variation, and reactive product concentration for instantaneous bimolecular irreversible reaction: (a) mean reactive product concentration; (b) variance of reactive product concentration

of variation is now strictly one-to-one, for all points in the mesh grid.

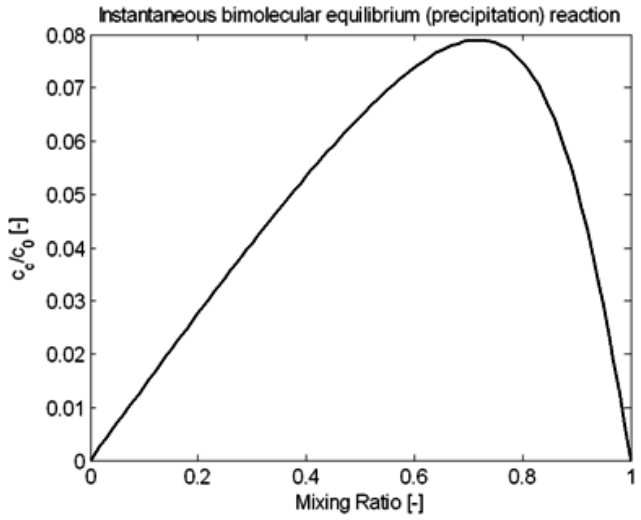

Figure 5.3: Schematic curve that demonstrates the relationship between reactive product concentration and mean concentration for instantaneous bimolecular irreversible reaction with 1:1:1 stoichiometry and local equilibrium constant K_{eq}

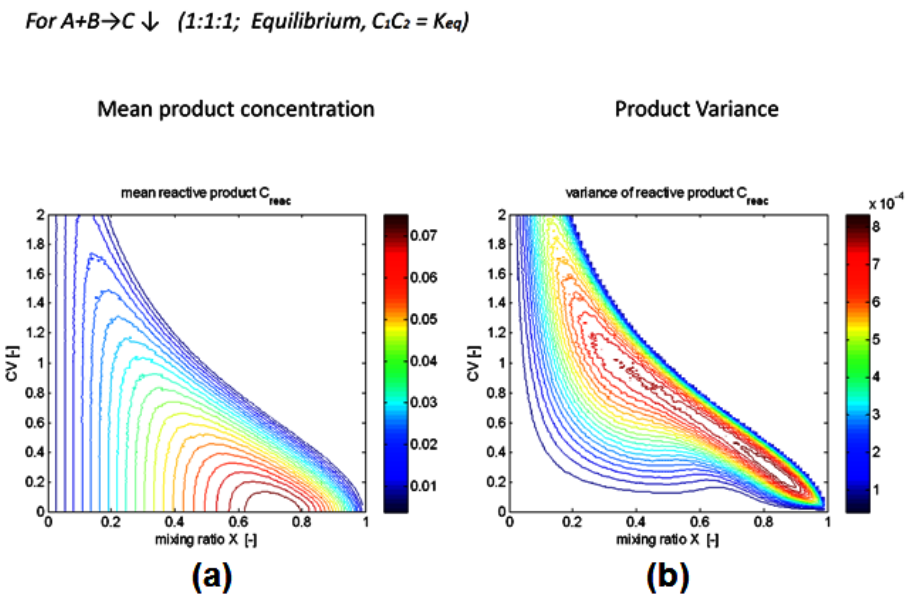

Figure 5.4: 2D mesh plot between mixing ratio, coefficient of variation, and reactive product concentration for instantaneous bimolecular irreversible reaction with 1:1:1 stoichiometry and local equilibrium constant K_{eq}: (a) mean reactive product concentration; (b) variance of reactive product concentration

Similarly, we consider an instantaneous bimolecular precipitation reaction with 1:1:1 stoichiometry and local equilibrium constant K_{eq}. Figure 5.3 is schematic plot that demonstrates the relationship between reactive product concentration and mean concentration for instantaneous bimolecular precipitation reaction with 1:1:1 stoichiometry and local equilibrium constant K_{eq}. Figure 5.4a shows the 2D contour mesh plot for mean product concentration, and Figure 5.4b shows the contour mesh plot for reactive product concentration variance. Similar results are obtained as those for instantaneous bimolecular irreversible reaction. Thus, for given relationships between conservative and reactive species concentrations, we can estimate the variance of conservative concentrations by sampling the beta distribution.

5.2.2 Predicting Reactive Transport

Once we have the concentration variance for both conservative and reactive transports, we can use the Eulerian concentration variance approach [*Gelhar and Axness*, 1983; *Kapoor and Gelhar*, 1994] with the advection-dispersion equation (ADE) for conservative mean concentrations and an equation for conservative concentration variances for predicting conservative and reactive transports with the same hydrogeological characteristics at arbitrary location and time.

In the Eulerian stochastic framework, solute concentration c and velocity v are treated as random variables, having a mean$(\overline{c}, \overline{v})$ and a zero-mean fluctuation(c', v'). The 1-dimensional transport model for conservative concentration mean$(\overline{c})$ and variance(σ_c^2) can be summarized by the following equations[*Gelhar and Axness*, 1983; *Kapoor and Gelhar*, 1994; *Oates*, 2007]:

$$\begin{aligned} \frac{\partial \overline{c}}{\partial t} &= -\overline{v}\frac{\partial \overline{c}}{\partial x} + \overline{v}A_x\frac{\partial^2 \overline{c}}{\partial x^2} \\ \frac{\partial \sigma_c^2}{\partial t} &= -\overline{v}\frac{\partial \sigma_c^2}{\partial x} + \overline{v}A_x\frac{\partial^2 \sigma_c^2}{\partial x^2} + 2\overline{v}A_x\left(\frac{\partial \overline{c}}{\partial x}\right)^2 - \frac{\overline{v}}{\chi_{L,t}}\sigma_c^2 \end{aligned} \tag{5.8}$$

where $\overline{v}$ is the mean velocity, A_x is the 1-dimensional macrodispersivity for the macrodispersion closure approximations, and $\chi_{L,t}$ is the variance length scale derived from variance destruction:

$$\begin{aligned} \overline{c'v'} &= -\overline{v}A_x\frac{\partial \overline{c}}{\partial x} \\ \left(\overline{v'c'^2}\right) &= -\overline{v}A_x\frac{\partial \sigma_c^2}{\partial x} \\ 2\alpha\overline{\left(\frac{\partial c'}{\partial x}\right)^2} &= \chi\sigma_c^2 = \frac{\overline{v}}{\chi_{L,t}}\sigma_c^2 \end{aligned} \tag{5.9}$$

where α is the local dispersivity, and $\chi_{L,t}$ can be considered as a characteristic length that a plume travels in order to destroy variance. In addition, $\chi_{L,t}$ is considered

time-dependent, especially at early time, and can be further expressed as [*Oates*, 2007]:

$$\chi_{L,t} = \chi_L \left(1 - e^{-(\overline{v}t)/\chi_G}\right) \tag{5.10}$$

where χ_L is the variance length scale that can be considered as characteristic distance a plume has to travel to destroy variance, and χ_G is the variance growth scale, which can be considered as a characteristic length that a plume travels in order to reach the asymptotic variance length scale χ_L.

In summary, the algorithm for predicting mixing-controlled reactive transport can be summarized as:

1. Conducting both conservative and reactive tracer tests with known reaction kinetics, such as bimolecular instantaneous reactions, and measure concentration breakthrough curves for both conservative and reactive species at a certain observation point, such as the outflow boundary;

2. Estimating the concentration variance by the sampling approach and using both mean conservative and reactive breakthrough curves;

3. Fitting the mean transport equations for both mean concentrations and variances, i.e., fitting Eqs. 5.8 to obtain coefficients $\overline{v}, A_x, \chi_L, \chi_G$;

4. Solving the transport equations for mean and variance for other locations;

5. Applying the sampling approach again for predicting the mean and variance of reactive species breakthrough curves.

5.3 The Numerical Case — Lab-scale Visualization Experiments for Conservative and Reactive Transports

We use the lab-scale visualization experiments from Dr. Harvey's research group at MIT (@ *http://web.mit.edu/ harveylab/Reactive_Transport.html*) to understand

fluid-fluid mixing, and utilize their experimental data for our numerical experiments. The experimental setup shown in Figure 5.5 (*Oates*, [2007]) was used for the Tiron-molybdate reaction as described by *Gramling et al.* [2002] and the tanks of heterogeneous porous media created by *Zinn et al.*, [2004]. Three $40 \times 20 \times 0.65cm$ glass-walled experimental chambers are filled with different size glass beads and have different spatially variable hydraulic conductivities. All chambers contain large glass beads ($2.1mm$ diameter) packed around circular inclusions ($2.5cm$ diameter) containing smaller glass beads: $0.9mm$ diameter for mildly heterogeneous media having a conductivity contrast of 6; $0.135mm$ diameter for intermediate heterogeneous media having a conductivity contrast of 300; and $0.057mm$ diameter for highly heterogeneous media having a conductivity contrast of 1800. The dominant solute transport processes in the three chambers are different: conservative solute transport in the mild heterogeneous chamber is dominated by advection-dispersion and can be fully described by the macroscopic advective-dispersive-equation (ADE) models; while advection mass transfer is dominated in the intermediate heterogeneous chamber; and diffusion mass transfer is dominated in the highly heterogeneous chamber can be reproduced by advective mass-transfer model [*Zinn et al.*, 2004; *Oates*, 2007].

We first briefly summarize the complex reaction of Tiron (Ti) and molybdate (Mo), and their representation in the absorbing imaging experiment. Next, we will show different patterns of the reactive transport in mild/intermediate/highly heterogeneous porous media. And finally, we are ready to demonstrate the developed innovative reactive-transport framework, based on the experimental data, and to test the effectiveness of the new method incorporating the evaluation of concentration variations.

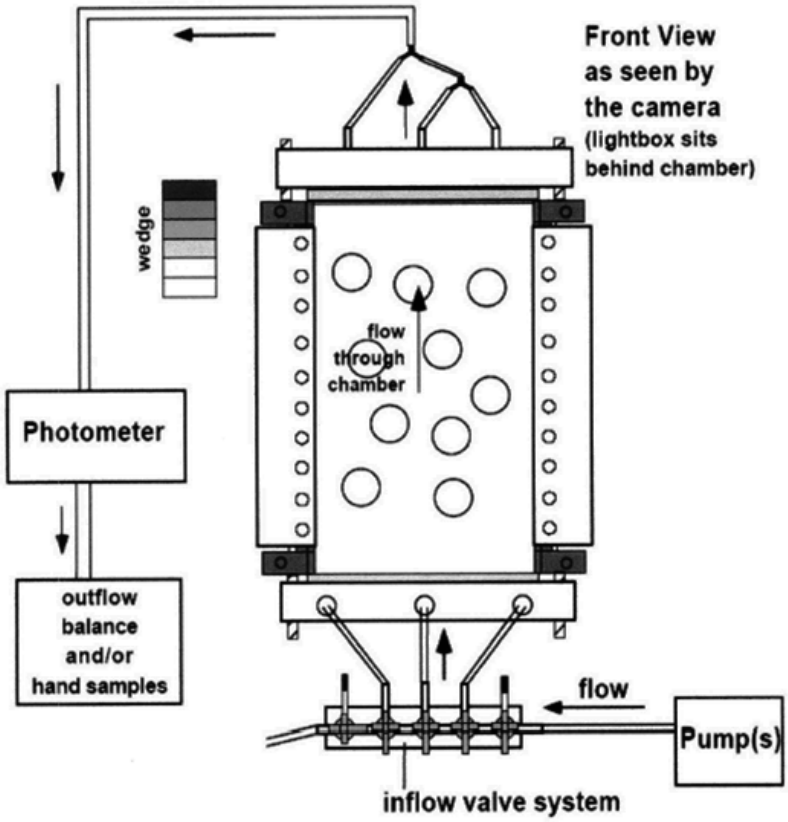

Figure 5.5: Experimental chamber containing circular inclusions of low conductivity as porous media *Oates*, [2007].

5.3.1 Tiron–Molybdate Reaction

Two tiron-molybdate species with a metal to ligand ratio of 1:1 and 1:2 have been reported by [*Sommer*, 1962; *Oates*, 2007]. The first complexation reaction can be written as:

$$Ti + Mo \rightleftharpoons MoTi \tag{5.11}$$

where Ti is the molar concentration of Tiron; Mo is the molar concentration of molybdate; and $MoTi$ is the molar concentration of the 1:1 complex. This reaction is assumed to be fast compared to typical transport times, so that this first reaction

can be treated as in local equilibrium:

$$K_1 = \frac{[MoTi]}{[Mo][Ti]} \tag{5.12}$$

where K_1 is the first equilibrium constant (liters/mol). This first product then undergoes an additional reaction with Tiron, and the second complexation reaction can be written as:

$$MoTi + Ti \rightleftharpoons MoTi_2 \tag{5.13}$$

where $MoTi_2$ is the second chelate formed. The second reaction can also be expressed in the equilibrium expression:

$$K_2 = \frac{[MoTi_2]}{[MoTi][Ti]} \tag{5.14}$$

where K_2 is the second equilibrium constant (liters/mol).

In the lab-scale visualization experiments conducted by Harvey's research group, two clear solutions of 0.05M Tiron and 0.025M molybdate are mixed and buffered at pH 6.1, which results in the progressive change of solute color as the reactants react and the products diluted[*Oates*, 2007].

5.3.2 Tiron and Molybdate Reaction Model

When the reactants Tiron and Molybdate are mixed, mass balances combined with equilibrium reaction rates (Eqs. 5.12, 5.14) give independent analytical solutions for each of the complexes [*Oates*, 2007]:

$$\begin{aligned} [MoTi] &= f([Ti_T], [Mo_T], K_1, K_2) \\ [MoTi_2] &= f([Ti_T], [Mo_T], K_1, K_2) \end{aligned} \tag{5.15}$$

where Mo_T is the total molybdate, and Ti_T is the total Tiron.

In addition, the additive property of Beer's Law ensures that the linear absorbance (A_1) of the two products ($MoTi$ and $MoTi_2$) can be expressed in a linear form:

$$-\log\left(\frac{T}{T_0}\right) = A_1 = \epsilon_1 [MoTi] + \epsilon_2 [MoTi_2] \tag{5.16}$$

where T/T_0 is the fraction of light transmitted, ϵ_1 and ϵ_2 are coefficients that include the transmittance path length and the corresponding molar absorptivity of the compound.

The equilibrium constants K_1 and K_2, and the linear absorbance coefficients ϵ_1 and ϵ_2, are determined by fitting observed absorbance at 580nm to Eqs. 5.15 and 5.16. The perfect fitting gives the following parameter values, as reported by [*Oates*, 2007]:

$$\begin{aligned} K_1 &= 3.4 \pm 0.8 \times 10^3 \text{ liter/mol} \\ K_2 &= 7.5 \pm 1 \times 10^2 \text{ liter/mol} \\ \epsilon_1 &= 4.3 \pm 2 \text{ liter/(mol*cm)} \\ \epsilon_2 &= 83 \pm 1 \text{ liter/(mol*cm)} \end{aligned} \tag{5.17}$$

Therefore, at a pH of 6.1 and a wavelength of 580nm, absorbance is dominated by the $MoTi_2$ species.

Finally, [*Oates*, 2007] obtained the relationship between the digital camera recorded polychromatic absorption and the monochromatic absorbance predicted by Beer's Law, which is found nonlinear, but very well described by an exponential function:

$$A_1 = 0.021 * (e^{3.7 * A/A_0} - 1) \tag{5.18}$$

where A_1 is the monochromatic absorbance at 580nm, and A/A_0 is the normalized camera imaged absorbance. Thus the camera absorbance are transformed into linear absorbance.

In the following numerical experiments, the actual solute concentration is the monochromatic absorbance, thus Eq. 5.18 need to be performed after we read in the data from the experimental video. Figure 5.6 demonstrates the relationships between

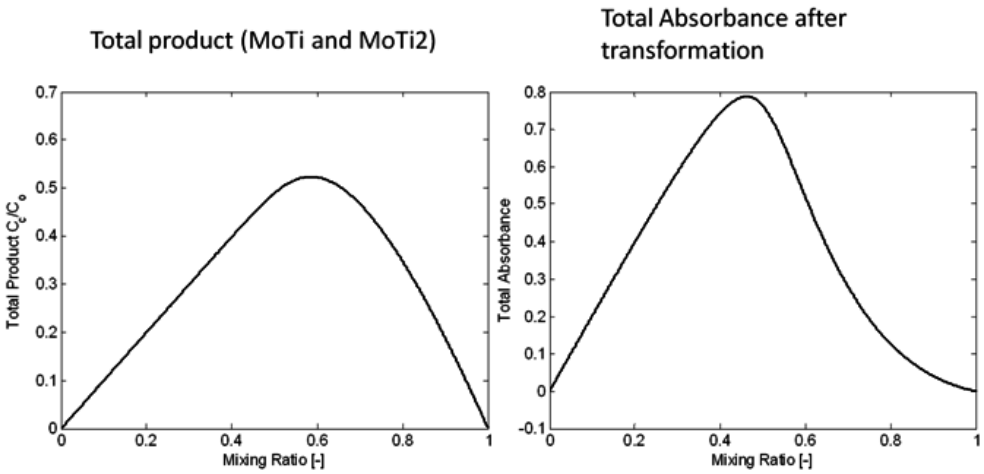

Figure 5.6: Schematic curves that demonstrate the relationship between total product characterized by the monochromatic absorbance in the Mo-Ti reaction and the image absorbance from the camera

total product characterized by the monochromatic absorbance in the Mo-Ti reaction and the image absorbance from the camera.

5.4 Results and Discussion

5.4.1 Conservative Transports

To utilize the experimental data from the visualization chamber experiment, we first capture the high resolution movie and convert the concentration data according to the colorbar values, and store the concentration data at different time t as snapshots for further calculation. Then the concentration mean and variance at the outflow boundary can be computed using the 2D snapshot concentration data.

Figure 5.7(a, b, c) are snapshots from the high-resolution video for conservative transports of mild, intermediate, and highly heterogeneous fields, respectively. The concentration value on each single grid can be read according to the colorbar, thus a detailed mapping of the concentration field can be obtained from the video. Therefore, mean concentration and concentration variance can easily be calculated subsequently.

Figure 5.8(a,b,c) show the mean concentration and concentration variation for

(a)

(b)

(c)

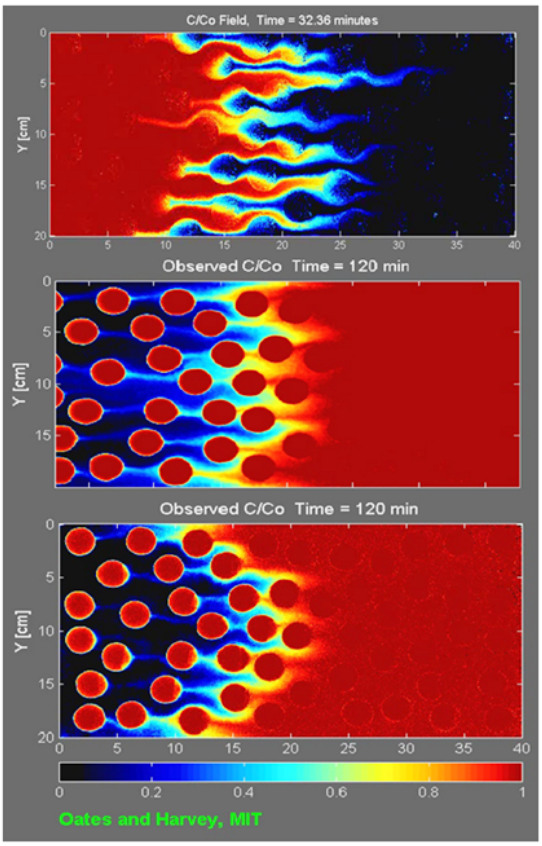

Figure 5.7: Snapshots from the high-resolution video for conservative transports of mild, intermediate, and highly heterogeneous fields, respectively (@*http://web.mit.edu/harvey-lab/Reactive_Transport.html*)

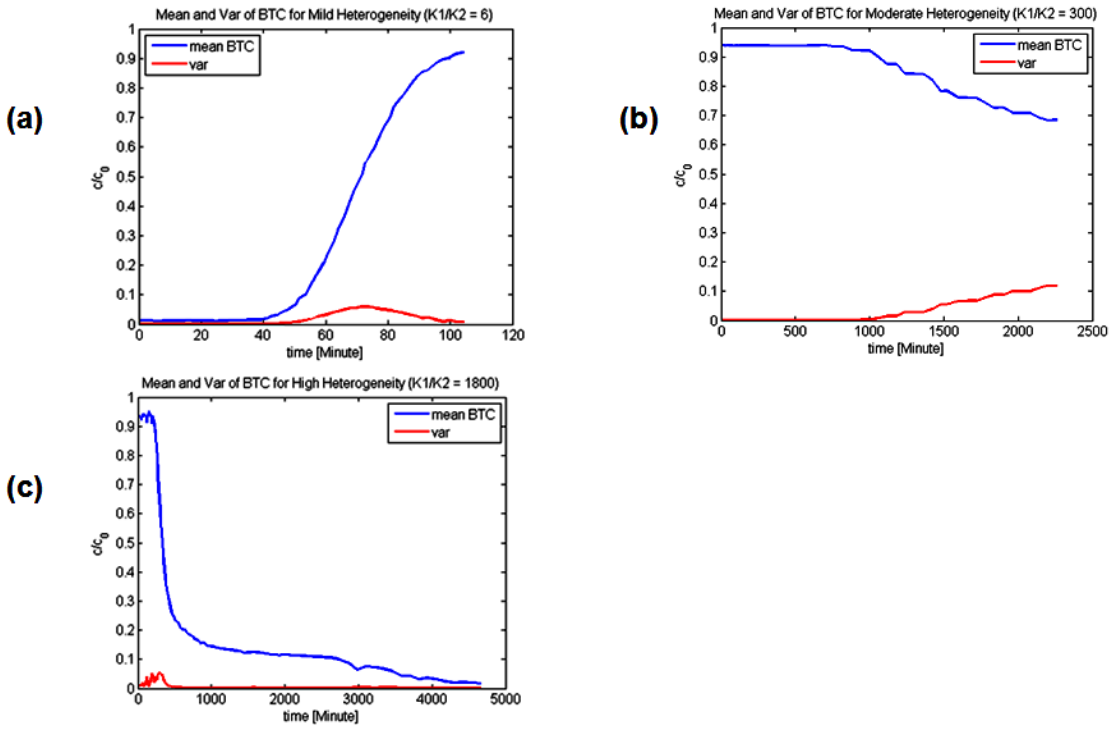

Figure 5.8: Mean and concentration variation for conservative transport breakthrough curve at outflow boundary for mild, intermediate, and highly heterogeneous fields, respectively

mild, intermediate, and highly heterogeneous media at the outflow boundary for conservative transport. As observed from the Figure 5.8b, the concentration data from the experimental video for intermediate heterogeneous media does not contain the full transport process. In the following of this work, we will only use the experimental data for mild and highly heterogeneous media ($K_1/K_2 = 6$ and $K_1/K_2 = 1800$, respectively).

In addition, we calculated the normalized mean square error (NRMSE) to quantify the concentration variance as:

$$NRMSE(X) = \frac{\sum Var(X)}{\sum \overline{X}^2} \tag{5.19}$$

For mild heterogeneous media, NRMSE = 0.054. For highly heterogeneous media, NRMSE = 0.029.

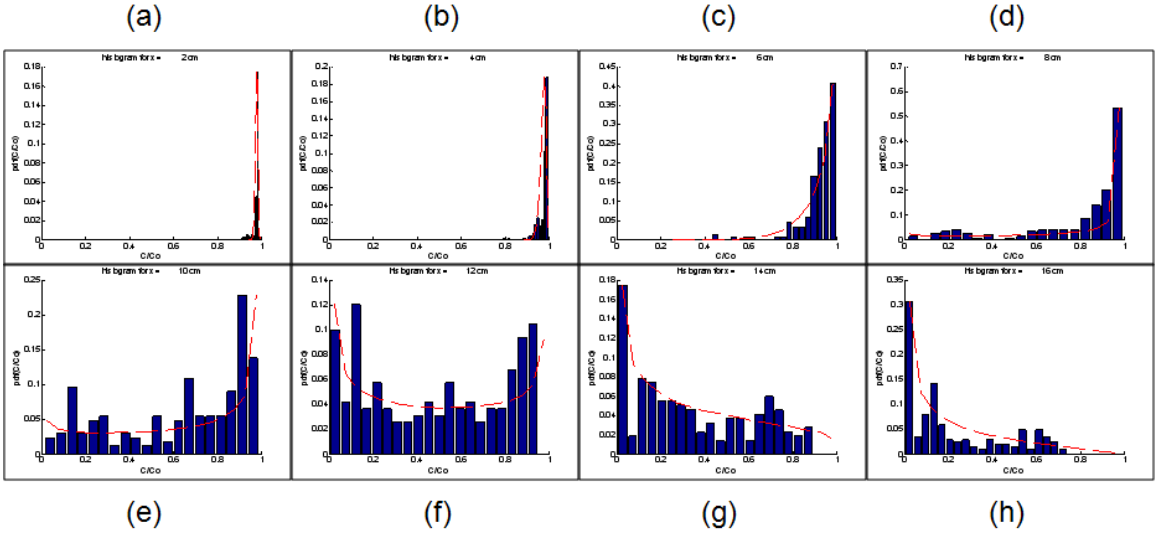

Figure 5.9: Compare histograms for data from video V.S. the fitted beta distributions, for mild heterogeneous field, at different locations along the x-axis. Subfigures from (a)-(h) are corresponding to concentration histograms at $x = 2, 4, 6, 8, 10, 12, 14, 16cm$, respectively. The blue histograms are from experimental video data, and the red lines are the fitted beta distributions, correspondingly

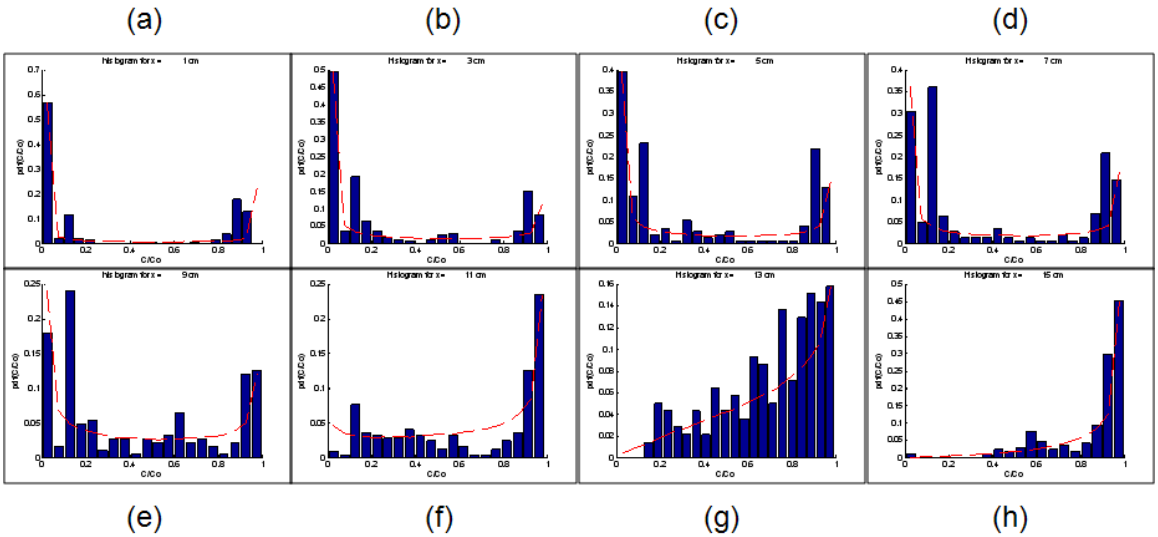

Figure 5.10: Compare histograms for data from video V.S. the fitted beta distributions, for highly heterogeneous field, at different locations along the x-axis. Subfigures from (a)-(h) are corresponding to concentration histograms at $x = 1, 3, 5, 7, 9, 11, 13, 15cm$, respectively. The blue histograms are from experimental video data, and the red lines are the fitted beta distributions, correspondingly

For both mildly and highly heterogeneous fields, the beta-distribution assumption can be validated by the conservative concentration data (Figures 5.9 and 5.10).The beta distribution match the experimental concentration histogram pretty well.

5.4.2 Mixing-controlled Reactive Transport

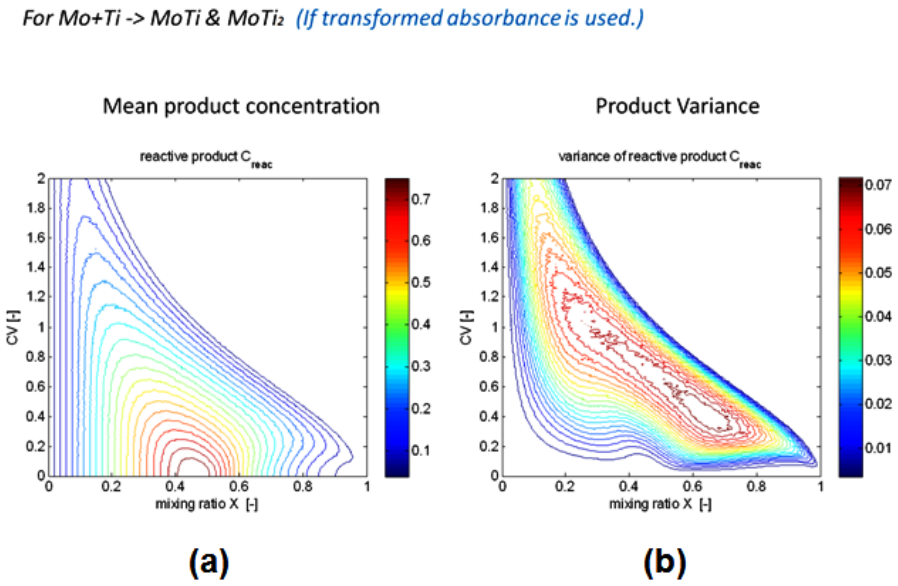

Figure 5.11: 2D mesh plot between mixing ratio, coefficient of variation, and reactive product concentration for Mo-Ti reaction: (a) mean reactive product concentration; (b) variance of reactive product concentration

For the particular Mo-Ti reaction, mean reactive product can be obtained by beta-distribution sampling (Eqs. 5.2 and 5.3) assuming mean concentration (μ) and coefficient of variation($CV = \sigma_c/\mu$) are known and on the mesh grids. Combining the reaction production curve in Figure 5.6, we can give a full contour mapping for mean product concentration and product variance, with respect to conservative mean concentration and concentration variation. Figure 5.11 shows the 2D contour mesh plot for mean product concentration for Mo-Ti reaction, which contains products of MoTi and $MoTi_2$. Except for (μ, CV) values that fall in the lower right corner of

the graph, there is a 1-1 mapping between mixing ratio(equivalent to mean conservative concentration) and concentration variation, thus fix the reactive product mean concentration for a given mean conservative concentration, and subsequently fix the concentration variation for reactive product.

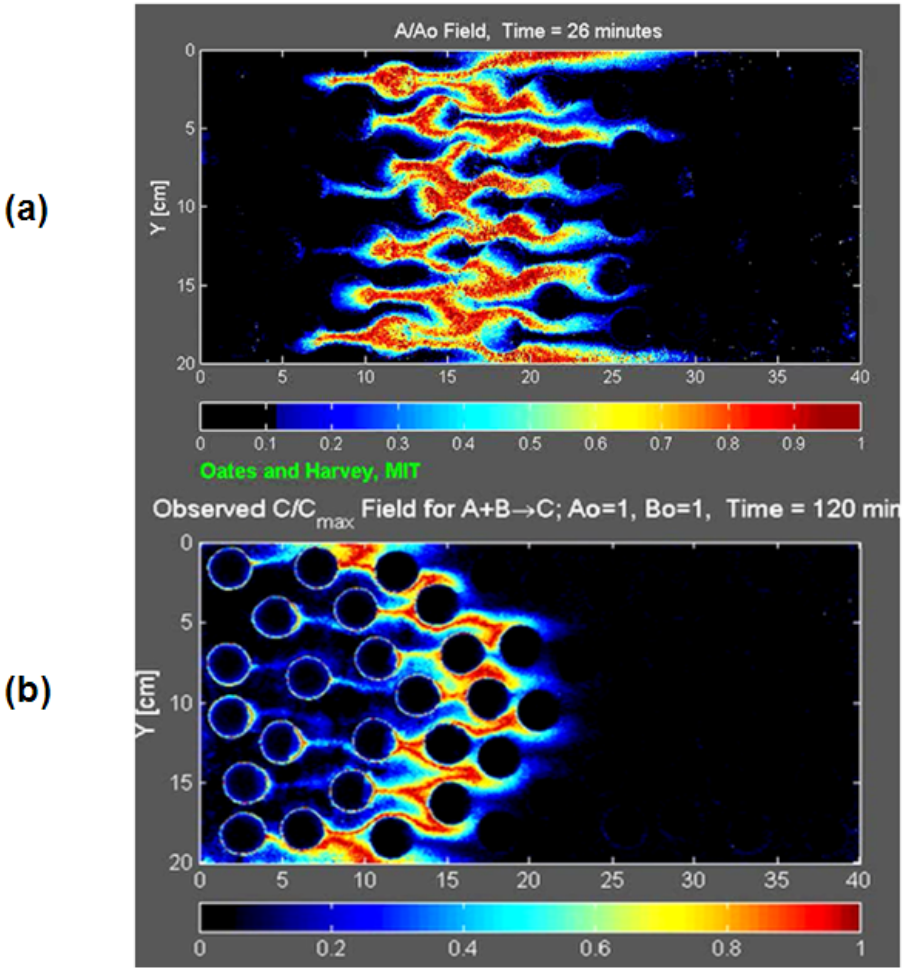

Figure 5.12: Snapshots of reactive transport for mild and highly heterogeneous fields, respectively (@*http://web.mit.edu/harvey-lab/Reactive_Transport.html*)

For the Tiron-molybdate reaction in the visualization experiments, the concentration of reactive product is available from the experimental data. Figures 5.12(a,b) are snapshots from the high-resolution video for conservative transports of mild and highly heterogeneous fields, respectively. The visual plots of concentrations also yield the concentration variance by extracting all local concentration. Figure 5.13(a,b)

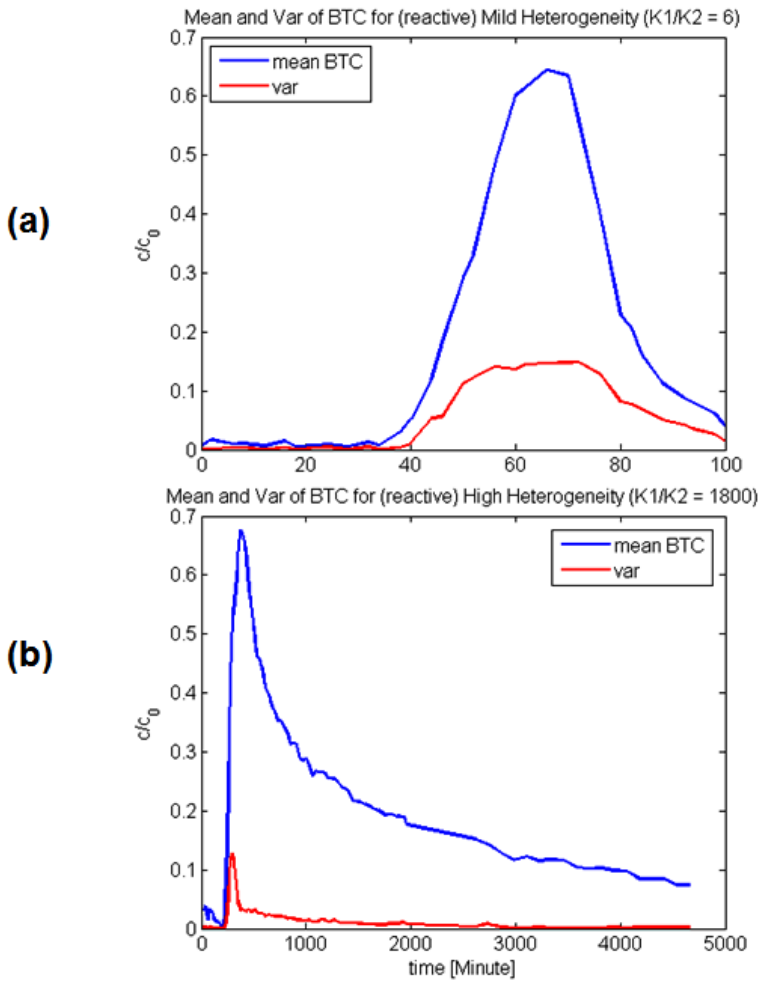

Figure 5.13: Mean and concentration variation for reactive transport breakthrough curve at outflow boundary for mild and highly heterogeneous fields, respectively

show the concentration mean and variance data for the concentration breakthrough curves of Tiron-molybdate reaction product at the outflow boundary, for mild and highly heterogeneous fields, respectively. For mild heterogeneous media, NRMSE = 0.220; and for highly heterogeneous media, with NRMSE = 0.057.

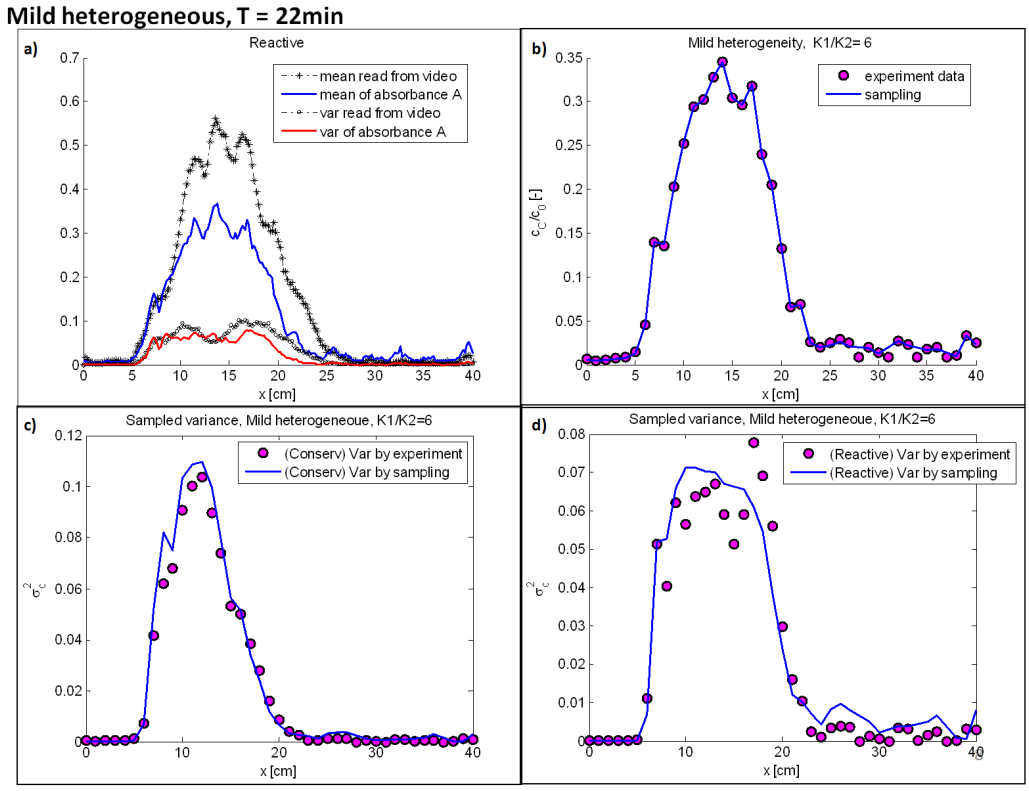

Figure 5.14: Performance of fitted beta-distributed conservative concentration variance for reactant A at snapshot time $T = 22\,\text{min}$, for mild heterogeneous media

Figure 5.14 shows a reactive concentration fitting at $T = 22\,\text{min}$ for mild heterogeneous field. By sampling the beta-distribution, we can fit the mean reactive concentration and the concentration variance for conservative concentration very well (Figure 5.14b, c). With these information, we obtain the sampled concentration variance for reactive concentration (Figure 5.14d), which is in accordance with experimental data. Figure 5.15 shows similar results for highly heterogeneous field.

Figure 5.16 shows that the developed approach yields very good prediction results for the breakthrough curves at the outflow boundary for highly heterogeneous media

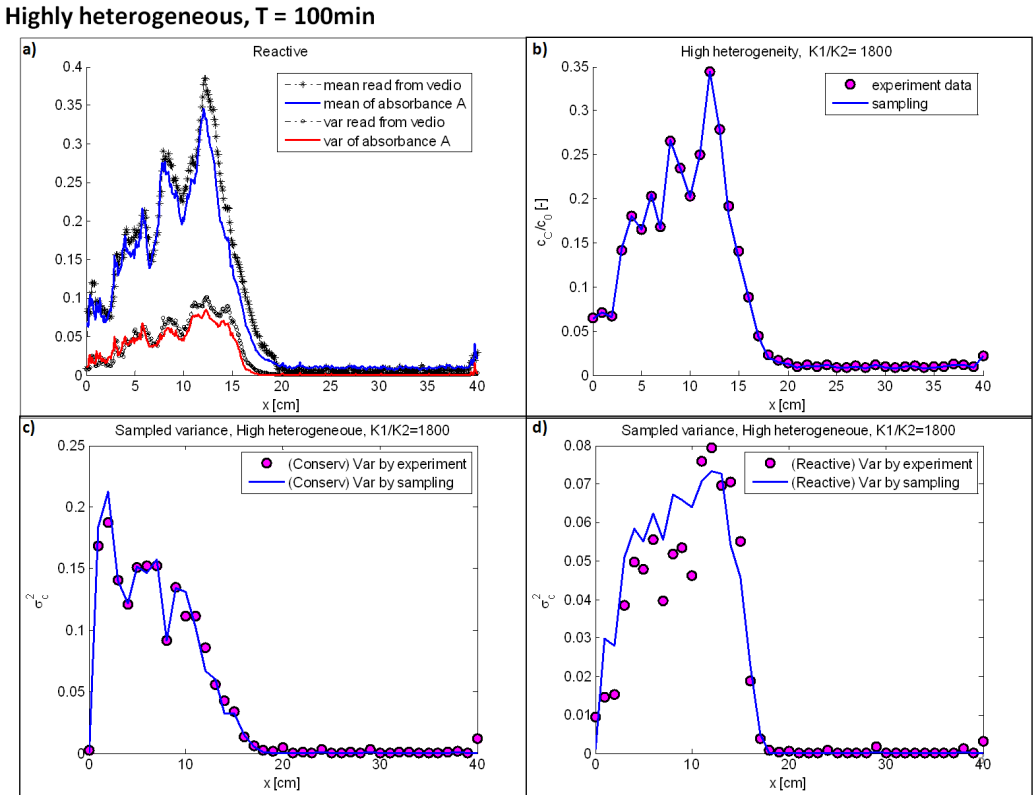

Figure 5.15: Performance of fitted beta-distributed conservative concentration variance for reactant A at snapshot time $T = 100\,\text{min}$, for highly heterogeneous media

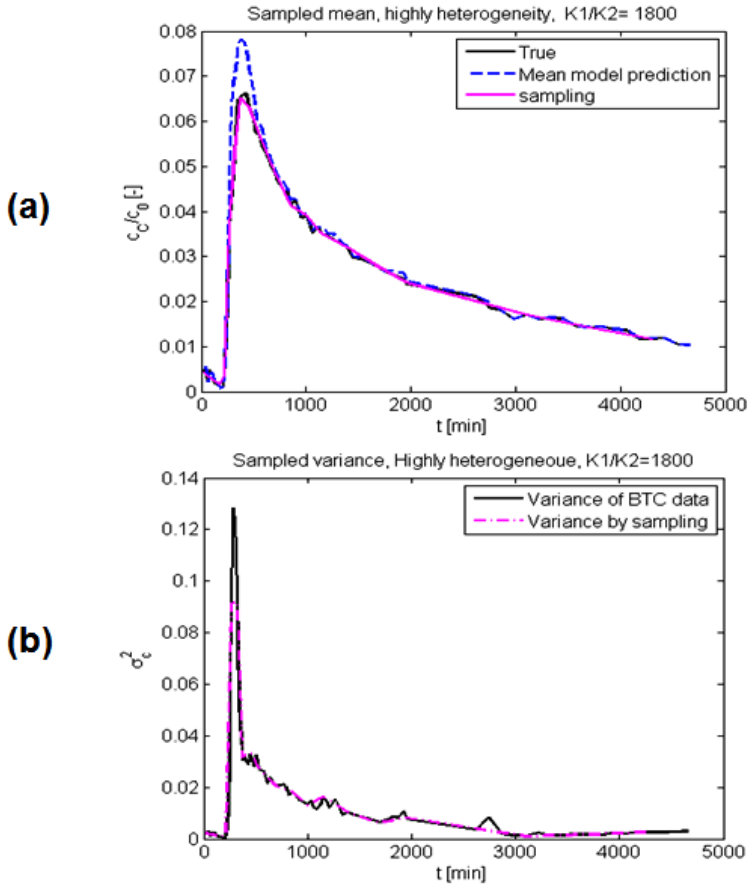

Figure 5.16: Reproduce concentration variance for reactive transport in highly heterogeneous media by sampling technique:(a) fitted mean breakthrough curve; (b) fitted concentration variance by sampling technique

by sampling the approximated beta distribution, while macroscopic model (mean model) from the conservative tracer test overestimated the peak. The uncertainty analysis is straightforward based on the samples. The mean concentration can either directly use the measured breakthrough curve because the step injection mode is applied to both conservative and reactive transport or use the predicted concentration breakthrough curve by the upscaled macroscopic model.

Figure 5.17 shows fitted macroscopic transport model for predicting conservative transport in mild heterogeneous chamber, at four different time snapshots: $T = 8, 22, 36, 50$ min. Figure 5.18 shows the corresponding reactive species concentrations

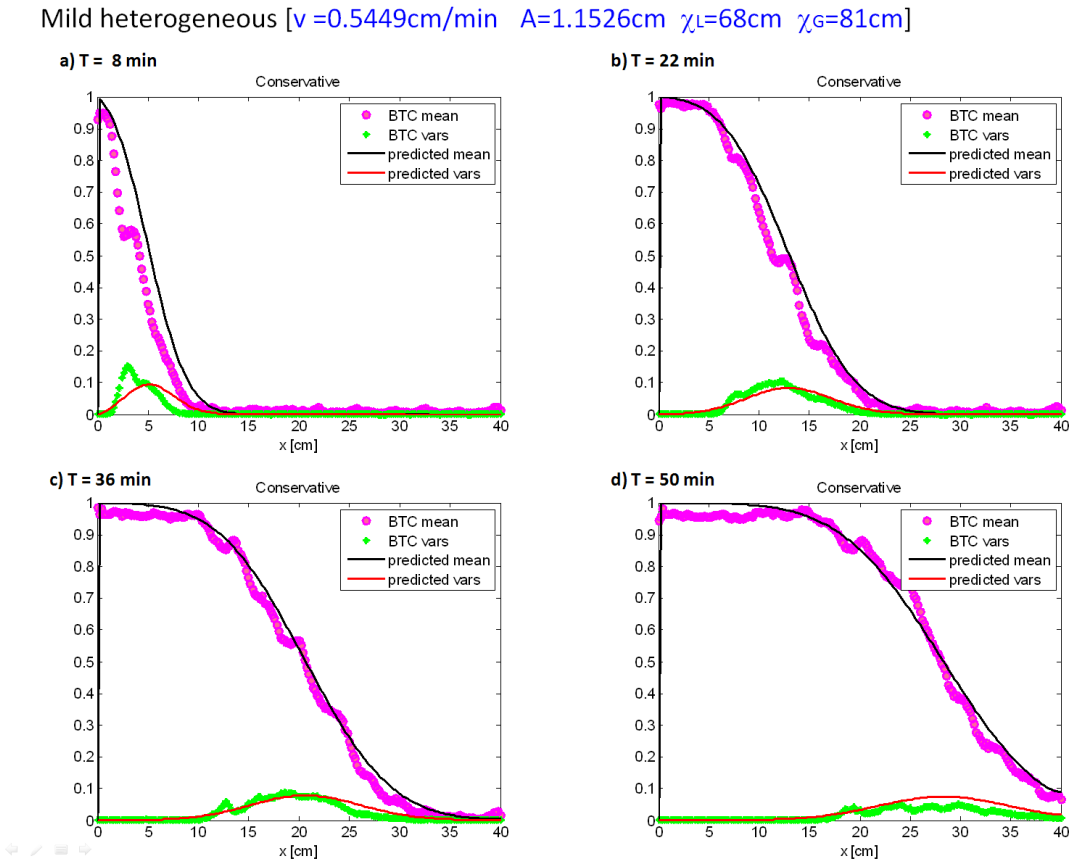

Figure 5.17: Predicted mean concentration and concentration variance for conservative transport in mild heterogeneous chamber, at four different time snapshots

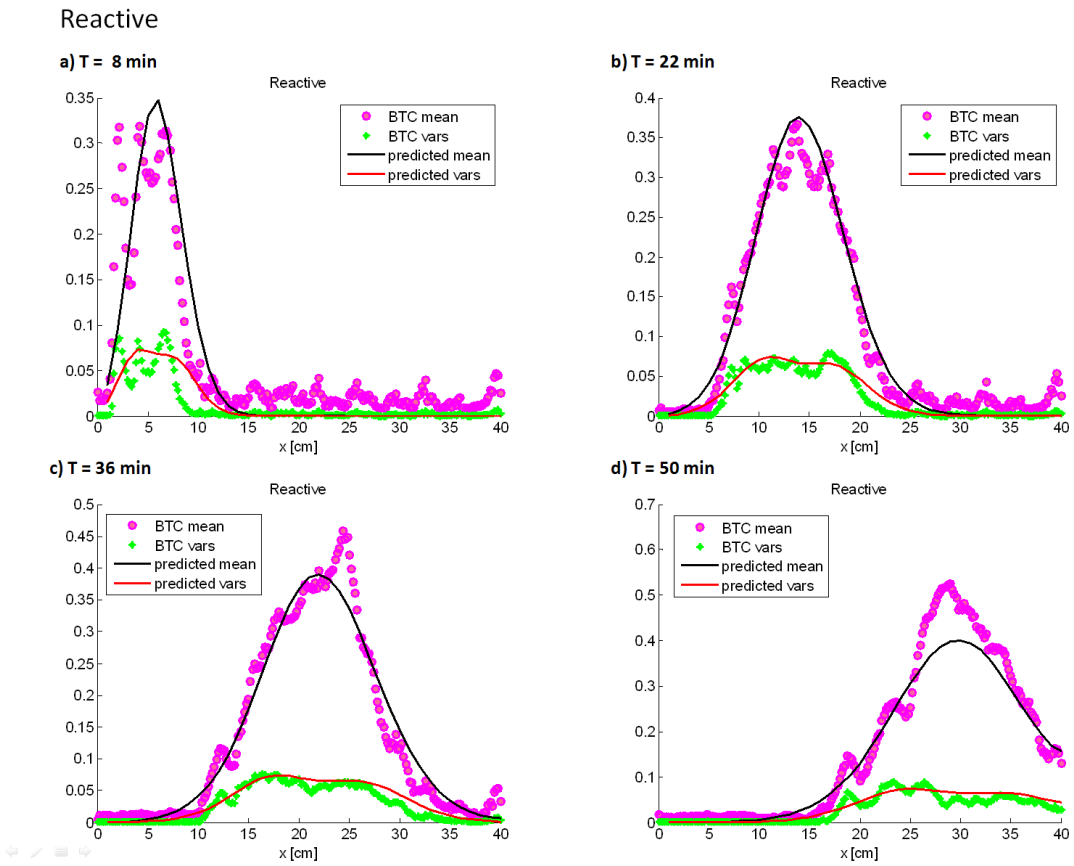

Figure 5.18: Predicted mean concentration and concentration variance for reactive transport in mild heterogeneous chamber, at four different time snapshots

for reactive transport. Our developed approach clearly demonstrate good predictive power for estimating concentration variance and predicting mixing-controlled reactive transport.

Figure 5.19 demonstrates the sensitivity of parameters χ_L and χ_G when fitting the 1-dimensional mean and concentration model (Eqs. 5.8). In fact, there is a range of values for the parameter pair (χ_L,χ_G) that gives similar fitting performance regarding the experimental data we used.

5.5 Conclusions

Characterization of concentration variance is the key for modeling mixing-controlled reactive transport. Concentration variance is usually difficult to measure because it

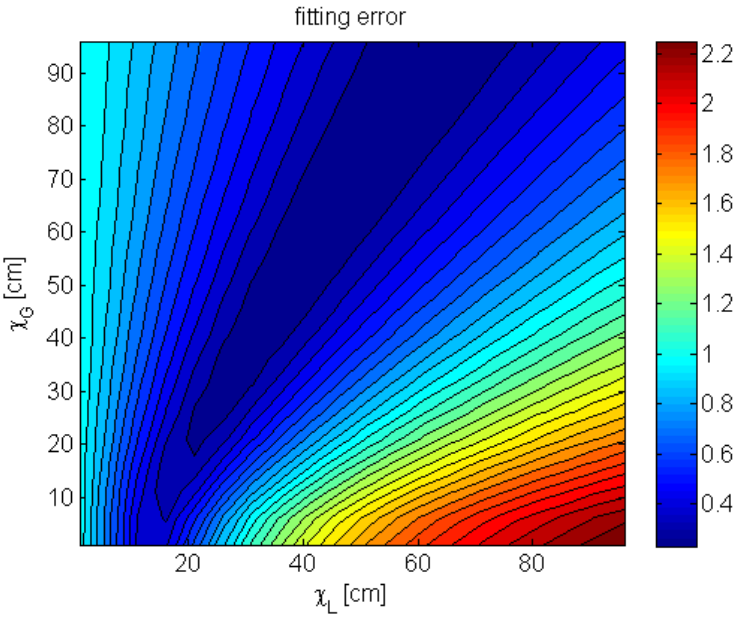

Figure 5.19: Sensitivity measurement for χ_L and χ_G

requires many local measurements. In this research, we propose to use mean concentration breakthrough curves of both conservative and reactive tracers to estimate the concentration variance. The conservative breakthrough curve only contains the information of mean concentrations, while the reactive breakthrough curves are results of both concentration mean and variance. Based on the relationship between conservative and reactive concentrations, we can estimate the variance by sampling the beta distribution to fit the mean reactive breakthrough curve. For prediction, both mean and fitted variance can be described by macroscopic transport models: one for mean concentration, and the other for the variance with additional parameters. Our approach is validated by the visualization experiments conducted at MIT. Although the experiments provide all concentration distributions, our approach only requires both conservative and reactive breakthrough curves at observation locations. In addition, our results suggest that one should conduct both conservative and reactive tracer tests for upscaling macroscopic transport models because conservative tracer

tests are insufficient for evaluating local concentration variations.

CHAPTER VI

A DUAL-PERMEABILITY TRANSPORT MODEL FOR SIMULATING MIXING-CONTROLLED REACTIVE TRANSPORT

6.1 Introduction

Upscaling macroscopic reactive transport models is necessary for predicting contaminant fate and transport in the heterogeneous subsurface because detailed characterization of spatial variability and uncertainty of hydraulic parameters is usually unavailable at field sites. Macroscopic models are usually calibrated by flux-averaged breakthrough curves of a conservative tracer and coupled with reaction kinetics determined in laboratory experiments. Such macroscopic models may inaccurately predict breakthrough curves of reactive species because they neglect concentration variations at local scale when evaluating effective reaction rates for nonlinear reactions limited by solute mixing [e.g., *Molz and Widdowson*, 1988; *MacQuarrie and Sudicky*, 1990; *Kitanidis*, 1994; *Kapoor et al.*, 1997; *Cirpka and Kitanidis*, 2000a; *Raje and Kapoor*, 2000; *Cirpka*, 2002; *Gramling et al.*, 2002; *Dentz and Carrera*, 2007; *Luo et al.*, 2008]. *Luo and Cirpka* [2011] showed that even a "perfect" macroscopic model, which may exactly reproduce the mean breakthrough curve of a conservative tracer, may yield significant errors in predicting concentration breakthrough curves of reactive species in mixing-controlled reactive transport. Such inconsistence between macroscopic mean models assuming perfect mixing and the inherent solute segregation or incomplete mixing at local scale has become a research focus in recent years (see a recent review by *Dentz et al.* [2010]).

In general, macroscopic models of mean concentrations can provide accurate prediction for mixing-controlled reactive transport only when concentration variations are negligible compared with mean concentrations or for linear reactions, the rate of which is independent of the degree of mixing. To improve the predictive ability of macroscopic mean models, many sophisticated models have been developed such as multi-rate mass transfer models [*Haggerty and Georelick*, 1995], and continuous time random walk [*Berkowitz and Scher*, 1997, 1998;], and fractal dispersion models [*Benson, et al*, 2000]. Such models are capable of describing anomalous behavior, particularly enhanced tailing, of concentration breakthrough curves, which cannot be characterized well by classical advection-macrodisperion models. Several recent studies showed that these models may improve the prediction of mixing-controlled reactive transport in heterogeneous media [*Edery et al.*, 2009; *Willmann et al.*, 2010]. However, *Luo and Cirpka* [2011] showed that only under specific conditions these improved models can be effective, such as in highly-heterogeneous media or nearly homogeneous media with low flux-averaged concentration variances. In media with intermediate hydraulic conductivity contrast, such models may still yield significant errors in predicting mixing-controlled reactive transport. The decisive point is that such models conceptualize a single concentration within the solute flux in the mobile domain. Therefore, they cannot account for any effects caused by concentration fluctuations within the flux. For example, the multirate mass transfer model can describe anomalous transport behavior by varying local memory functions for characterizing incomplete mixing in the immobile domains. However, for the flow flux leaving a domain, only the mobile contributions count. Thus, such models with a single mobile flux concentration are strictly incapable to account for variations within the flux, no matter whether reactions are considered in the immobile domain(s) or not. We see a clear research need in deriving upscaled nonlocal transport formalisms that go beyond ensemble mean concentrations so that both long-tails or other anomalous features of

the flux-averaged breakthrough curves can be captured and concentration variations be quantified.

A good macroscopic model should be able to describe both spreading and mixing. In cases when concentration fluctuations cannot be neglected, both mean concentrations and concentration variances should be evaluated for predicting mixing-controlled reactive transport. A specific modeling framework, which accounts for both the mean concentration and its variance, is based on transport equations of the concentration variance in addition to macroscopic mean models [*Kapoor et al.*, 1997]. The variance transport equation involves terms for the generation and destruction of the concentration variance, which are difficult to measure or to predict from statistical metrics of the flow field. From conservative-concentration statistics (mean and variance), attempts have been made to estimate the concentration covariance of reactive species in nonlinear mixing-controlled reactive transport, which is subsequently used to correct reaction rates [*Oates*, 2007]. More elaborate models have targeted the full concentration distribution of conservative species [e.g., *Fiorotto and Caroni*, 2002, 2003], which has been shown to resemble a beta distribution. For specific cases, such as instantaneous bimolecular reactions or biokinetic reactions at steady state, the local statistics of conservative species can be mapped to those of reactive species without relying on linearization [*Cirpka et al.*, 2008, 2011].

An alternative modeling framework is based on the effective mixing concept and multi-scale measurements. In the analysis of point-like observations of solute breakthrough, longitudinal dispersion does not alter the mean breakthrough time at any location, whereas transverse dispersion balances differences of mean breakthrough time between adjacent streamtubes in heterogeneous formations. Both processes lead to wider local breakthrough curves. Thus, a particular set of point-like measured breakthrough curves within an observation plane may be interpreted as caused by transport with transverse dispersion in a highly variable velocity field or by transport

with enhanced longitudinal dispersion rather than transverse exchange, but in a less variable velocity field. This ambiguity is used in the advective-dispersive streamtube (ADS) approach within an Eulerian-Lagrangian framework [*Cirpka and Kitanidis*, 2000a, b; *Ginn*, 2001; *Ginn et al.*, 2001; *Cirpka*, 2002; *Janssen et al.*, 2006; *Luo and Cirpka*, 2008]. The essence of this approach is to characterize the "right" mixing and "right" variability of advection. The dispersion of the mean concentration breakthrough curve or macrodisperion is the summation of the mean dispersion of local-scale breakthrough curves and the variance of the mean of local breakthrough curves (also referred as the two-particle covariance [*Fiori and Dagan*, 2000; *Pannone and Kitanidis*, 2004]). The "right" mixing is the mean dispersion of local-scale measurements, while the variance of the mean describing the advection variations should not be included for evaluating mixing. The "right" advection is then described by an advective travel-time distribution. Integration of all local concentration breakthrough curves over the entire travel-time distribution yields the mean concentration breakthrough curve at the outflow boundary. *Cirpka* [2002] studied a bimolecular reactive transport case, in which the original reaction terms were maintained, i.e., concentration covariance was not included in the reaction rate, while effective heterogeneity-induced mixing was characterized by the effective dispersion tensor [*Dentz et al.*, 2000].

Both numerical and experimental work showed good applicability of these two modeling frameworks [*Cirpka*, 2002; *Janssen et al.*, 2006; *Oates*, 2007; *Cirpka et al.*, 2008]. The essential difference between them is that the first one aims to evaluate effective reaction rates by explicitly accounting for the concentration covariance or the entire distribution, while the latter approximates solute segregation by a number of non-interacting streamtubes. The first approach may become complicated for non-linear, heterogeneous reactions involving many species and different phases because of the challenges in evaluating the covariance matrix [*Miralles-Wilhelm et al.*, 1997]. The

latter is more efficient for simulating multi-species reactive transport given the "right" advective travel-time distribution and the effective mixing parameters because within each streamtube it is a classical one-dimensional transport problem. However, it is only applicable at locations where both point-scale and integral-scale measurements are available, and it is difficult to make predictions at locations without multi-scale measurements because it is challenging to predict apparent "right" mixing parameters and "right" advective travel-time distributions [*Luo and Cirpka*, 2008]. Furthermore, numerical solutions of both modeling frameworks require sophisticated numerical approaches, such as inverse modeling of travel-time distributions [*Luo and Cirpka*, 2008] and evaluation of concentration curvature fields [*Kapoor and Kitanidis*, 2000; *Luo et al.*, 2008], which are usually unavailable in widely-applied solute transport codes.

In this study, we present a dual-permeability modeling framework to upscale mixing-controlled reactive transport in heterogeneous media. Its conceptualization is similar to the dual-porosity model in which the medium is assumed to consist of two distinct pore systems with different hydraulic properties and kinetic mass transfer between them [*Dykhulzen*, 1987; *Gerke and van Genuchten*, 1993]. The dual-porosity model has successfully been applied to simulate the preferential movement of water and solutes in structured soils or fractured rocks [*Gerke and van Genuchten*, 1993]. Stochastic analysis was also conducted for solute transport in heterogeneous, dual-permeability media [e.g., *Hu et al.*, 2002]. However, it has not been applied to upscale mixing-controlled reactive transport in heterogeneous media. The dual-permeability model considers the concentration at any location as a flux-weighted or volume-weighted mean of the two concentrations in two pore systems, which naturally yield the evaluation of the concentration variance within the flux and within the volume. The present research aims to use the dual-permeability model to quantify both concentration mean and variance for evaluating mixing-controlled reactive transport, while most previous studies of the dual-permeability model focused on

the mean behavior of conservative transport. In some sense, the dual-permeability model is the simplest streamtube method with only two streamtubes. However, the dual-permeability model considers kinetic mass transfer between the two streamtubes that cannot be incorporated in the non-interacting streamtube method. Furthermore, solution of the dual-permeability model is much simpler than the models discussed above. An analytical solution was recently reported for conservative transport [*Leij et al.*, 2012]. Finally, we shall notice that the dual-permeability model for simulating mixing-controlled reactive transport is not just a mathematical manipulation. Both laboratory and numerical experiments have demonstrated that it may be necessary to include one more advection term to simulate solute transport in media with intermediate hydraulic conductivity contrast [*Gramling et al.*, 2002; *Luo and Cirpka*, 2011; *Leij et al.*, 2012].

6.2 Dual-Permeability Model

6.2.1 Governing Equations

The subsurface medium is conceptualized as two overlapped domains with different flow velocities and dispersion coefficients and a linear kinetic mass transfer term between. The transport governing equations for a conservative tracer are given by [*Dykhulzen*, 1987; *Gerke and van Genuchten*, 1993; *Leij et al.*, 2012]:

$$\theta_f \frac{\partial c_f}{\partial t} = -q_f \frac{\partial c_f}{\partial x} + \theta_f D_f \frac{\partial^2 c_f}{\partial x^2} + \alpha \left(c_s - c_f \right) \tag{6.1}$$

$$\theta_s \frac{\partial c_s}{\partial t} = -q_s \frac{\partial c_s}{\partial x} + \theta_s D_s \frac{\partial^2 c_s}{\partial x^2} + \alpha \left(c_f - c_s \right) \tag{6.2}$$

where c_f and c_s are concentrations in the fast- and slow-flow domain, respectively; t is time; x is travel distance; θ_f and θ_s are porosities of the fast- and slow-flow domains, respectively; q_f and q_s are specific discharges; D_f and D_s are dispersion coefficients, and α is the first-order mass transfer rate coefficient. By neglecting molecular diffusion and assuming the same dispersivity, D_f and D_s are written as:

$$D_f = \alpha_l v_f = \alpha_l q_f / \theta_f \tag{6.3}$$

$$D_s = \alpha_l v_s = \alpha_l q_s / \theta_s \tag{6.4}$$

in which α_l is the apparent longitudinal dispersivity, and v_f and v_s are fast and slow velocities. Different dispersivities may be defined but analytical solution may not be available [*Leij et al.*, 2012].

For a Dirac impulse input of mass at the inlet of an initially free, semi-infinite domain, the boundary and initial conditions are defined as:

$$v_f c_f - D_f \left.\frac{\partial c_f}{\partial x}\right|_{x=0} = \frac{m_{in} v_f}{A\left(v_f + v_s\right)} \delta\left(t\right) \tag{6.5}$$

$$v_s c_s - D_s \left.\frac{\partial c_s}{\partial x}\right|_{x=0} = \frac{m_{in} v_s}{A\left(v_f + v_s\right)} \delta\left(t\right) \tag{6.6}$$

$$\left.\frac{\partial c_f}{\partial x}\right|_{x=\infty} = \left.\frac{\partial c_s}{\partial x}\right|_{x=\infty} = 0 \tag{6.7}$$

$$c_f\left(x, 0\right) = c_s\left(x, 0\right) = 0 \tag{6.8}$$

where m_{in} is the input mass at the domain inlet, and δ is the Dirac delta function.

6.2.2 Dimensional Analysis

For the transport model presented above, it will be more convenient to consider its dimensionless form. First, we introduce the porosity and discharge flow ratios:

$$\beta = \frac{\theta_f}{\theta_s} \tag{6.9}$$

$$\eta = \frac{q_f}{q_s} \tag{6.10}$$

in which β is the porosity ratio and η is the discharge ratio, which may be interpreted as the hydraulic conductivity or permeability contrast given the same hydraulic gradient for the fast- and slow-flow domain. The velocity contrast can then be expressed as:

$$\frac{v_f}{v_s} = \frac{q_f/\theta_f}{q_s/\theta_s} = \eta/\beta \geq 1 \tag{6.11}$$

For a transport system with a total flow discharge $q = q_f + q_s$ and a total porosity $\theta = \theta_f + \theta_s$, we have:

$$q_f = \frac{\eta}{1+\eta} q \tag{6.12}$$

$$q_s = \frac{1}{1+\eta} q \tag{6.13}$$

$$\theta_f = \frac{\beta}{1+\beta} \theta \tag{6.14}$$

$$\theta_s = \frac{1}{1+\beta} \theta \tag{6.15}$$

We introduce dimensionless parameters in terms of the total specific discharge q and total porosity θ:

$$\text{Concentration: } C_f = \frac{Ac_f}{m_{in}}, C_s = \frac{Ac_s}{m_{in}} \tag{6.16}$$

$$\text{Travel distance: } X = \frac{x}{L} \tag{6.17}$$

$$\text{Time:} T = \frac{qt}{\theta L} \tag{6.18}$$

$$\text{Péclet number:} P_e = \frac{L}{\alpha_l} \tag{6.19}$$

$$\text{Damköhler number: } D_a = \frac{\alpha L}{q} \tag{6.20}$$

in which L is the travel distance at the domain outlet, and $T = 1$ corresponds to one pore volume (PV) of the entire domain.

Eqs. (6.1) and (6.2) can be transformed to:

$$\frac{\partial C_f}{\partial T} = \frac{\eta\,(1+\beta)}{(1+\eta)\,\beta} \left(-\frac{\partial C_f}{\partial X} + \frac{1}{P_e} \frac{\partial^2 C_f}{\partial X^2} \right) + \frac{1+\beta}{\beta} D_a \left(C_s - C_f \right) \tag{6.21}$$

$$\frac{\partial C_s}{\partial T} = \frac{1+\beta}{1+\eta} \left(-\frac{\partial C_s}{\partial X} + \frac{1}{P_e} \frac{\partial^2 C_s}{\partial X^2} \right) + (1+\beta)\, D_a \left(C_f - C_s \right) \tag{6.22}$$

and the boundary and initial conditions become:

$$C_f - \frac{1}{Pe}\frac{\partial C_f}{\partial X}\bigg|_{X=0} = \delta(T) \tag{6.23}$$

$$C_s - \frac{1}{Pe}\frac{\partial C_s}{\partial X}\bigg|_{X=0} = \delta(T) \tag{6.24}$$

$$\frac{\partial C_f}{\partial X}\bigg|_{X=\infty} = \frac{\partial C_s}{\partial X}\bigg|_{X=\infty} = 0 \tag{6.25}$$

$$C_f(X,0) = C_s(X,0) = 0 \tag{6.26}$$

6.2.3 Analytical Solution

For investigating concentration breakthrough curves, we focus on the flux concentration:

$$C_f^* = C_f - \frac{1}{Pe}\frac{\partial C_f}{\partial X} \tag{6.27}$$

$$C_s^* = C_s - \frac{1}{Pe}\frac{\partial C_s}{\partial X} \tag{6.28}$$

Leij et al. [2012] presented an analytical solution for residence concentrations with a first-type step input boundary condition. Following the same procedure, we obtain the Laplace solutions for flux concentrations with the defined input boundary condition of the third type:

$$\bar{C}_f^* = \frac{V_1 - V_1V_2}{V_1 - V_2}\exp\left[\frac{XP_e}{2}\left(1-\sqrt{1+4\lambda_1/P_e}\right)\right] + \frac{-V_2 + V_1V_2}{V_1 - V_2}\exp\left[\frac{XP_e}{2}\left(1-\sqrt{1+4\lambda_2/P_e}\right)\right] \tag{6.29}$$

$$\bar{C}_s^* = \frac{1 - V_2}{V_1 - V_2}\exp\left[\frac{XP_e}{2}\left(1-\sqrt{1+4\lambda_1/P_e}\right)\right] + \frac{-1 + V_1}{V_1 - V_2}\exp\left[\frac{XP_e}{2}\left(1-\sqrt{1+4\lambda_2/P_e}\right)\right] \tag{6.30}$$

in which λ_1 and λ_2 are:

$$\lambda_1 = \frac{1+\eta}{2(1+\beta)\eta}\left(D_a b_1 + s a_1 + r\right) \tag{6.31}$$

$$\lambda_2 = \frac{1+\eta}{2(1+\beta)\eta}\left(D_a b_1 + s a_1 - r\right) \tag{6.32}$$

and V_1 and V_2 are:

$$V_1 = \frac{D_a b_2 + s a_2 - r}{2 D_a \eta(\beta+1)} \tag{6.33}$$

$$V_2 = \frac{D_a b_2 + s a_2 + r}{2 D_a \eta(\beta+1)} \tag{6.34}$$

with the defined variables:

$$a_1 = \eta + \beta, \quad a_2 = \eta - \beta \tag{6.35}$$

$$b_1 = (1+\beta)(\eta+1), \quad b_2 = (1+\beta)(\eta-1) \tag{6.36}$$

$$r(s) = \sqrt{D_a^2 b_1^2 + 2 D_a s a_2 b_2 + a_2^2 s^2} \tag{6.37}$$

The flux-averaged breakthrough curve is the mixture of solutions in the two pore systems. Thus, the mean concentration is given by:

$$C_m^* = \frac{q_f}{q} C_f^* + \frac{q_s}{q} C_s^* = \frac{\eta}{1+\eta} C_f^* + \frac{1}{1+\eta} C_s^* \tag{6.38}$$

and its Laplace solution is

$$\bar{C}_m^* = \frac{\eta}{1+\eta} \bar{C}_f^* + \frac{1}{1+\eta} \bar{C}_s^*$$

The concentration variance within the flux is given by:

$$\begin{aligned} \sigma_C^2 &= \frac{\eta}{1+\eta}\left(C_f^* - C_m^*\right)^2 + \frac{1}{1+\eta}\left(C_s^* - C_m^*\right)^2 \\ &= \frac{\eta}{(1+\eta)^2}\left(C_f^* - C_s^*\right)^2 \end{aligned} \tag{6.39}$$

and

$$\bar{C}_f^* - \bar{C}_s^* = \frac{(V_1 - 1)(V_2 - 1)}{V_1 - V_2} \left\{ \exp\left[\frac{XP_e}{2} \left(1 - \sqrt{1 + 4\lambda_2 / P_e} \right) \right] - \exp\left[\frac{XP_e}{2} \left(1 - \sqrt{1 + 4\lambda_1 / P_e} \right) \right] \right\} \tag{6.40}$$

The mean concentration and variance may also be defined for the residence concentration weighted by the porosities.

6.3 Behavior of Concentration Variance within the Flux

The concentration variance within the flux at a given location, $X = 1$ for the outlet, is controlled by the dimensionless parameters: β, η, P_e and D_a, in which β and η mainly control the flow velocity and discharge contrast, whereas P_e and D_a describe the mixing effects. In the following, we will focus on the concentration variance within the flux for a step input at the inlet, which is also the displacement reactive transport case that will be studied in the next section. The concentration breakthrough curves are simply the time integrals of the solutions presented in the previous section. The normalized root mean squared error (NRMSE) is used to quantify the concentration variance within the flux,

$$NRMSE = \frac{\sqrt{\int \sigma_C^2 dT}}{C_{\max}^* - C_{\min}^*} \tag{6.41}$$

in which $C_{\max}^* = 1$ and $C_{\min}^* = 0$ for a step input.

6.3.1 Effects of Flow Contrast

Figure 6.1 shows the effects of the porosity ratio and discharge contrast (or hydraulic conductivity contrast). For given constant mixing parameters, P_e and D_a, and porosity ratio, β, the concentration variance within the flux is a non-monotonic function of the discharge contrast, η (Figure 6.1a). The maximum concentration variance occurs at an intermediate value of η. This observation is consistent to the findings of

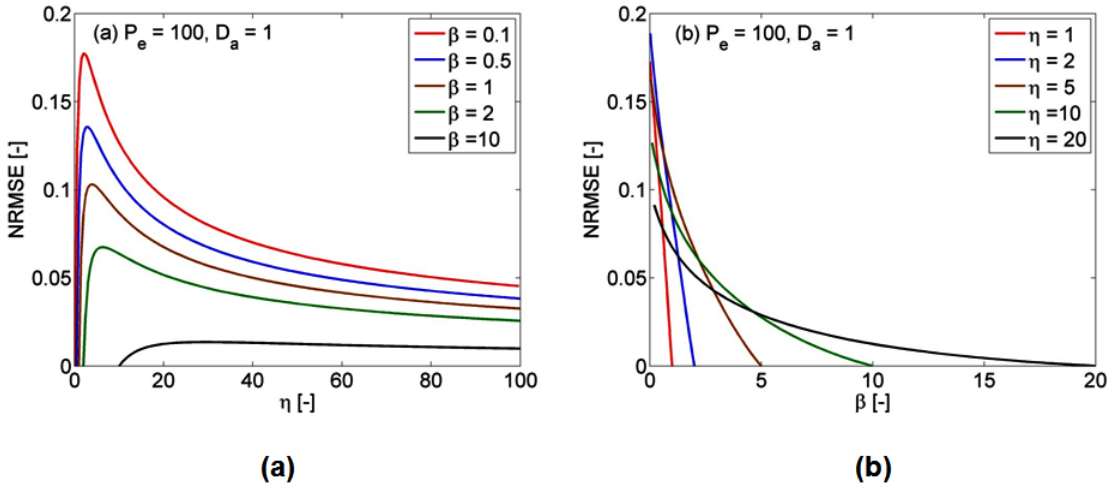

Figure 6.1: The concentration variance (quantified by NRMSE) within the flux, for given constant mixing parameters, P_e and D_a, and porosity ratio, β

Luo and Cirpka [2011]: Macroscopic mean models that perfectly fit flux-averaged conservative concentration breakthrough curves may not improve the prediction of mixing-controlled reactive transport in cases with intermediate hydraulic conductivity contrast, because it is necessary to quantify and account for the variability of conservative concentrations in the flux. In high contrast cases, most flow takes place in the fast flow paths, which results in a small variance of the flux-weighted concentration even though the offset in the breakthrough between the slow and fast travel paths is substantial. Figure 6.1b shows that the concentration variance monotonically decreases with the porosity ratio for given discharge contrast. Since the discharge contrast relates to the ratio of specific discharge, an increase in the ratio of porosities implies a decrease in the ratio of effective velocity thus reducing the concentration variance.

Figure 6.2 shows several breakthrough curves of concentrations in the two domain and flux averaged as well as breakthrough curves of the concentration variance. The NRMSE or the overall variance, Eq. (6.41), is determined by both the magnitude of the variance and the duration over which the concentrations in the two domains

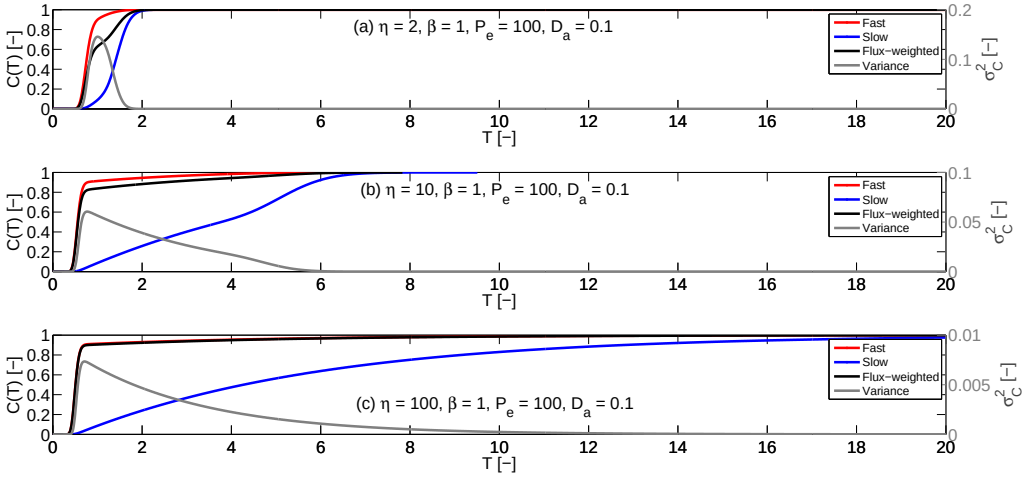

Figure 6.2: Breakthrough curves of concentrations in the two domain and flux averaged, and breakthrough curves of the concentration variance

significantly differ. At a smaller discharge and velocity contrast (Figure 6.2a), the variance magnitude (see the peaks of variances in Figure 6.2a, b, and c) is greater, but the duration of large concentration variance is shorter. At a larger discharge and velocity contrast (Figure 6.2c), the mean breakthrough curve has a long tail because of the slow flow, but the mean value is dominated by the concentration in the fast flow, resulting in a small concentration variance. At an intermediate discharge contrast (Figure 6.2b), the integral effects of both variance magnitude and duration result in a larger overall variance.

6.3.2 Effects of Mixing Processes

Figure 6.3 shows the effects of longitudinal dispersion and first-order mass transfer on the overall concentration variance. Figure 6.3a shows that the concentration variance increases with the Péclet number, which implies that a larger dispersivitiy or a longer travel distance yields a smaller normalized concentration variance. Figure 6.3b shows that a higher Damköhler number (e.g., a larger first-order mass transfer rate coefficient) yields a smaller concentration variance because mass transfer between

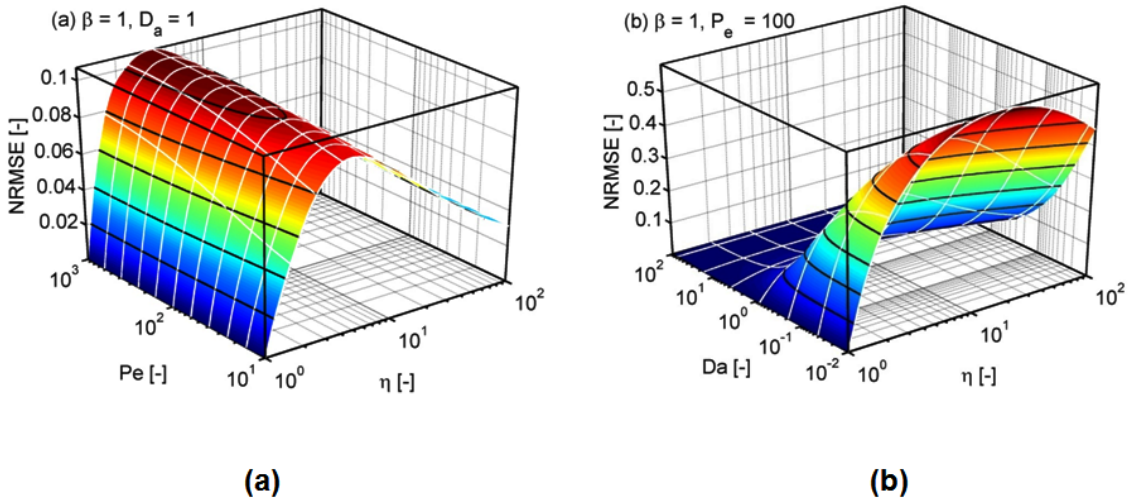

Figure 6.3: Overall concentration variance (quantified by NRMSE) as a function of (a) Péclet number and discharge contrast, η; and (b) Damköhler number and discharge contrast, η

the fast and slow domains diminishes concentration differences between the two domains. At the limit of very large D_a values, the kinetic mass transfer instantaneously reaches equilibrium, resulting in identical concentrations in the two domains and thus zero concentration variance. For small D_a values, the dual-permeability model approaches the limit of two non-interacting streamtubes. Figure 6.3 essentially implies that larger mixing effects in both longitudinal and transverse directions yield smaller concentration variances within the flux.

However, there is a fundamental difference between the cases with zero and non-zero D_a numbers. Within the dual-permeability model, kinetic mass transfer is the only mechanism that causes transverse mixing between the fast and slow domains, functioning similarly as transverse dispersion in continuous models. With the decrease of D_a, the magnitude of the concentration variance increases (comparing Figure 6.3a with Figure 6.4a, and the non-monotonic behavior with the discharge contrast is still valid. However, the non-monotonic behavior becomes monotonically increasing if the kinetic mass transfer is completely ignored (Figure 6.4b). The appendix shows the

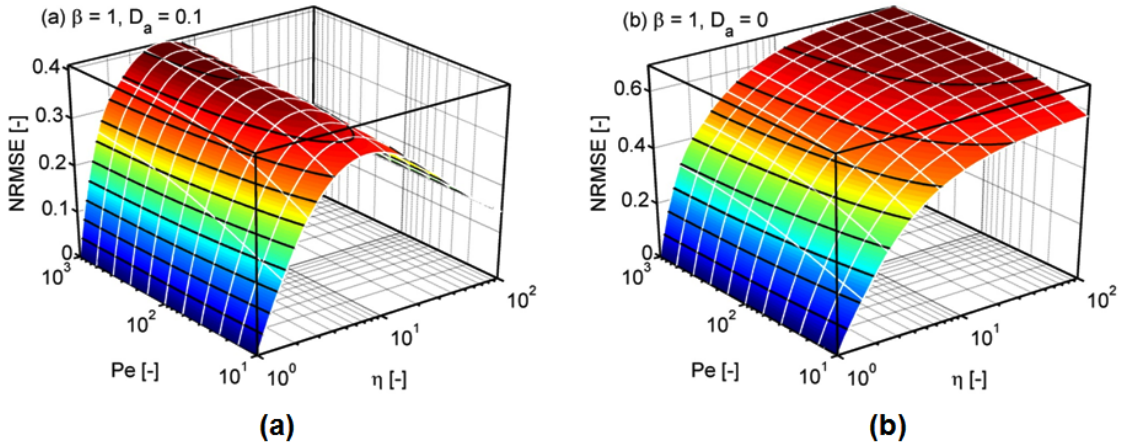

Figure 6.4: Overall concentration variance (quantified by NRMSE) as a function of Péclet number and discharge contrast, η, for Damköhler numbers being (a)non-zero and (b)zero

analytical proof for the monotonic behavior of the non-interacting case.

6.4 Application to Mixing-Controlled Reactive Transport

It is straightforward to extend the dual-permeability model to reactive transport by incorporating reaction kinetics in the fast and slow domains.

$$\theta_f \frac{\partial c_{f,i}}{\partial t} = -q_f \frac{\partial c_{f,i}}{\partial x} + \theta_f D_f \frac{\partial^2 c_{f,i}}{\partial x^2} + \alpha \left(c_{s,i} - c_{f,i} \right) + r_{f,i} \left(c_{f,1}, c_{f,2}, ... \right) \tag{6.42}$$

$$\theta_s \frac{\partial c_{s,i}}{\partial t} = -q_s \frac{\partial c_{s,i}}{\partial x} + \theta_s D_s \frac{\partial^2 c_{s,i}}{\partial x^2} + \alpha \left(c_{f,i} - c_{s,i} \right) + r_{s,i} \left(c_{s,1}, c_{s,2}, ... \right) \tag{6.43}$$

in which $c_{f,i}$ and $c_{s,i}$ are the concentrations of ith reactive species in the fast and slow flow domains, and $r_{f,i}$ and $r_{s,i}$ are reaction rates. Reactions are treated separately in these two domains and mass exchange occurs through kinetic mass transfer. One may also include equilibrium or kinetic sorption by including solid phases in both domains.

Similarly to conservative transport, the reactive concentration breakthrough curves are weighted by the discharge fluxes, and the residence concentrations are weighted

by porosities. Unlike other models involving the evaluation of concentration variations or distributions, the dual-permeability model can be conveniently solved by modifying existing numerical codes. In addition, if concentration variances are available, one may jointly fit the flux-weighted mean and variance. We shall notice that the dual-permeability model yields two concentrations at each time and location, which essentially uses a binomial distribution to approximate the actual concentration distribution. However, the dual-permeability model aims to approximate the concentration variance instead of evaluating the concentration distribution.

6.5 Numerical Experiments

The general procedure to develop a dual-permeability model is similar to that for the classical advection-dispersion equation or the mobile-immobile transport model. Transport parameters are estimated by fitting flux-weighted breakthrough curves of conservative tracers. Reaction kinetics are then included in the transport model to predict breakthrough curves of reactive species. Comparing with the classical mobile-immobile model, there is only one more parameter, i.e., the velocity in the slow flow domain or the discharge contrast, to be estimated. To examine the performance of the dual-permeability model, we will compare the dual-permeability model with an approach in which a single domain is assumed characterized by exactly meeting the flux-averaged breakthrough curve of a conservative compound. This is considered as the "perfect" transport model based on a single concentration within the flux. We will present two numerical studies of mixing-controlled reactive transport: one in a structured medium with a single, elliptical, low-permeability inclusion within a homogeneous, isotropic medium [see, *Luo and Cirpka*, 2011]; and the other in random heterogeneous media with different variances of hydraulic conductivity. We will consider the most practical cases in which the only known information is the measured flux-weighted breakthrough curve of a conservative tracer at the domain

outlet.

6.5.1 Hydrogeological Settings

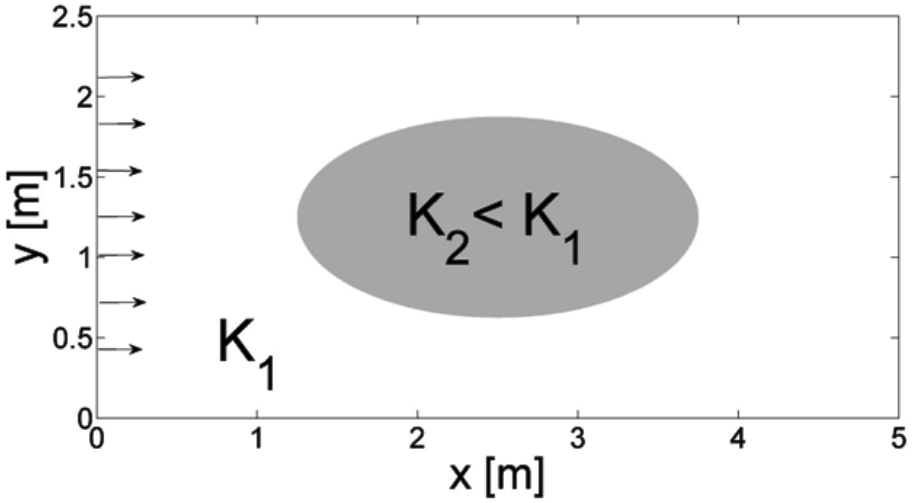

Figure 6.5: The elliptical inclusion setup: an elliptical low-permeability inclusion is embedded in a rectangular two-dimensional homogeneous, isotropic domain

Figure 6.5 shows the first setup used in our simulations: an elliptical low-permeability inclusion is embedded in a rectangular two-dimensional homogeneous, isotropic domain. The hydraulic head is fixed at the left and right boundaries, whereas no flow crosses the top and bottom boundaries. The major and minor axes of the ellipse are half of the domain length and width, respectively. Table 6.1 summarizes the hydrogeological parameters used in the numerical case. Solute transport in this domain is essentially controlled by two dimensionless parameters

$$K_r = \frac{K_1}{K_2} \tag{6.44}$$

$$Pe = \frac{\overline{v}b^2}{D_t L} \tag{6.45}$$

in which K_1 and K_2 are the hydraulic conductivity in the inclusion and matrix, respectively; K_r represents the hydraulic conductivity contrast; $\overline{v}$ is the effective mean velocity within the entire domain; b is the half width of the elliptical inclusion;

L is the domain length; D_t is the transverse dispersion coefficient; and Pe is the transverse Péclet number.

Table 6.1: Hydrogeologic parameters for heterogeneous cases with an elliptical, low-permeability inclusion

Parameter	Symbol	Values
Dimension of domain	$L \times W$	$5m \times 2.5m$
Dimension of elliptical inclusion	$2a \times 2b$	$2.5m \times 1.25m$
Discretization	$\Delta x \times \Delta y$	$0.005m \times 0.005m$
Hydraulic conductivity	K_1	$10^{-3}m/s$
Hydraulic conductivity Contrast	K_{rel}	$1.8, 10, 100$
Mean hydraulic gradient	J	0.01
Effective porosity	θ	0.4
Péclet number	Pe	$396, 588, 560$

The second set of simulations is performed in random heterogeneous fields, which may be considered as a composition of many low- or high-permeable inclusions [*Suribhatla et al.*, 2004]. We consider sets of two-dimensional heterogeneous fields in which the mean flow is in direction x. The length and width of the domain are $20m$ and $10m$, respectively. Variances of log hydraulic conductivity, 0.2, 0.5, 0.8, 1, 2, ..., and 6, are chosen to represent mildly to strongly heterogeneous fields. All hydrogeological parameters are listed in Table 6.2. 100 log-conductivities fields are generated for each variance by the spectral method of *Dykaar and Kitanidis* [1992] on a rectangular 1000×500 cell grid. The steady-state flow field is solved for a mean hydraulic gradient of 0.01 in direction x. A streamline-oriented grid for transport with grid resolution identical to that of the rectangular grid is generated using the streamline method of *Cirpka et al.* [1999a, 1999b]. The flow rate in each stream tube is identical. The numerical schemes for solving the transport problem have been presented elsewhere [*Cirpka et al.*, 1999a].

6.5.2 Mixing-Controlled Reaction

We consider reactive transport of compounds undergoing an instantaneous bimolecular precipitation reaction with 1:1:1 stoichiometry:

Table 6.2: Hydrogeologic parameters for two-dimensional Gaussian random heterogenous cases

Parameter	Symbol	Values
Dimension of domain	$L \times W$	$20m \times 10m$
Discretization	$\Delta x \times \Delta y$	$0.02m \times 0.02m$
Mean hydraulic conductivity	$e^{\langle \ln K \rangle}$	$1.16 \times 10^{-5} m/s$
Variance of hydraulic conductivity	$\sigma^2_{\ln K}$	$0.2, 0.5, 0.8, 1, 2, 3, 4, 5, 6$
Correlation length	$I_x \times I_y$	$0.4m \times 0.4m$
Mean hydraulic gradient	J	0.01
Effective porosity	θ	0.3
Longitudinal dispersivity	α_ℓ	$0.02m$
Transverse dispersivity	α_t	$0.02m$
Molecular diffusion	D_m	$10^{-9} m^2/s$

$$\text{A+B} \rightarrow \text{C} \downarrow \tag{6.46}$$

in which A and B are aqueous species (solutes) and C is a mineral, present throughout the domain. This reaction is assumed to be fast compared to typical transport processes, so that it can be treated as being in local equilibrium. The concentrations of the aqueous species A and B satisfy:

$$c_A c_B = K_{eq} \tag{6.47}$$

where c_A and c_B are the molar concentrations of the reactive species A and B, respectively, and K_{eq} is the solubility product. The same reaction rates of A and B are identical due to the stoichiometry considered. In the following, we consider that Eq. (6.47) is satisfied at all locations and times and $K_{eq} = 0.01$ (with a unit of squared concentration). Replacement simulations are considered for the bimolecular precipitation reaction, i.e., we assume that the domain is initially uniformly filled with a solution containing species A, and a solution of species A and B with a constant concentration is continuously injected into the domain at the inflow boundary. This reactive transport case can be solved completely relying on the mixing ratio of conservative transport [*De Simoni et al.,* 2005, 2007; *Luo and Cirpka*, 2011].

6.5.3 Measure of Goodness

To obtain measures of goodness for the transport models, we consider the concentration of compound A consumed in the reaction, denoted c_A^{miss}, which is the difference between $c_A(t)$ in calculations where A behaves like a conservative compound and in calculations where it undergoes the precipitation reaction with compound B. We analyze the total mass of consumed A and the maximum value of c_A^{miss}. The measures of goodness are relative errors of the macroscopic model predictions and the true values obtained at the outflow boundary, which are defined as relative error in total precipitated mass, ϵ_T, and relative error in peak precipitated mass, ϵ_P[*Luo and Cirpka*, 2011]:

$$\varepsilon_{\mathrm{T}} = \frac{\int \langle c_A^{miss} \rangle^* \, dt}{\int \langle c_A^{miss} \rangle \, dt} - 1 \tag{6.48}$$

$$\varepsilon_{\mathrm{P}} = \frac{\langle c_A^{miss} \rangle^*_{\max}}{\langle c_A^{miss} \rangle_{\max}} - 1 \tag{6.49}$$

in which $\langle c_A^{miss} \rangle^*$ is the flux average of c_A^{miss} predicted by the macroscopic models, and $\langle c_A^{miss} \rangle$ is the true value.

6.6 Results

Figure 6.6 shows the mean breakthrough curves of the conservative-species concentration and the associated concentration variance, the travel-time distributions and the mean reactive breakthrough curves averaged over the outflow boundary for three specific cases with hydraulic conductivity contrasts of 1.8, 10 and 100 at similar Péclet numbers. All travel-time distributions are bimodal, resulting from a fraction of the total flux to pass through the low-conductivity inclusion while the remaining flux surpasses the inclusion. The variability in concentration results mainly from different times (and shapes) of breakthrough between stream tubes passing through

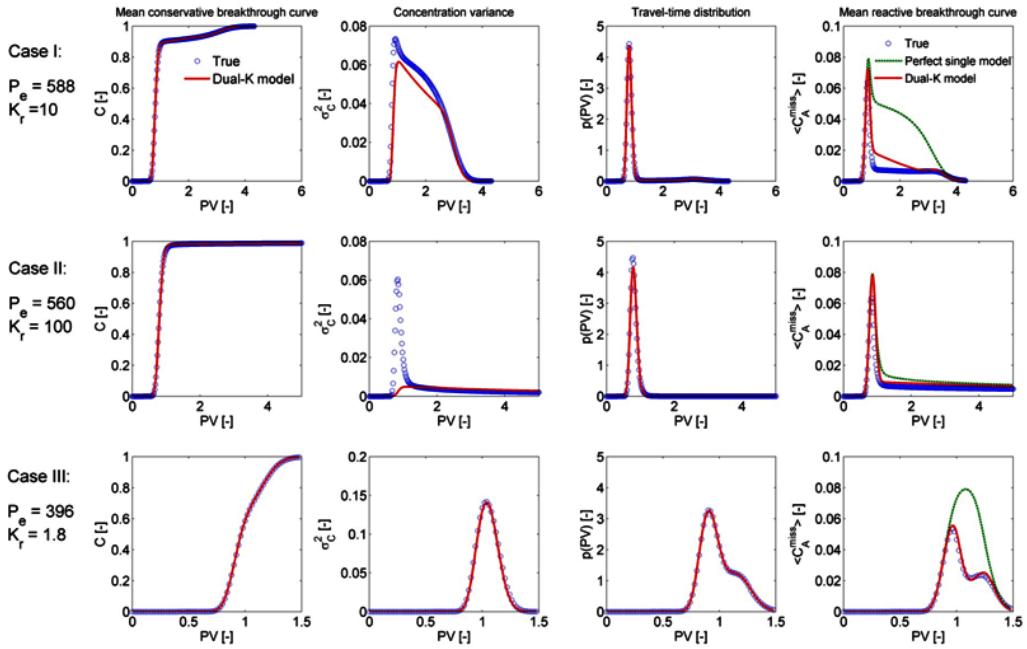

Figure 6.6: The mean breakthrough curves of the conservative-species concentration and the associated concentration variance, the travel-time distributions and the mean reactive breakthrough curves averaged over the outflow boundary for three specific cases with hydraulic conductivity contrasts of 1.8, 10 and 100 at similar Péclet numbers

the low-permeability inclusion and those bypassing it. The case with larger conductivity contrast shows a significantly enhanced tail after the first peak in both mean concentration and concentration variance. All cases could not be reproduced by a 1-D ADE model, and more sophisticated, most likely nonlocal macroscopic models may be needed to capture the observed anomalous transport behavior in the conservative breakthrough curves. However, even such models cannot describe the concentration variances in the flux because only a single concentration can be predicted. The dual-permeability model yields very good descriptions of the conservative breakthrough curves for all cases. With the breakthrough curve fitting, the dual-permeability model predicts the concentration variance well, particularly for the cases with intermediate hydraulic conductivity contrasts, $K_r = 1.8$ and 10. For the

high contrast case, $K_r = 100$, the dual-permeability model reproduces the long tail of the concentration variance, but misses the peak. For reactive breakthrough curves, the dual-permeability model yields much better prediction than the "perfect" model relying on a single flux concentration.

Table 6.3: Fitted parameters and prediction errors for heterogeneous cases with an elliptical, low-permeability inclusion

Elliptical Inclusion Cases	I. $P_e = 588, K_{rel} = 10$	II. $P_e = 560, K_{rel} = 100$	III. $P_e = 396, K_r = 1.8$
Péclet number	197	143	231
Damköhler number	0.034	0.015	0.012
Porosity ratio	2.97	3.99	1.73
Discharge ratio	11.7	185.7	2.2
ε_{T} (Dual-K model)	0.41	0.12	0.03
ε_{T} ("Perfect" model)	2.65	0.44	0.80
ε_{P} (Dual-K model)	0.14	0.24	0.04
ε_{P} ("Perfect" model)	0.24	0.25	0.48

Table 6.3 summarizes the fitted parameters and the prediction errors. The fitted discharge ratios follow the same order of the hydraulic conductivity contrasts. The dual-permeability model significantly improves the prediction of the reactive transport in terms of the total mass consumed and the peak of the consumed concentration. Specifically, for $K_r = 1.8$, the overestimation of the total precipitated mass and the peak concentration consumed (ε_{T} and ε_{P}) drops from 80% and 48% to 3% and 4%, respectively; for $K_r = 10$, ε_{T} and ε_{P} drop from 265% and 24% to 41% and 14%; for $K_r = 100$, the total error improves from 44% to 12%, while the peak does not change much because the variance peak is not captured. These cases demonstrate that the dual-permeability model can significantly improve the prediction of mixing-controlled reactive transport by including only one more parameter than the classical mobile-immobile model, particularly for media with intermediate hydraulic conductivity contrasts, where the concentration variations are important.

Figure 6.7 shows the prediction errors for the Gaussian heterogeneous cases. With the increase of the hydraulic conductivity variance, the errors of the "perfect" model

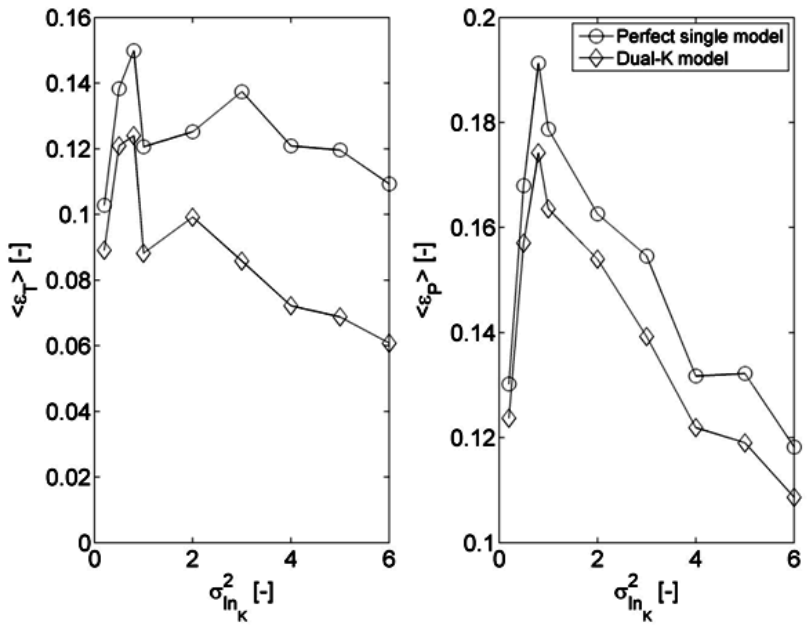

Figure 6.7: Prediction errors for Gaussian heterogeneous cases: relative error in total precipitated mass, ϵ_T, and relative error in peak precipitated mass, ϵ_P

with a single flux concentration decreases because highly heterogeneous hydraulic conductivity fields do not necessarily lead to high concentration variations. In these cases, the majority of flow occurs in preferential paths, which dominate the evaluation of the flux-averaged concentration. Thus, macroscopic, single flux-domain models perform better in highly than in mildly heterogeneous cases. For all cases, the dual-permeability model yields a better prediction in general in terms of both the total precipitated mass and the peak of missing concentration. We want to remark that the predictions in the random fields are better than for the elliptical cases because the domain size is 50 integral scales and the prediction error decreases with increasing travel distance, which is consistent with the common understanding, that mixing can catch up with spreading in the large-distance limit.

6.7 Conclusions

Macroscopic models with a single flux concentration are incapable of representing incomplete mixing, and thus concentration variations, within the solute flux. This has been identified as the major mechanism responsible for inaccurate predictions of mixing-controlled reactive transport. From a strict point of view, such models work well only when the concentration variations within the flux are small or when the reaction is linear. Because the transfer from conservative to reactive compound concentrations is usually nonlinear, it is clear that neglecting such variations must lead to a mass-balance error. Thus, it is generally necessary to consider concentration variations in the upscaling of mixing-controlled reactive transport. In the present study, we propose adopting the dual-permeability model for such purposes. Because the dual-permeability model gives two local flux concentrations, one in the fast- and the other in the slow-flow domain, it conveniently predicts both the mean and variance of the flux concentration.

Dimensionless analytical solutions were developed for the dual-permeability model. The concentration variance within the flux is controlled by four dimensionless parameters, namely the porosity ratio, discharge ratio, the Péclet number, and the Damköhler number. The normalized total concentration variance decreases with the increase of the porosity ratio and the Damköhler number and with the decrease of the Péclet number, while it changes non-monotonically with the discharge ratio. The maximum concentration variance occurs at intermediate discharge contrasts.

We have numerically tested the dual-permeability model for mixing-controlled reactive transport with a bimolecular precipitation reaction at local equilibrium in heterogeneous domains. The case of a single inclusion could be characterized by two dimensionless variables: the hydraulic conductivity contrast and the transverse Péclet number. In the simulations using random fields, the hydraulic conductivity contrast was replaced by the variance of log-conductivity. Our results indicate that the

dual-permeability model generally better predicts breakthrough curves of the reactive compounds for both the structured and random heterogeneous media. Particularly, in the cases of elliptical inclusions with intermediate hydraulic conductivity contrast, the total precipitated mass and the peak difference between reactive and conservative concentrations are significantly improved. For the case with a long concentration tail, the dual-permeability model yields performed well with respect to the total precipitated mass, but the peak difference was not well captured.

If conservative concentration breakthrough curves can be well characterized by macroscopic models with a single flux concentration, such as the classical advection-dispersion and mobile-immobile models, the fitted dual-permeability model usually approaches such macroscopic models. In such cases, the dual-permeability model underestimates the concentration variance the same way as the single flux-domain models, yielding identical predictions of reactive breakthrough curves. However, in general the dual-permeability model yields the chance of better predicting mixing-controlled reactive transport than macroscopic models with a single flux concentration. Under which conditions flux averaged breakthrough curves of conservative compounds are sufficient to unanimously identify multiple flux domains is beyond the scope of the current study.

Appendix

Consider the dual-permeable domain as two parallel non-interacting plug flow of pure advection. For a domain-free initial condition, i.e., $C_f\left(t=0\right)=C_s\left(t=0\right)=0$, and unit step inputs, i.e., $C_f\left(x=0\right)=C_s\left(x=0\right)=1$, the solutions of C_f and C_s at $X=1$ are given by:

$$C_f(T) = H\left(\frac{(1+\eta)\beta}{\eta(1+\beta)}\right) \tag{6.50}$$

$$C_s(T) = H\left(\frac{1+\eta}{1+\beta}\right) \tag{6.51}$$

where H is the Heaviside step function. The flux-averaged breakthrough curve is

$$C_m(T) = \frac{\eta}{1+\eta}H\left(\frac{(1+\eta)\beta}{\eta(1+\beta)}\right) + \frac{1}{1+\eta}H\left(\frac{1+\eta}{1+\beta}\right) \tag{6.52}$$

which can be expanded as

$$C_m = \begin{cases} 0, & T < \frac{(1+\eta)\beta}{\eta(1+\beta)} \\ \frac{\eta}{1+\eta}, & \frac{(1+\eta)\beta}{\eta(1+\beta)} \leq T < \frac{1+\eta}{1+\beta} \\ 1, & T \geq \frac{1+\eta}{1+\beta} \end{cases} \tag{6.53}$$

Thus, for $T < \frac{(1+\eta)\beta}{\eta(1+\beta)}$ and $T \geq \frac{1+\eta}{1+\beta}$, no concentration variation occurs between the local and flux-averaged breakthrough curves. For $\frac{(1+\eta)\beta}{\eta(1+\beta)} \leq T < \frac{1+\eta}{1+\beta}$, the concentrations in the fast and slow flow are 1 and 0, respectively, and the variance is constant:

$$\sigma_C^2 = \frac{\eta}{(1+\eta)^2} \tag{6.54}$$

The total variance over the time course is

$$\Omega = \int_{\frac{(1+\eta)\beta}{\eta(1+\beta)}}^{\frac{1+\eta}{1+\beta}} \frac{\eta}{(1+\eta)^2} dT = \frac{\eta}{(1+\eta)^2}\left[\frac{1+\eta}{1+\beta} - \frac{(1+\eta)\beta}{\eta(1+\beta)}\right] = \frac{\eta-\beta}{(1+\eta)(1+\beta)} \tag{6.55}$$

and the NRMSE is

$$NRMSE = \frac{\Omega}{C^*_{\max} - C^*_{\min}} = \frac{\eta-\beta}{(1+\eta)(1+\beta)} \tag{6.56}$$

Taking the first derivatives of Eq. (6.55) with respect to β and η yields:

$$\frac{\partial\Omega}{\partial\beta} = -\frac{1}{(1+\beta)^2} < 0 \tag{6.57}$$

$$\frac{\partial\Omega}{\partial\eta} = \frac{1}{(1+\eta)^2} > 0 \tag{6.58}$$

CHAPTER VII

SUMMARY, CONCLUSIONS AND RECOMMENDATIONS

7.1 Summary

This dissertation investigates the extent of mixing and improves upscaling effective macroscopic models for mixing-controlled reactive transport in connected heterogeneous formations, which usually exhibit strongly anomalous transport behavior.

A numerical framework is developed for an accurate geostatistical characterization of connected heterogeneous formations transformed from Gaussian random fields. Numerical experiments are conducted in such heterogeneous fields with different connectivity to investigate the performance of macroscopic mean transport models for simulating mixing-controlled reactive transport. Results show that good characterization of anomalous transport of a conservative tracer does not necessarily mean that the models may characterize mixing well and that, consequently, it is questionable that the models capable of characterizing anomalous transport behavior of a conservative tracer are appropriate for simulating mixing-controlled reactive transport. In connected heterogeneous fields with large hydraulic conductivity variances, macroscopic mean models ignoring concentration variations yield good prediction, while in fields with intermediate conductivity variances, the models must consider both the mean concentration and concentration variations, which are very difficult to evaluate both theoretically and experimentally.

An innovative and practical approach is developed by combining mean conservative and reactive breakthrough curves for estimating concentration variations, which can be subsequently used by variance transport models for prediction. Furthermore,

a new macroscopic framework based on the dual-permeability conceptualization is developed for describing both mean and concentration variation for mixing-controlled reactive transport. The developed approach and models are validated by numerical and laboratory visualization experiments. In particular, the new dual-permeability model demonstrates significant improvement for simulating mixing-controlled reactive transport in heterogeneous media with intermediate conductivity variances.

Overall, results, approaches and models from this dissertation advance the understanding of subsurface mixing in anomalous transport and significantly improve the predictive ability for modeling mixing-controlled reactive transport in connected heterogeneous media.

7.2 Research Conclusions

Major conclusions that can be drawn from this research include:

1. Geostatistical characterization of connected random fields

Application of the numerical approach to geostatistically characterize connected heterogeneous formations transformed from Gaussian random fields provides a quantitative view of the change of correlation length of connected random fields before and after the transformation. The Monte-Carlo simulation and the results indicate that

- The absolute-value transformation has slight effect on changing the types of covariance models;
- The correlation length of the original field is 1.67 or 2.64 times of that of the connected field for Gaussian or exponential covariance models, respectively;
- Anisotropy is not changed by the absolute-value transformation.

- Connectivity measures in the literature and two-point cluster function is also discussed in details, by which we conclude that two-point cluster functions can identify different degrees of connectivity for Gaussian fields, but not as reliable as for exponential fields, which may be due to the fact that exponential covariance models are continuous but not differentiable.

2. Performance of macroscopic mean models

Numerical test cases of mixing controlled reactive transport with a bimolecular precipitation reaction at local equilibrium in different heterogeneous domains are conducted on random heterogeneous fields with same variance of hydraulic conductivity and different connectivity. Specifically, we study Gaussian heterogeneous fields, high-conductivity connected fields, and low-conductivity connected fields. The key objective was to analyze to what extent concentration fluctuations within the solute flux could be neglected in the transfer from breakthrough curves of conservative to reactive compounds. The numerical results indicate that largest errors occur in macroscopic one-dimensional models for intermediate conductivity variances. With respect to total mass balance and peak concentration errors, increasing the degree of heterogeneity beyond a critical value led to an improvement of the performance. Our results clearly indicate the need for developing other modeling frameworks to evaluate both mean and concentration variance for simulating mixing-controlled reactive transport in heterogeneous media, particularly in media with intermediate variances of hydraulic conductivity.

3. Estimating concentration variance

Characterization of concentration variance is the key for modeling mixing-controlled reactive transport, but concentration variance is usually difficult to measure because it requires many local measurements. The innovative and practical approach we proposed uses mean concentration breakthrough curves of both conservative and reactive

tracers to estimate the concentration variance. The conservative breakthrough curve only contains the information of mean concentrations, while the reactive breakthrough curves are results of both concentration mean and variance. Based on the relationship between conservative and reactive concentrations, concentration variance can be estimated by sampling the beta distribution to fit the mean reactive breakthrough curve. In addition, both mean and fitted variance can be described by macroscopic transport models for prediction purpose: one for mean concentration, and the other for the variance with additional parameters. Our approach is validated by the visualization experiments conducted at MIT. Although the experiments provide all concentration distributions, our approach only requires both conservative and reactive breakthrough curves at observation locations. Furthermore, our results suggest that one should conduct both conservative and reactive tracer tests for upscaling macroscopic transport models because conservative tracer tests are insufficient for evaluating local concentration variations.

4. New macroscopic model

Macroscopic models with a single flux concentration are incapable of representing incomplete mixing, and thus concentration variations, within the solute flux. A dual-permeability model is presented in this dissertation to include concentration variations in the upscaling of mixing-controlled reactive transport. Because the dual-permeability model gives two local flux concentrations, one in the fast- and the other in the slow-flow domain, both the mean and variance of the flux concentration can be conveniently predicted. Dimensionless analytical solutions were developed for the dual-permeability model. The concentration variance within the flux is controlled by four dimensionless parameters, namely the porosity ratio, discharge ratio, the Péclet number, and the Damköhler number. The normalized total concentration variance decreases with the increase of the porosity ratio and the Damköhler number and with

the decrease of the Péclet number, while it changes non-monotonically with the discharge ratio. The maximum concentration variance occurs at intermediate discharge contrasts. Numerical tests for the dual-permeability model for mixing-controlled reactive transport with a bimolecular precipitation reaction at local equilibrium in heterogeneous domains are conducted. The case of a single inclusion could be characterized by two dimensionless variables: the hydraulic conductivity contrast and the transverse Péclet number. In the simulations using random fields, the hydraulic conductivity contrast was replaced by the variance of log-conductivity. Our results indicate that the dual-permeability model generally better predicts breakthrough curves of the reactive compounds for both the structured and random heterogeneous media. Particularly, in the cases of elliptical inclusions with intermediate hydraulic conductivity contrast, the total precipitated mass and the peak difference between reactive and conservative concentrations are significantly improved. For the case with a long concentration tail, the dual-permeability model performed well with respect to the total precipitated mass, but the peak difference was not well captured.

7.3 Recommended Future Work

Based on the research conducted in this dissertation, I recommend the following topics that worth further investigation:

1. Although we have investigated the characterization of geostatistical (or "static") connectivity by two-cluster function, flow connectivity and transport connectivity, or "dynamic" connectivities, have not been discussed. In general, flow and transport connectivities are often controlled by the connected high-permeability areas such as "channels" or by the presence of hydraulic barriers. Techniques that already been developed in the framework of percolation theory and fractured media would be good candidates for quantification. There have been some recent research on flow and transport connectivities such as S*anchez-Vila, et al.*,

[1996], *Knudby and Carrera*[2005,2006], *Renard and Allard* [2011], and multiple definitions and quantifications have been carried out, which indicated that flow and transport connecivities are more process-dependent. They not only depend on the geometry of the heterogeneous field, but also depend on physical parameters in flow and transport dynamics. The concept of flow and transport connectivity and their quantifications would be worth further studying. For example, which connectivity definition shall we use to quantify a specific solute flow or transport process? What information do we gain if we properly choose connectivity quantifications? Numerical and experimental studies need to be conducted to answer these questions. In addition, the approach used to generate connected random fields is absolute-value transformation of Gaussian random fields because it can generate connected fields given a geostatistical structural model. Connected random fields generated by other methods should be investigated.

2. The performance of macroscopic mean models is examined using the Monte-Carlo method, which is computationally expensive. Model reduction is helpful for examining large amount of realizations. For example, the temporal moment method may be applied to transfer the transient transport cases to steady-state equations, and the concentration breakthrough curves can be reconstructed by the temporal moments. In addition, the mixing-controlled reactive transport uses instantaneous reactions, which can be expressed as a function of the conservative concentrations. There is a need to examine the reactive transport with kinetic reactions. Furthermore, our method relates the performance with the discrete conductivity variances. Finer discretization of conductivity variances are needed to identify more accurate turning points of the macroscopic mean model performance.

3. We propose to use both conservative and reactive tracer tests to estimate concentration variations and assume that reactive species concentrations are functions of conservative concentrations. In practice, there is always a reaction timescale. For kinetic reactions, a simple relationship between conservative and reactive tracer concentrations may not be available. It is needed to develop a method to estimate concentration variances based on kinetic, multi-component reactions. Furthermore, concentration breakthrough curves are usually flux-weighted. The local fluxes are difficult to measure. Thus, the estimated concentration variances may be considered as flux concentration variances. How to relate it to residence concentration variances needs further study.

4. The proposed dual-permeability modeling framework upscales mixing-controlled reactive transport in heterogeneous media. The general procedure to develop a dual-permeability model is similar to that for the classical advection-dispersion equation or the mobile-immobile transport model. Transport parameters are estimated by fitting flux-weighted breakthrough curves of conservative tracers. Reaction kinetics are then included in the transport model to predict breakthrough curves of reactive species. Comparing with the classical mobile-immobile model, there is only one more parameter, i.e., the velocity in the slow flow domain or the discharge contrast, to be estimated. The difference between daul-permeability model and mobil-immobile model would be worth discussing. The method of temporal moment analysis, in this case, would be a convenient tool for characterization, which has been used by *Valocchi*[1983] to address the difference between mobil-immobile model and advection-dispersion model. A rigorous model selection procedure can be helpful for determining which model is more appropriate. In addition, we may need to examine the applicability of multi-permeability model, in which the mass transfer among all permeability zones needs to be appropriately characterized. The previous multi-tube method

completely neglected such mass transfer.

5. Much of the verification and validation of the developed methods has focused on the numerical cases and lab-scale experimental cases. Less effort has been spent on field studies. Flow and transport processes may be influenced by the field geometry, geochemical reactions, and even pore structure change, which will affect the performance of our theoretical models. Effort should be made to conduct field studies, and results should be included in evaluating the model effectiveness and reliability.

REFERENCES

[1] Ababou, R., L.W., Gelhar, and D. McLaughlin (1988), Three-dimensional flow in random porous media, Report No. 318, Ralph Parsons Laboratory for Water Resources & Hydrodynamics, Massachusetts Institute of Tech., Cambridge, MA.

[2] Ababou, R., D. McLaughlin, L.W. Gelhar, and A.F.B. Tompson (1989), Numerical-simulation of 3-dimensional saturated flow in randomly heterogeneous porous-media, Transport in Porous Media, 4(6), 549-565.

[3] Bardossy, A., and J. Li (2008), Geostatistical interpolation using copulas, Water Resour. Res., 44,W07412, doi:10.1029/2007WR006115.

[4] Barlebo, H.C., M.C. Hill, and D. Rosbjerg (2004), Investigating the Macrodisperion Experiment (MADE) site in Columbus, Mississippi, using a three-dimensional inverse flow and transport model, Water Resour. Res., 40, W04211.

[5] Bear, J. (1972), Dynamics of Fluids in Porous Media, Dover Publications, Inc, New York.

[6] Bellin, A., P. Salandin, and A. Rinaldo (1992), Simulation of dispersion in heterogeneous porous formations - Statistics, 1st-order theories, convergence of computations, Water Resour. Res. 28 (9), 2211-2227.

[7] Bellin, A., A. Rinaldo, W.J.P. Bosma, S.E.A.T.M. van de Zee, and Y. Rubin (1993), Linear equilibrium adsorbing solute transport in physically and chemically heterogeneous porous formations. 1. Analytical solutions, Water Resour. Res. , 29(12), 4019-4030.

[8] Bellin, A., Y. Rubin, and A. Rinaldo (1994), Eulerian-Lagrangian approach for modeling of flow and transport in heterogeneous geological formations, Water Resour. Res. , 30(11), 2913-2924.

[9] Bellin, A., and Y. Rubin (1996), HYDRO_GEN: A spatially distributed random field generator for correlated properties, Stochastic Hydrology and Hydraulics, 10(4), 253-278.

[10] Benson, D. A., S. W. Wheatcraft, and M. M. Meerschaert (2000), Application of a fractional advection-dispersion equation, Water Resour. Res., 36, 1413-1423.

[11] Berkowitz, B., and H. Scher (1997), Anomalous transport in random fracture networks, Phys. Rev. Lett., 79, 4038-4041.

[12] Berkowitz, B., and H. Scher (1998), Theory of anomalous chemical transport in random fracture networks, Phys. Rev. E, 57, 5858-5869.

[13] Berkowitz, B., H. Scher, and S.E. Silliman (2000), Anomalous transport in laboratory-scale, heterogeneous porous media, Water Resour. Res., 36, 149-158.

[14] Berkowitz, B., S. Emmanuel, and H. Scher (2008), Non-Fickian transport and multiple-rate mass transfer in porous media, Water Resour. Res., 44(3), W03402, DOI: 10.1029/2007WR005906.

[15] Carrera, J., X. Sanchez-Vila, I. Benet, A. Medina, G. Galarza, and J. Guimera (1998), On matrix diffusion: formulations, solution methods, and qualitative effects, Hydrogeology Journal, 6, 178-190.

[16] Chin, D.A., and T. Z. Wang (1992), An investigation of the validity of 1st-order stochastic dispersion theories in isotropic porous-media, Water Resour. Res., 28(6), 1531-1542.

[17] Cirpka, O.A., E.O. Frind, and R. Helmig (1999a), Numerical methods for reactive transport on rectangular and streamline-oriented grids, Adv. Water Resour., 22, 711-728.

[18] Cirpka, O.A., E.O. Frind, and R. Helmig (1999b), Numerical simulation of biodegradation controlled by transverse mixing, J. Contam. Hydrol., 40, 159-182.

[19] Cirpka, O.A., and P.K. Kitanidis (2000a), An advective-dispersive streamtube approach for the transfer of conservative tracer data to reactive transport, Water Resour. Res., 36, 1209-1220.

[20] Cirpka, O.A., and P.K. Kitanidis (2000b), Characterization of mixing and dilution in heterogeneous aquifers by means of local temporal moments, Water Resour. Res., 36, 1221-1236.

[21] Cirpka, O.A. (2002), Choice of dispersion coefficients in reactive transport calculations on smoothed fields, J. Contam. Hydrol., 58, 261-282.

[22] Cirpka, O. A. (2005), Effects of sorption on transverse mixing in transient flows, Journal of Contaminant Hydrology, 78(3), 207-229.

[23] Cirpka, O.A. (2006), Stochastic Methods in Subsurface Hydrology, Course notes, Swiss Federal Institute for environmental Science and Technology.

[24] Cirpka, O.A., and A.J. Valocchi (2007), Two-dimensional concentration distribution for mixing-controlled bio-reactive transport in steady state, Adv. Water Resour., 30(6-7): 1668-1679.

[25] Cirpka, O. A., R.L. Schwede, J. Luo, and M. Dentz (2008), Concentration statistics for mixing-controlled reactive transport in random heterogeneous media, Journal of Contaminant Hydrology, 98(1-2), 61-74, DOI: 10.1016/j.jconhyd.2008.03.005.

[26] Cirpka, O. A., F.P.J. de Barrows, G. Chiogna, M. Rolle, and W. Nowak (2011), Stochastic flux-related analysis of transverse mixing in two-dimensional heterogeneous porous media, Water Resour. Res., 47, W06515.

[27] Chrysikopoulos, C., Kitanidis, P. K. & Roberts, P. V. (1990), Analysis of one-dimensional solute transport through porous media with spatially variable retardation factor. Water Resour. Res. 26, 437 - 446.

[28] Cushman, J.H., and T.R. Ginn (2000), Fraction advection-dispersion equation: A classical mass balance with convolution-Fickian flux, Water Resour. Res., 36, 3763-3766.

[29] Dagan, G. (1984), Solute transport in heterogeneous porous formations, J. Fluid Mech., 145, 151-177.

[30] Dagan G. (1986), Statistical theory of groundwater flow and transport: pore to laboratory, laboratory to formation, and formation to regional scale. Water Resour Res; 22(9):120S–34S.

[31] Dagan, G. (1988), Time-dependent macrodispersion for solute transport in anisotropic heterogeneous aquifers, Water Resour. Res., 24(9), 1491-1500.

[32] Dagan, G. (1989), Flow and Transport in Porous Formations, Springer-Verlag, New York.

[33] Dagan, G. (1991), Dispersion of a passive solute in nonergodic transport by steady velocity-fields in heterogeneous formations, Journal of Fluid Mechanics, 233, 197-210.

[34] Dentz, M., H. Kinzelbach, S. Attinger, and W. Kinzelbach (2000), Temporal behavior of a solute cloud in a heterogeneous porous medium - 1. Point-like injection, Water Resour. Res., 36, 3591-3604.

[35] Dentz, M., H. Kinzelbach, S. Attinger, and W. Kinzelbach (2002), Temporal behavior of a solute cloud in a heterogeneous porous media - 3. Numerical Simulations, Water Resour. Res., 38(7), 10.1029/2001WR000436.

[36] Dentz, M., and J. Carrera (2007), Mixing and spreading in stratified flow, Phy. Fluids, 19, 017107.

[37] Dentz, M., T. Le Borgne, A. Englert, and B. Bijeljic (2010), Mixing, spreading and reaction in heterogeneous media: A brief review, J. Contam. Hydrol., doi:10.1016/j.jconhyd.2010.05.002.

[38] De Simoni, M., J. Carrera, X. Sanchez-Vila, and A. Guadagnini (2005), A procedure for the solution of multicomponent reactive transport problems, Water Resour. Res., 41(11), W11410, DOI: 10.1029/2005WR004056.

[39] De Simoni, M., X. Sanchez-Vila, J. Carrera, and M.W. Saaltink (2007), A mixing ratios-based formulation for multicomponent reactive transport, Water Resour. Res., 43, W07419.

[40] Dykaar, B. B., and P. K. Kitanidis (1992), Determination of the effective hydraulic conductivity for heterogeneous porous media using a numerical spectral approach: 1. Method, Water Resour. Res., 28, 1155–1166.

[41] Dykaar, B. B., and P. K. Kitanidis (1992b), Determination of the effective hydraulic conductivity for heterogeneous porous media using a numerical spectral approach: 2. Results, Water Resour. Res., 28, 1167-1178.

[42] Dykhulzen, R. C.(1987), Transport of solutes through unsaturated fractured media, Water Research, 21, 1531-1539.

[43] Edery, Y., H. Scher, and B. Berkowitz (2009), Modeling bimolecular reactions and transport in porous media, Geophys. Res. Lett., 36, L02407, doi:10.1029/2008GL036381.

[44] Fiori, A., and G. Dagan (2000), Concentration fluctuations in aquifer transport: A rigorous first-order solution and applications, J. Contam. Hydrol., 45, 139-162.

[45] Fiori, A., F. Boso, F. P. J. de Barros, S. De Bartolo, A. Frampton, G. Severino, S. Suweis, and G. Dagan (2010), An indirect assessment on the impact of connectivity of conductivity classes upon longitudinal asymptotic macrodispersivity, Water Resour. Res., 46, W08601, doi:10.1029/2009WR008590.

[46] Fiorotto, V., and E. Caroni (2002), Solute concentration statistics in heterogeneous aquifers for finite Peclet values, Transport Porous Media, 48, 331– 351, (Erratum, Transp. Porous Media, 50(3), 373, 2003.)

[47] Fiorotto, V., and E. Caroni (2003), Solute concentration statistics in heterogeneous aquifers for finite Peclet values, Transport Porous Media, 50, 373-373.

[48] Janssen, G., O.A. Cirpka and S.E.A.T.M. van der Zee (2006), Stochastic analysis of nonlinear biodegradation in regimes controlled by both chromatographic and dispersive mixing, Water Resour. Res., 42, W01417.

[49] Gelhar, L.W., and C.L. Axness (1983), 3-dimensional stochastic-analysis of macrodispersion in aquifers, Water Resour. Res., 19, 161-180.

[50] Gelhar, L.W. (1993), Stochastic Subsurface Hydrology, Prentice-Hall Inc., Englewood, Cliffs, NJ.

[51] Gerke, H.H., and M.T. van Genuchten (1993), A dual-porosity model for simulating the preferential movement of water and solutes in structured porous-media, Water Resour. Res. 29, 305-319.

[52] Ginn, T.R., C. S. Simmons, and B.D. Wood (1995), Stochastic-convective transport with nonlinear reaction - Biodegradation with microbial-growth, Water Resour. Res., 31(11), 2689-2700.

[53] Ginn, T.R. (2001), Stochastic-convective transport with nonlinear reactions and mixing: finite streamtube ensemble formulation for multicomponent reaction systems with intra-streamtube dispersion, J. Contam. Hydrol., 47, 1-28.

[54] Ginn, T.R., E.M. Murphy, A. Chilakapati, and U. Seeboonruang (2001), Stochastic-convective transport with nonlinear reaction and mixing: application to intermediate-scale experiments in aerobic biodegradation in saturated porous media, J. Contam. Hydrol., 48, 121-149.

[55] Ginn, T.R., B.D. Wood, K.E., Nelson, T.D. Scheibe, E.M. Murphy, and T.P. Clement (2002), Prosesses in microbil transport in the natural subsurface, Adv. Water Resour., 25, 1017-1042.

[56] Gomez-Hernandez, J. J., and X. Wen (1998), To be or not to be multi-Gaussian? A reflection on stochastic hydrogeology, Adv. Water Resour., 21, 47–61.

[57] Gorelick, S.M., G. Liu, and C. Zheng (2005), Quantifying mass transfer in permeable media containing conductive dentritic networks, Geophys. Res. Lett., 32, L18402.

[58] Gramling, C.M., C.F. Harvey, and L.C. Meigs (2002), Reactive transport in porous media: A comparison of model prediction with laboratory visualization, Environ. Sci. Technol., 36, 2508-2514.

[59] Guswa, A.J., and D. L. Freyberg (2000), Slow advection and diffusion through low permeability inclusions, Journal of Contaminant Hydrology, 46, 205-232.

[60] Hadermann, J., and W. Heer (1996), The Grimsel (Switzerland) migration experiment: Integrating field experiments, laboratory investigations and modelling, J. Contam. Hydrol., 21, 87– 100.

[61] Haggerty, R. , and S. M. Gorelick (1995), Multiple-rate mass-transfer for modeling diffusion and surface-reactions in media with pore-scale heterogeneity, Water Resour. Res., 31, 2383-2400.

[62] Haggerty, R., and S. M. Gorelick (1998), Modeling mass transfer process in soil columns with pore-scale heterogeneity, Soil Science Society of America Journal, 62(1), 62-74.

[63] Haggerty, R., S. a. McKenna, and L. C. Meigs (2000), On the late-time behavior of tracer test breakthrough curves, Water Resour. Res., 36, 3467-3479.

[64] Haggerty, R., S.W. Fleming, and L.C. Meigs (2001), Tracer tests in a fractured dolomite 2. Analysis of mass transfer in single-well injection-withdrawal tests, Water Resour. Res., 37, 1129-1142.

[65] Hanssen, A.E., J.H. Cushman, and J.W. Delleur (1998a), A Monte Carlo assessment of Eulerian flow and transport perturbation models, Water Resour. Res., 34(5), 1143-1163.

[66] Hanssen, A.E., J.H. Cushman, and J.W. Delleur (1998b), Significance of porosity variability to transport in heterogeneous porous media, Water Resour. Res., 34(9), 2249-2259.

[67] Harvey, C., and S.M. Gorelick (2000), Rate-limited mass transfer or macrodispersion: Which dominates plume evolution at the Macrodispersion Experiment (MADE) site? Water Resour. Res., 36, 637-650.

[68] Haslauer, C. P., P. Guthke, A. B ardossy, and E. A. Sudicky (2012), Effects of non-Gaussian copula-based hydraulic conductivity fields on macrodispersion,Water Resour. Res., 48,W07507, doi:10.1029/2011WR011425.

[69] Hu, B. X., H. Huang, and D. X. Zhang (2002), Stochastic analysis of solute transport in heterogeneous, dual-permeability media, Water Resour. Res., 38(9), DOI: 10.1029/2001WR000442

[70] Hu, L., and T. Chugunova (2008), Multiple-point geostatistics for modeling subsurface heterogeneity: A comprehensive review, Water Resour. Res., 44, W11413, doi:10.1029/2008WR006993.

[71] Janssen, G., O.A. Cirpka and S.E.A.T.M. van der Zee (2006), Stochastic analysis of nonlinear biodegradation in regimes controlled by both chromatographic and dispersive mixing, Water Resour. Res., 42, W01417.

[72] Journel, A.G., Alabert, F.G. (1990), New method for reservoir mapping, J. Petrol. Tech., 42(2), 212–218.

[73] Journel, A.G., Deutsch, C.V. (1993), Entropy and spatial disorder, Math. Geol., 25(3), 329–355.

[74] Kapoor, V., and L.W. Gelhar (1994), Transport in three-dimensionally heterogeneous aquifers 1. Dynamics of concentration fluctuations, Water Resour. Res., 30, 527–536.

[75] Kapoor, V., and P.K. Kitanidis (1996), Concentration fluctuations and dilution in two-dimensionally periodic heterogeneous porous media, Transp. Porous Media, 22, 91–119.

[76] Kapoor, V., L.W. Gelhar, and F. Miralles-Wilhelm (1997), Bimolecular second order reactions in spatially varying flows: Segregation induced scale-dependent transformation rates, Water Resour. Res., 33, 527–536.

[77] Kapoor, V., and P.K. Kitanidis (1998), Concentration fluctuations and dilution in aquifers, Water Resour. Res., 34, 1181-1193.

[78] Kitanidis, P.K. (1988), Prediction by the method of moments of transport in a heterogeneous formation, J. Hydrol., 102, 453-473.

[79] Kitanidis, P.K. (1994), The concept of the dilution index, Water Resour. Res., 30, 2011–2026.

[80] Knudby, C., and J. Carrera (2005), On the relationship between indicators of geostatistical, flow and transport connectivity, Adv. Water Resour., 28, 405-421.

[81] Knudby, C., and J. Carrera (2006), On the use of apparent hydraulic diffusivity as an indicator of connectivity, J. Hydrol., 329, 377-389, doi:10.1016/j.jhydrol.2006.02.026

[82] LaBolle, E. M., and G. E. Fogg (2001), Role of molecular diffusion in contaminant migration and recovery in an alluvial aquifer system, Trans. Porous Med., 42, 155–179.

[83] Lawrence, A. E., X. Sanchez-Vila, and Y. Rubin (2002), Conditional moments of the breakthrough curves of kinetically sorbing solute in heterogeneous porous media using multirate mass transfer models for sorption and desorption, Water Resour. Res., 38(11), 1248.

[84] Leij, F. J., N. Torike, M. S. Field, and A. Sciortino (2012), Solute transport in dual-permeability porous media, Water Resour. Res., 48, W04523, DOI: 10.1029/2011WR011502.

[85] Liu, G., C. Zheng, and S.M. Gorelick (2004), Limits of applicability of the advection-dispersion model in aquifers containing connected high-conductivity channels, Water Resour. Res., 40, W08308.

[86] Liu, G., C. Zheng, and S.M. Gorelick (2007), Evaluation of the applicability of the dual-domain mass transfer model in porous media containing connected high-conductivity channels, Water Resour. Res., 43, W12407.

[87] Luo, J., and O.A. Cirpka (2008), Travel-time based descriptions of transport and mixing in heterogeneous domains, Water Resour. Res., doi:10.1029/2007WR006035.

[88] Luo, J., M. Dentz, J. Carrera, and P.K. Kitanidis (2008), Transport controlled effective reaction parameters in heterogeneous media, Water Resour. Res., 44, W02416.

[89] Luo, J., and O.A. Cirpka (2008), Travel-time based descriptions of transport and mixing in heterogeneous domains, Water Resour. Res., doi:10.1029/2007WR006035.

[90] Luo, J., and O.A. Cirpka (2011), How well do mean breakthrough curve predict mixing-controlled reactive transport? Water Resour. Res., 47, W02520, doi: 10.1029/2010WR009461.

[91] MacQuarrie, K.T.B., and E.A. Sudicky (1990), Simulation of biodegradable organic contaminants in groundwater 2. Plume behavior in uniform and random flow fields, Water Resour. Res., 26, 223-239.

[92] Margolin, G., M. Dentz, and B. Berkowitz (2003), Continuous time random walk and multirate mass transfer modeling of sorption, Chemical Physics, 295(1), 71-80.

[93] Miralles-Wilhelm, F. and L.W. Gelhar (1996), Stochastic analysis of sorption macrokinetics in heterogeneous aquifers. Water Resour. Res. 32, 1541-1549.

[94] Miralles-Wilhelm, F., L.W. Gelhar, and V. Kapoor (1997), Stochastic analysis of oxygen-limited biodegradation in three-dimensionally heterogeneous aquifers, Water Resour. Res., 33, 1251–1263.

[95] Molz, F.J., and M.A. Widdowson (1988), Internal inconsistencies in dispersion-dominated models that incorporate chemical and microbial kinetics, Water Resour. Res., 24, 615-619.

[96] Neuman, S.P., C.L. Winter, and C.M. Newman (1987), Stochastic-theory of field-scale Fickian dispersion in anisotropic porous-media, Water Resour. Res., 23(3), 453-466.

[97] Neuman SP (1997). Stochastic approach to subsurface flow and transport: a view to the future. In: Dagan G, Neuman SP, editors. Subsurface flow and transport—A stochastic approach. International Hydrology Series. Unesco.

[98] Neuweiler, I., and O.A. Cirpka (2005), Homogenization of Richards equation in permeability fields with different connectivity, Water Resour. Res., 41, W02009, doi:D R10.1029/2004WR003329172 .

[99] Oates, P., and C. F. Harvey (2006), A colorimetric reaction to quantify fluid mixing, Exp Fluids, 41:673-683, doi: 10.1007/s00348-006-0184-z.

[100] Oates, P. (2007), Upscaling reactive transport in porous media: Laboratory visualization and stochastic models, MIT Dissertation.

[101] Pannone, M., and P. K. Kitanidis (2004), On the asymptotic behavior of dilution parameters for Gaussian and hole-Gaussian log-conductivity covariance functions, Transport in Porous Media, 56, 257-281.

[102] Raje, D.S., and V. Kapoor (2000), Experimental study of bimolecular reaction kinetics in porous media, Environ. Sci. Technol., 34, 1234-1239.

[103] Renard, P., and D. Allard (2011), Connectivity metrics for subsurface flow and transport, doi:10.1016/j.advwatres.2011.12.001.

[104] Rezaei, M., E. Sanz, E. Raeisi, C. Ayora, E. Vazquez-Sune, and J. Carrera (2005), Reactive transport modeling of calcite dissolution in the fresh-salt water mixing zone, Journal of Hydrology, 311(1-4), 282-298.

[105] Roth, K., and W.A. Jury (1993), Linear transport models for adsorbing solutes, Water Resour. Res., 29(4), 1195-1203.

[106] Rubin, Y., M.A. Cushey, and A. Wilson (1997), The moments of the breakthrough curves of instantaneously and kinetically sorbing solutes in heterogeneous geologic media: Prediction and parameter inference from field measurements, Water Resour. Res., 33(11), 2465-2481.

[107] Rubin, Y. (2003), Applied Stochastic Hydrogeology, Oxford University Press, Inc., New York.

[108] Salamon, P., D. Fernandez-Garcia, and J.J. Gomez-Hernandez (2007), Modeling tracer transport at the MADE site: The importance of heterogeneity, Water Resour. Res., 43, W08404.

[109] Salandin, P., and V. Fiorotto (1998), Solute transport in highly heterogeneous aquifers, Water Resour. Res., 34(5),949-961.

[110] Sanchez-Vila, X., J. Carrera, and J.P. Girardi (1996), Scale effects in transmissivity, J. Hydrol., 183, 1-22.

[111] Schwede, R. L., O. A. Cirpka, W. Nowak, and I. Neuweiler (2008), Impact of sampling volume on the probability density function of steady state concentration, Water Resour. Res., 44, W12433, doi:10.1029/2007WR006668.

[112] Selroos, J.O., and V. Cvetkovic (1992), Modeling solute advection coupled with sorption kinetics in heterogenous formations, Water Resour. Res., 28, 1271-1278.

[113] Silliman, S. E., and A. L. Wright (1988), Stochastic analysis of paths of high hydraulic conductivity in porous media, Water Resour. Res., 24(11), 1901–1910.

[114] Silva, O., J. Carrera, M. Dentz, S. Kumar, A. Alcolea, and M Willmann (2009), A general real-time formulation for multi-rate mass transfer problems, Hydrology and Earth Sciences, 13, 1399-1411.

[115] Stark, C.P. (1991), An invasion percolation model of drainage network evolution, Nature, 352, 423-425.

[116] Strebelle, S. (2002), Conditional simulation of complex geological structures using multiple-point statistics, Math. Geol., 34, 1-21.

[117] Sturman, P.J., P.S. Stewart, A.B. Cunningham, E. J. Bouwer, and J.H. Wolfram (1995), Engineering scale-up of in situ bioremediation processes: A review, J. Contam. Hydrol., 19, 171-203.

[118] Tartakovsky, A.M., Tartakovsky, G.D., Scheibe, T.D., (2009). Effects of incomplete mixing on multicomponent reactive transport. Adv. Water Resour. 32, 1674–1679.

[119] Tidwell, V. C., and J. L. Wilson (1999), Permeability upscaling measured on a block of Berea Sandstone: Results and interpretation, Math. Geol., 31(7), 749–769.

[120] Tompson, A. F. B., and L. W. Gelhar(1990), Numerical-simulation of solute transport in 3-dimensional, randomly heterogeneous porous-media, Water Resour. Res., 26(10), 2541-2562.

[121] Torquato, S., J. D. Beasley, and Y. C. Chiew (1988), 2-point cluster function for continuum percolation, Journal of Chemical Physics, 88, 6540-6547.

[122] Valocchi, A. J.(1985), Validity of the local equilibrium assumption for modeling sorbing solute transport through homogeneous soils, Water Resour. Res., 21, 808-820.

[123] Wen, X.-H., and J. J. Gomez-Hernandez (1997), Numerical modeling of macrodispersion in heterogeneous media: A comparison of multi-Gaussian and non-multi-Gaussian models, J. Contam. Hydrol., 30, 129– 156.

[124] Wen, X.-H., and J. Gomez-Hernandez (1998), Journal of Contaminant Hydrology, 30, 129-156.

[125] Western, A. W., G. Bloschl, and R. B. Grayson (1998), Geostatistical characterisation of soil moisture patterns in the Rarrawarra catchment, Journal of Hydrology, 205, 20-37.

[126] Western, A. W., G. Bloschl, and R. B. Grayson (2001), Toward capturing hydrologically significant connectivity in spatial patterns, Water Resour. Res. , 37, 83-97.

[127] Willmann, W., J. Carrera, X. Sanchez-Vila, O. Silva, and M. Dentz (2010), Coupling of mass transfer and reactive transport for nonlinear reactions in heterogeneous media, Water Resour. Res., 46, W07512.

[128] Zheng, C., and S.M. Gorelick (2003), Analysis of solute transport in flow fields influenced by preferential flowpaths at the decimeter scale, Ground Water, 41, 142-155.

[129] Zinn, B., and C.F. Harvey (2003), When good statistical models of aquifer heterogeneity go bad: A comparison of flow, dispersion, and mass transfer in connected and multivariate Gaussian hydraulic conductivity fields, Water Resour. Res., 39, 1051.

[130] Zinn, B., L. C. Meigs, C. F. Harvey, R. Haggerty, W. J. Peplinski, and C. F. von Schwerin (2004), Experimental visualization of solute transport and mass transfer processes in two-dimensional conductivity fields with connected regions of high conductivity, Environmental Science and Technology, 38, 3916-3926.